# Kinetics of the photocatalytic reduction of platinum(IV) in a batch and flow reactor

**A. Petzer**

Dissertation submitted in partial fulfilment of the requirements for the degree of Master of Science in Chemistry at the Potchefstroom Campus of the North-West University

Supervisor: Dr. R.J Kriek
Co-supervisor: Prof. E.L.J Breet

August 2011

# DECLARATION

I declare that this dissertation entitled “Kinetics of the photocatalytic reduction of platinum(IV) in a batch and flow reactor” is my own work apart form the contributions mentioned in the acknowledgements. It has not been submitted for any degree or examination at any other university, and all sources used or quoted have been indicated and acknowledged by complete references.

(Signature)

Adéle Petzer (Full name)

Date: 25 August 2011

# ACKNOWLEDGEMENTS

I would like to thank the following institutions and persons:

- Anglo Platinum for funding of the project, without their interest none of this would have been possible.
- Dr. R.J Kriek, my project leader, for all his contributions and support throughout the study.
- Professor E.L.J. Breet for his guidance in interpreting the results and support as assistant supervisor.
- The North-West University for the use of their facilities and the friendly personnel that was always ready with advice.
- My dad, Dickie, and my mom, Marinda, for giving me this opportunity always encouraging me to follow my dreams and for their ongoing love and support.
- Mike Breytenbach for being my motivation and sounding board during the project.
- To the rest of my family and friends, for keeping me sane all this time.

Thank you.

# SUMMARY

Semiconductor photocatalysis has received considerable attention in recent years as an alternative for treating water polluted with hazardous organic chemicals. The process, as a means of removal of persistent water contaminants such as pesticides, which exhibit chemical stability and resistance to biodegradation, has attracted the attention of many researchers. To a lesser extent, it has also been studied for decontamination of water containing toxic metals.

Precious and common metals enter waters through washing, rinsing, pickling and surface treatment procedures of industrial processes, such as hydrometallurgy, plating and photography. As a result we are living in an environment with a multitude of potentially harmful toxic metal ions. In contrast, the demand for metals increases significantly with the development and growth of industry.

Even though research on the photocatalytic recovery of waste and noble metals has escalated in the past 10 years, the practical implementation of these processes is not yet justified. The successful implementation of large scale reactors, for industrial application, has to consider several reactor design parameters that must be optimised, such as reactor geometry and the utilization of radiated energy.

In this study the effect of various parameters such as initial platinum(IV)chloride concentrations, initial sacrificial reducing agent (ethanol) concentrations, catalyst ($TiO_2$) concentration, pH, temperature and light intensity has been investigated as a first step towards optimising a photocatalytic batch and photocatalytic flow reactor. Langmuir-Hinshelwood kinetics has been applied to calculate the photocatalytic rate constant $k_r$ as well as the adsorption equilibrium constant $K_e$ for both the initial platinum(IV) dependency as well as the initial ethanol concentration dependency.

The results in this study may be used in future work for the optimisation and comparison of both batch and flow reactors towards the industrial implementation of these processes.

**Keywords:** semiconductor; photocatalysis; photocatalytic; reduction; platinum; Langmuir-Hinshelwood; kinetic; $TiO_2$; ethanol

# CONTENTS

# LIST OF FIGURES

# LIST OF TABLES

# CHAPTER 1

# INTRODUCTION

In today's highly industrialized society we are faced with tremendous environmental problems related to remediation of hazardous wastes, contaminated ground waters and control of toxic air contaminants [3].

Semiconductor photocatalysis has received considerable attention in recent years as an alternative for treating water polluted with hazardous organic chemicals. The process, as a means of removal of persistent water contaminants such as pesticides, which exhibit chemical stability and resistance to biodegradation, has attracted the attention of many researchers. To a lesser extent, it has also been studied for decontamination of water containing toxic metals [4, 5].

Metal ions are non-degradable. They have infinite lifetimes and build up to toxic levels in food chains. In recent years, arrays of industrial activities have been disturbing the geological equilibrium of metal ions through release of large quantities of toxic metal ions, such as Hg(II), Pb(II), Cd(II), Ag(I), Ni(II) and Cr(VI), into the environment [6]. Precious and common metals enter waters through washing, rinsing, pickling and surface treatment procedures of industrial processes, such as hydrometallurgy, plating and photography [1]. As a result we are living in an environment with a multitude of potentially harmful toxic metal ions [2]. In contrast, the demand for metals increases significantly with the development and growth of industry. Noble metals such as platinum and palladium are extensively used in catalytic converters in motor vehicles for the conversion of hazardous exhaust gases such as carbon monoxide (CO), hydrogen carbons ($C_xH_y$) and nitrous oxides ($NO_x$) into more acceptable gases and water.

Transition metal ions can be converted into the metallic form and deposited on semiconductor surfaces, or transformed into different soluble species by means of photocatalytic reduction. Photodeposition of metals on a semiconductor surface is related to applications such as the enhancement of the photocatalytic activity of the

semiconductor photocatalyst (for the oxidation of organic compounds as well as the recovery of metal ions), water splitting, light-energy storage systems, photographic imaging systems as well as anti-corrosion of the semiconductor [1]. Waste metal recovery can thus potentially resolve two issues: metal pollution remediation and, simultaneously, resource conservation.

South Africa is home to the largest platinum reserve in the world in the Bushveld Complex. The country currently supplies over 75% of the world's platinum consumption. Within this reserve, metals such as platinum, palladium, rhodium, ruthenium, osmium and iridium are found, and are often referred to as the Platinum Group Metals (PGMs). During the production of these PGMs the metal containing ore is processed by milling, flotation and concentration, and refined. During each of these processes small amounts of PGMs end up in effluent streams. These streams eventually go to large landfill areas. Several techniques, such as precipitation, solvent extraction, ion-exchange or reduction-collection, have been used to recover these low concentration PGMs. However, photocatalytic deposition may be a less expensive and simpler alternative. The metal can be separated from the photocatalyst with aqua regia or chlorine in HCl without altering the semiconductor, which may be recycled [1, 6].

Even though research on the photocatalytic recovery of waste and noble metals has escalated in the past 10 years, practical implementation of these processes is not yet justified. The successful implementation of large scale reactors for industrial application has to consider several reactor design parameters that needs to be optimised, such as reactor geometry and utilization of radiated energy. This study is a first step by investigating kinetically each of the parameters that may have an influence on the rate of metal ion reduction. Parameters such as pH, temperature, metal ion and catalyst concentration, as well as an added sacrificial reducing agent, will be investigated for both a continuously stirred batch reactor and a recirculating flow reactor. The influence of each parameter will be investigated individually in order to identify the rate-controlling parameters. This will allow future studies to optimise photocatalytic reactors for metal ion treatment and contribute towards the industrialisation of photocatalytic processes.

# CHAPTER 2

# LITERATURE REVIEW

## 2.1 Heterogeneous Photocatalysis

The term photocatalysis implies a combination of photochemistry and catalysis for which both light and a catalyst are necessary to bring about or accelerate a photochemical transformation in the presence of a catalyst. This is important since the reaction can only be called photocatalytic if no reaction takes place in the absence of either a suitable light source or a semiconductor catalyst. In photogenerated catalysis the photocatalytic activity (PCA) depends on the ability of the catalyst to create electron–hole pairs, which generate free radicals (hydroxyl radicals: •OH) capable of undergoing secondary reactions. The catalyst may accelerate the photoreaction through interaction with the substrate in its ground or excited state and/or with a primary photoproduct, depending on the mechanism of photoreaction [7].

Semiconductor catalysts are characterized by a filled, low-energy valence band (VB) and an empty, high-energy conduction band (CB). Electrons cannot exist in the band-gap region between the VB and the CB. When the semiconductor is exposed to ultraviolet light with energy larger than that of the band gap, electrons in the low-energy VB will absorb energy, become excited and migrate to the high-energy CB. The result of this excitation is a positive hole in the valence band ($h^+_{VB}$) and an electron in the conduction band ($e^-_{CB}$) [3, 8, 9]. Both the positive hole and the electron must migrate to the surface of the catalyst particle in order to be exposed/available for reaction with the medium. The excited electron can either be used directly to create electricity or to drive a chemical reaction i.e. photocatalysis.

The absorption of photons with the resulting creation of a positive hole in the valence band and an electron in the conduction band is represented in Figure 1.

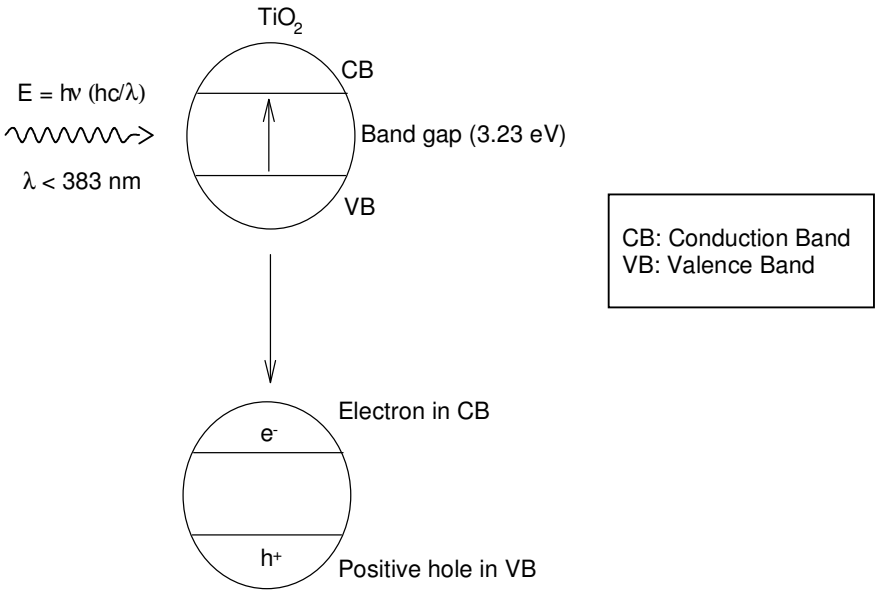


**Figure 1** Schematic representation of the activation of $TiO_2$ semiconductor photocatalyst

The electron-hole pair formed is in an unstable, excited state. This excited state can return to its original ground state by three possible pathways: (i) Recombination of the electron and the positive hole which occurs within nanoseconds. (ii) A sacrificial reducing agent (SRA) can donate an electron to the positive hole, allowing the electron in the CB to be used for reduction. (iii) A sacrificial oxidizing agent (SOA) can be reduced by the electron in the CB and the positive hole can then be used for oxidation.

## 2.2 Photocatalyst

A photocatalyst is defined as a substance that is activated by the absorption of a photon and helps accelerate a reaction without being consumed. Factors that influence the photocatalyst's activity include structure (crystal defects and impurities), particle size, surface properties, preparation, spectral activation and resistance to mechanical stress [10]. Semiconductor photocatalysts can act as sensitizers for

light-reduced redox processes due to their electronic structure, which is characterised by a filled valence band and an empty conduction band [3].

Several catalysts have been studied over the years for the photocatalytic removal of organic and inorganic species from water. These include CdS, ZnS, α-$Fe_2O_3$, γ-$Fe_2O_3$, α-FeOOH, β-FeOOH, and γ-FeOOH, ZnO, $ZrO_2$, $SnO_2$, and $WO_3$, $CN^-$, $Cr_2O_7^{2-}$, $AgCl/Al_2O_3$, $ZnO/TiO_2$ , $TiO_2/SiO_2$, $TiO_2/Al_2O_3$, nobium oxides and lanthanide tantallates ($LnTaO_4$, where Ln can be La, Ce, Pr, Nd, or Sm) [5]. Amongst the semiconductors used $TiO_2$ is one of the most popular and promising materials, because of its photostability under harsh conditions, non-toxicity, strong oxidizing power, commercial availability, low cost, possibility of coating it as a thin film on solid support and ease of preparation in the laboratory [5]. Another advantage is that the photocatalytic activity of $TiO_2$ can be studied in the fixed bed form as well as in suspension.

### 2.2.1 Titanium Dioxide as Photocatalyst

Titanium is the world's fourth most abundant metal and ninth most abundant element. Titanium metal is bound to other elements, found in various igneous rocks and sediments. Three crystalline configurations of $TiO_2$ exist: anatase, rutile and brookite. The rate of formation of the hydroxyl radical is dependent upon the crystalline structure of $TiO_2$ present. Of the three configurations of $TiO_2$, the anatase structure, has the highest level of photoconductivity with an energy band gap of 3.23 eV (384 nm). Rutile is considered much less photoreactive than anatase, with an energy band gap of 2.03 eV (411 nm) [11]. This is attributed to a more efficient recombination of the electron-hole pair and a smaller surface area in the rutile structure [12]. Rutile is the most common structure of $TiO_2$ and is also the most stable. Both anatase and brookite convert to rutile upon heating [13].

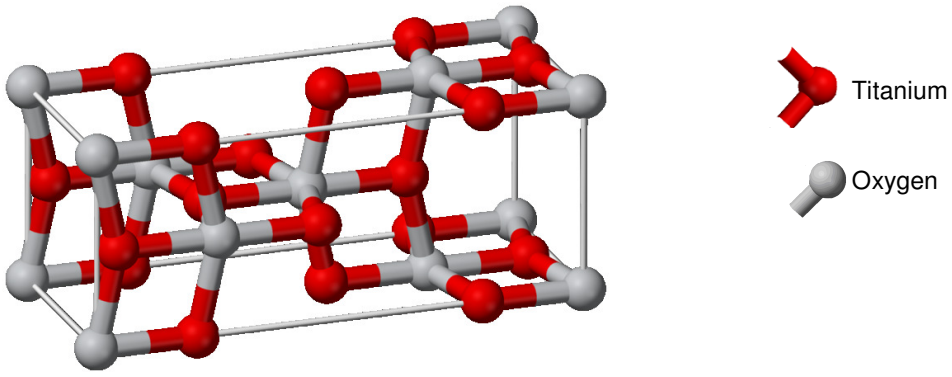


**Figure 2** Crystalline structure of anatase $TiO_2$

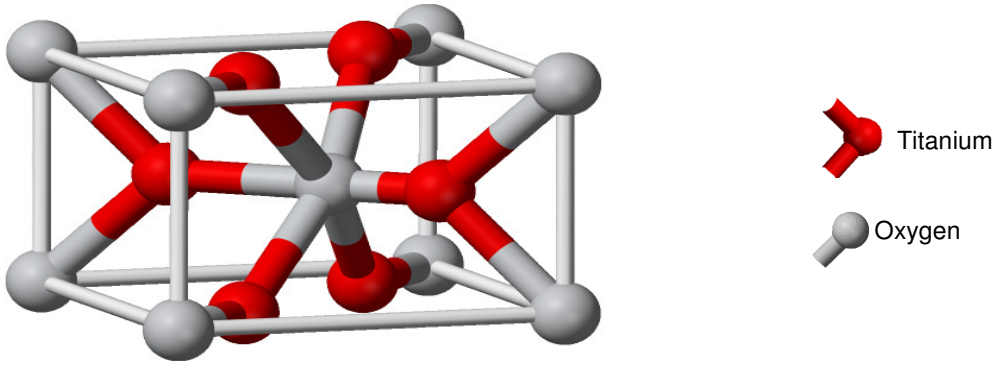


**Figure 3** Crystalline structure of rutile $TiO_2$

Several researchers have indicated that there may be an optimum combination of rutile and anatase crystals for photocatalysis [14]. Degussa P25 is a commercially available 70:30 mixture of anatase and rutile and is generally accepted as the standard photocatalytic form of $TiO_2$ and produces excellent activity. Degussa P25 has an average surface area of 55 ±15 $m^2/g$ and crystalline sizes range from 30 nm to 0.1 mm in diameter.

Key to semiconductor-induced reactions is the light source that will emit photons at the optimum wavelength for excitation of valence band electrons, an optimum that varies among semiconductors. To excite $TiO_2$ valence band electrons, the light source must have a wavelength shorter than 387.5 nm to overcome the band gap

energy [12]. $TiO_2$ absorbs radiation below the visible range of the light spectrum; hence at least near UV light is required [15]. Medium-pressure UV lamps provide the most effective source of photons for $TiO_2$ systems, emitting wavelengths in the 200 to 400 nm range. The absorption spectrum of titanium dioxides overlaps with the solar spectrum and hence opens up the possibility of using solar energy as the source of irradiation [5]. Wavelengths shorter than 387.5 nm are emitted by the sun but in a much less concentrated and consistent manner, making the utilisation of solar energy possible but much less advantageous than artificial light sources [12].

$TiO_2$/UV systems have been developed for a variety of chemical species with much success. However, the potential fatal flaw of heterogeneous $TiO_2$/UV systems is the recovery of suspended $TiO_2$ particles, which have a very slow settling rate and must be centrifuged or micro-filtered, neither of which are economically advantageous separation mechanisms.

$TiO_2$ has a wide variety of applications, from paint to sunscreen to food colouring. $TiO_2$ is the most widely used white pigment because of its brightness and very high refractive index (n = 2.7), which is surpassed only by a few materials. $TiO_2$ is found in most sunscreens because of its high refractive index, its strong UV light absorbing capabilities as well as its resistance to discolouration under UV light.

## 2.3 Photocatalytic Oxidation of Organic Compounds

Industrialised countries adopted a protocol stating that all water must be purified. This has become the driving force for research on photocatalytic oxidation of organic compounds [16]. The degradation or organic compounds is possible via chemical, photochemical en biological processes. Most of these processes are dependent on long treatment times and removal of waste can be a practical problem.

### 2.3.1 Reactions Involved in Photocatalytic Oxidation

The absorption of light photons with energy larger than that of the band gap of the semiconductor particle leads to the formation of electron-hole pairs (Eq. 1).

Electrons in the CB and the positive hole in the VB migrate to the surface of the $TiO_2$ particle making oxidation and reduction of absorbed species possible.

$$TiO_2 + h\nu \leftrightarrow TiO_2(e^- + h^+) \quad (1)$$

Experimentally two types of oxidation reactions can be observed, electron transfer from the adsorbed substrate molecule RX (Eq. 2) as well as electron transfer from the adsorbed solution molecule ($H_2O$ and $OH^-$) (Eq. 3 and 4) [16].

$$TiO_2(h^+) + RX_{ads} \rightarrow TiO_2 + RX^{\bullet +}_{ads} \quad (2)$$

$$TiO_2(h^+) + H_2O_{ads} \rightarrow TiO_2 + OH^{\bullet}_{ads} + H^+ \quad (3)$$

$$TiO_2(h^+) + OH^-_{ads} \rightarrow TiO_2 + OH^{\bullet}_{ads} \quad (4)$$

The OH-radical has an oxidation potential of 2.85 eV and is an extremely strong oxidizing agent. It is, together with the positive hole in the VB, responsible for the oxidation of organic compounds (Eq. 5).

$$OH^{\bullet}_{ads} + RX_{ads} \rightarrow OH^-_{ads} + RX^{\bullet +}_{ads} \quad (5)$$

The presence of molecular oxygen promotes the oxidation process since oxygen is a sacrificial oxidizing agent (Eq. 6) inhibiting recombination of the electron-hole pair.

$$TiO_2(e^-) + O_2 \rightarrow TiO_2 + O_2^{\bullet -} \quad (6)$$

Addition of hydrogen peroxide enhances this oxidation process even further, and it was found that the rate of photocatalytic oxidation increases in the sequence $O_2 < H_2O_2 < O_2 + H_2O_2$ [17]. The reason for this is, firstly, that hydrogen peroxide is a better electron receptor than oxygen, and the excited electrons from the $TiO_2$ surface will be removed at an improved rate and, therefore, the recombination rate of the electron-hole pair and the efficiency of hole utilization for reactions 2 – 4 will increase. Secondly, hydrogen peroxide leads to the creation of more OH-radicals that favors oxidation (Eq. 7 and 8).

$$TiO_2(e^-) + H_2O_2 \rightarrow TiO_2 + OH^- + OH\bullet \quad (7)$$

$$H_2O_2 + h\nu \rightarrow 2HO\bullet \quad (8)$$

If an oxidizing agent, such as $O_2$ and $H_2O_2$, is absent already, oxidized species are reduced (Eq. 9 and 10) and the resulting effect is that electron-hole pair recombination occurs more rapidly and oxidation is inhibited.

$$TiO_2(e^-) + HO^\bullet \rightarrow TiO_2 + OH^- \quad (9)$$

$$TiO_2(e^-) + RX^{\bullet+} \rightarrow TiO_2 + RX \quad (10)$$

The efficiency of photocatalytic oxidation can further increase by increasing the photocatalytic activity of the semiconducter particle. This can be achieved by depositing, especially platinum group metals (PGMs), on the surface of the semiconductor. Wang et al. [18] reported that the rate of photocatalytic oxidation of organic compounds is determined by the rate of electron transfer to molecular oxygen. The rate of electron transfer to molecular oxygen can be increased by deposition of PGMs on the $TiO_2$ particle, as the PGMs stabilises the excited electron, thereby prolonging the recombination of electron hole pairs.

## 2.4 Photocatalytic Reduction of Metallic Species

Since the early days of heterogeneous photocatalysis, photo-transformation and photodeposition of metals, such as noble, expensive and toxic species, have been envisaged as one of the most useful applications of the technique for both economic and environmental aspects involved.

Photocatalytic transformation and deposition of various metals in aqueous solutions have been extensively researched in recent years. Among these metals are chromium, gold, silver, platinum, palladium, rhodium, mercury, lead, manganese, thallium and copper [2, 4, 10, 19, 20]. At the back end of the process, the metallic species can generally be extracted from the slurry by mechanical or chemical means.

According to Rajeshwar et al. [21] three types of mechanisms are possible for the photocatalytic removal of metal ions, viz. (i) direct reduction of ions by photogenerated electrons; (ii) indirect reduction by intermediates generated by hole oxidation of added organics; and (iii) oxidative removal of metals such as $Pb^{2+}$, $Mn^{2+}$ or $Tl^{+}$. The direct reduction pathway is the simplest one; for deposition of a metal M, the energy of the conduction band (CB) electron must be more negative than the $E^0$ of the $M^{n+}/M$ couple as shown in Figure 4 (adapted from Rajeshwar et al. [21]). A few of the metallic couples can be influenced by pH and this must be taken into account. $Ag^{+}$, $Cd^{2+}$, $Cu^{2+}$, $Hg^{2+}$, $Ni^{2+}$ and $Cr^{6+}$ can be reduced by $TiO_2$ conduction band electrons when in an appropriate pH range.

Praire *et al.* [4] investigated the photocatalytic reduction of a variety of dissolved metal ions in 0.1 wt% $TiO_2$. They found that only those metals with half-reaction standard reduction potentials more positive than 0.4 V can be reduced using $TiO_2$ as photocatalyst. Oxygen inhibits the reduction in cases of silver, mercury, palladium, rhodium and platinum, through competition for conduction band electrons. The enhancement of metal deposition is generally reinforced by the addition of a sacrificial reducing agent. The results of Praire et al. [4, 22, 23] reported that $Cr^{6+}$, $Au^{3+}$, $Hg^{2+}$, $Pd^{2+}$, $Pt^{4+}$ and $Ag^{+}$ can be reduced to a large extent after short UV illumination times in the presence of salicylic acid, while no reduction of $Cu^{2+}$, $Cd^{2+}$ and $Ni^{2+}$ took place.

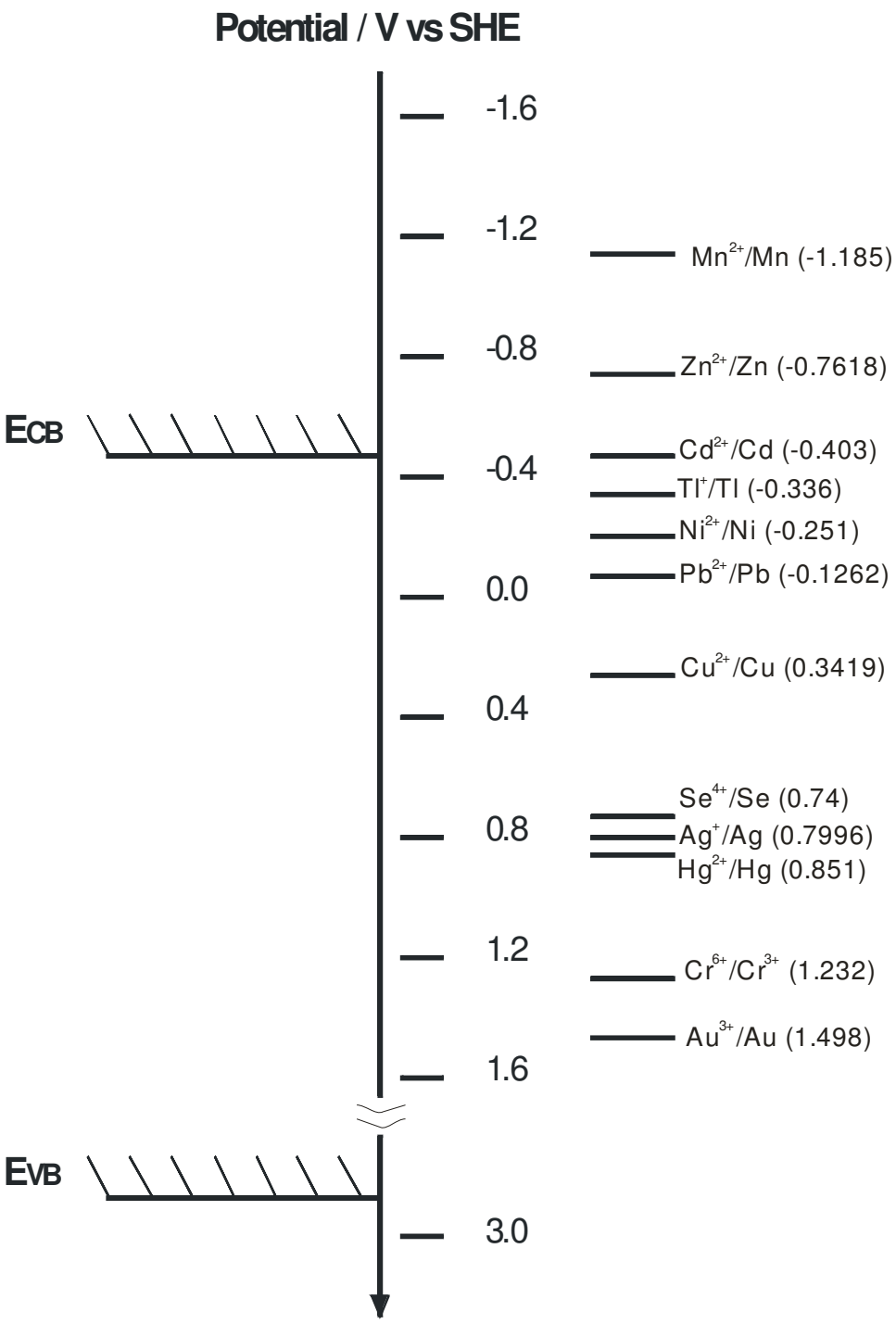


**Figure 4** Positions of redox potentials of various metallic couples related to the energy levels of the conduction and valence bands of $TiO_2$ Degussa P-25 at pH 0

### 2.4.1 Reactions Involved in Photocatalytic Reduction

The majority of platinum group metals is halide complexes $MX_m^{n-}$ (X = Cl, Br, I) in solution. In contrast to photocatalytic oxidation, where the excited electron is responsible for reduction of molecular oxygen, the electron is now responsible for the reduction of the metal complex (Eq. 11)

$$(m\text{-}n)TiO_2(e^-) + MX_m^{n-} \rightarrow M^0 + mX^- \quad (11)$$

For reaction 11 to occur, an electron must be donated to the positive hole in the VB in order for the $TiO_2$ particle to return to its neutral state. If there is no sacrificial reducing agent (SRA), water will be oxidised according to reactions 12 and 13.

$$4TiO_2(h^+) + 2H_2O \rightarrow TiO_2 + O_2 + 4H^+ \quad (12)$$

$$TiO_2(h^+) + H_2O \rightarrow TiO_2 + H^+ + HO\bullet \quad (13)$$

OH-radicals as well as molecular oxygen are formed, and these can lead to formation of more OH-radicals. OH-radicals inhibit the reduction process by acting as a strong oxidizing agent. The oxidation of water is reduced by the use of a sacrificial reducing agent that does not react in the oxidised form and, therefore, the effectivity of the photocatalytic reduction of most metals increases. Alcohols are popular sacrificial reducing agents, e.g. methanol or ethanol.

The oxidation of ethanol [24], with the simultaneous reduction of platinum on the surface of the semiconductor, $TiO_2$, is illustrated in Figure 5. The oxidation-reduction process continues according to Equation 11 until the metal is completely deposited on the semiconductor surface.

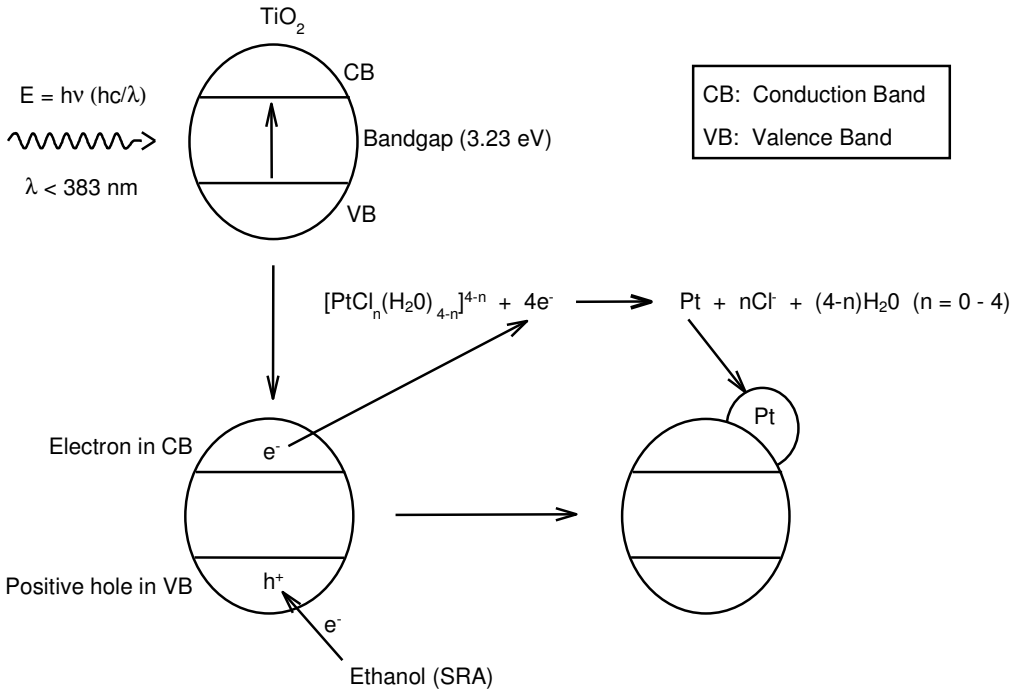


**Figure 5** Schematic representation of simultaneous ethanol (SRA) oxidation and platinum reduction

## 2.4.2 Platinum Group Metals (PGMs)

The recent extended use of PGMs (Pt, Pd, Rh, Ru, Ir and Os) in applications such as catalytic converters for controlling emission of pollutants in automobile exhaust gases and in cancer-inhibiting drugs has raised the concern for environmental pollution by these metallic species. In the zero-valence form their toxicities are low, but the soluble forms (e.g. chlorides) can be poisonous at levels as low as 1 ppb. Catalytic converters, on the other hand, have introduced problems such as the emission of noble metal particulate matter in the respirable size range [25].

Generally, platinum production results in effluent streams containing small amounts of the metal, which must be recovered. Several techniques have been employed, e.g. precipitation, solvent extraction, ion-exchange or reduction-collection. However, the costs of these processes are critical, especially in the case of Pt recovery from the main secondary source, i.e. automotive three-way catalysts. Photocatalytic deposition may be a less expensive and simpler alternative since the metal can be

separated from the photocatalyst by means of aqua regia or chlorine in HCl and recycled. The photocatalytic reduction of Pt is thermodynamically possible since $E^0_{PtCl_6^{2-}/Pt^0} = 0.691\,\text{V}$, but in the absence of a hole scavenger the reaction is difficult to perform [10].

Ward and Bard [26] found that addition of $H_2PtCl_6$ to degassed $TiO_2$ aqueous suspensions resulted in irreversible $Pt^0$ deposition on the particles with no re-oxidation of the metal. In another study [20], the photocatalytic recovery of low $PtCl_6^{2-}$ concentrations from P-25 aqueous suspensions at low pH and high chloride concentration (conditions similar to those of hydrometallurgical processes) was investigated in a continuous flow system with recirculation through an illuminated column and methanol as hole scavenger. The product was a $Pt/TiO_2$ sponge, easily separable by centrifugation. Almost quantitative recovery of Pt was achieved by selective dissolution of Pt by aqua regia or chlorinated hydrochloric acid.

Photocatalytic reduction of $PdCl_4^{2-}$ to $TiO_2$ degassed aqueous suspensions resulted in irreversible $Pd^0$ deposition on the particles [26]. Oxygen competed with the reduction, particularly at low pH. The reaction did not take place at pH 0 and was a maximum in the range 3–5. It was found that in acidic media $Pd^{2+}$ is completely reduced to $Pd^0$, while at pH 11.8 it is only adsorbed or precipitated onto $TiO_2$ [27].

Borgarello et al. [28] studied the light-induced reduction of $Rh^{3+}$ on $TiO_2$ dispersions from $RhCl_3.3H_2O$ aqueous solutions irradiated with simulated sunlight. Complete reduction of $Rh^{3+}$ at pH 0 in oxygen-free solutions occurred only in the presence of methanol, with a change in the colour of the slurry from white to dark grey ($Rh^0$) on $TiO_2$.

### 2.4.3 Selective Photocatalytic Reduction of PGMs

The photocatalytic reduction of the PGMs in a suspension of $TiO_2$ with resulting deposition and accumulation of the metal on the semiconductor has led to investigations of the possibility to selectively remove PGMs from solution by selective photocatalytic reduction.

The standard reduction potential of chloride complexes of some of the platinum group metals is given in Table 1. From the differences in the reduction potential of the PGMs one can assume that there will be a difference in the ease of photocatalytic reduction of the metals.

**Table 1** Standard reduction potentials of chloride complexes of PGMs relative to the standard hydrogen electrode (SHE)

| Reaction | $E^0$ (V) |
|---|---|
| $[PtCl_4]^{2-} + 2e^- \leftrightarrow Pt + 4Cl^-$ | 0.755 |
| $[PtCl_6]^{2-} + 2e^- \leftrightarrow [PtCl_4]^{2-} + 2Cl^-$ | 0.68 |
| $[PdCl_4]^{2-} + 2e^- \leftrightarrow Pd + 4Cl^-$ | 0.591 |
| $[PdCl_6]^{2-} + 2e^- \leftrightarrow [PdCl_4]^{2-} + 2Cl^-$ | 1.288 |
| $[RhCl_6]^{3-} + 3e^- \leftrightarrow Rh + 6Cl$ | 0.431 |
| $[IrCl_6]^{3-} + 3e^- \leftrightarrow Ir + 6Cl^-$ | 0.77 |
| $[IrCl_6]^{2-} + e^- \leftrightarrow [IrCl_6]^{3-}$ | 0.8665 |
| $[RuCl_5]^{2-} + 3e^- \leftrightarrow Ru + 5Cl^-$ | ≈ 0.4 |

Kriek [16] investigated the selective photocatalytic reduction of three PGMs, viz. platinum, palladium and rhodium. He found that these metals can be separated by differential photocatalytic reduction. Pt(IV) is in solution at pH ≈ 12, while both Pd(II) and Rh(III) will absorb onto the photocatalyst. This makes the separation of platinum possible. Palladium and rhodium can be brought back into solution by reducing the pH (pH ≈ 2). Pd(II) and Rh(III) can then be separated by differential photocatalytic reduction, where rhodium remains in solution and palladium is reduced to $Pd^0$ on $TiO_2$ at a pH of exactly 3.1. It is important that the pH remains at 3.1 because rhodium is reduced at pH values below 3.1 and adsorption of rhodium occurs at pH values higher than 3.1.

## 2.5 Photocatalytic Reactors

Photocatalytic reactors differ from the more conventional reactors (of thermal or thermal-catalytic nature) due to the presence of a radiation field that produces the activation of the catalyst. The catalyst most widely employed, titanium dioxide, absorbs radiation below the visible range of the light spectrum, hence at least near UV light is required. The light that gives rise to the required radiation field can be produced by artificial lamps or by solar irradiation. In both cases, optimization of this light activated step is, together with catalyst selection, very likely to be the key points for the design of these reactors [15].

To implement a commercial reactor, several design parameters must be optimized, such as photoreactor geometry, type of photocatalyst and utilization of radiated energy [29]. A fundamental issue regarding successful implementation of photocatalytic reactors is the transmission of irradiation in a highly scattering and absorbing medium composed of water and fine $TiO_2$ particles. The successful scaling-up of photocatalytic reactors involves increasing the number of photons absorbed per unit time per unit volume as well as efficiently using the electron holes created during photocatalytic transformations.

While a few of the physico-chemical principles of photocatalysis are relatively well understood, reactor design and reactor engineering of photocatalytic units still require consideration [14, 30] This is particularly true in the case of scaled reactors processing large volumes of water and using high levels of irradiation. Cassano et al. [31] stressed that several aspects of design, optimization and operation of photochemical reactors that are not usually considered in the design of conventional chemical reactors should be taken into account. A few of these aspects are:

- selection of radiation sources including output power, source efficiency, spectral distribution, shape, dimensions, maintenance and operating requirements;
- design of reactor geometry with respect to the irradiation source;
- design of reactor irradiation devices including mirrors, reflectors and windows, their construction materials, shape and cleaning procedures.

Photocatalytic reactors for water treatment can be classified according to their design [29].

1. **Three main photocatalytic reactor configurations**
    - Photocatalytic Batch Reactors (PBR)
    - Photocatalytic Continuous Flow Reactors (PCFR)
    - Photocatalytic Plug Flow Reactors (PPFR)
2. **State of photocatalyst**
    - Photocatalytic slurry reactors (suspended catalyst)
    - Photocatalytic reactors with immobilized photocatalyst
3. **Type of illumination**
    - UV polychromatic lamps
    - Solar light
        1. Non-concentrating irradiated reactors
        2. Concentrating irradiated reactors
4. **Position of irradiation source**
    - Reactors with an immersed light source
    - Reactors with an external light source
    - Reactors with distributed light sources (reflectors of light guides) [32]

Photocatalytic reactors for treating wastewater exhibit difficulty in handling fluids which have different compositions and/or concentrations; thus, a detailed kinetic representation may not be possible. For comparing different reaction systems under similar operating conditions and to provide approximate estimations for scaling-up purposes, simplified models may be useful. These should be based on a few simple and observable variables that, in the ideal situation, must not exceed those used to control the reactor operation [15, 33, 34].

### 2.5.1 Photocatalytic Reactor Configurations

The photocatalytic batch reactor (PBR) is by definition an unsteady-state system. It is assumed to function under isothermal and perfectly mixed conditions. This operation mode is an approximation. In normal practice these reactors operate at ambient temperature that can experience changes during the day. The hypothesis is true for stable species in most of the fluid region. Close to the catalytic particles stirring should be extremely vigorous to make sure that the boundary layer close to the solid is well mixed with the rest of the liquid. Moreover, the radiation field is

intrinsically non-uniform an there is no mechanical way to successfully mix photons that travel at the speed of light [32]. This fact could place some doubts about the possibility of having good mixing conditions for radical species of very short lifetime, unless the mixing time of the system would also be very short. In liquid systems we can also assume that the reaction volume is constant.

A continuous flow reactor (CFR) is a device that allows chemical reactions to be performed as a continual process rather than batch-wise. Continuous flow reactors allow good control over reaction conditions including heat transfer, time and mixing. The residence time of the reagents in the reactor is calculated from the volume of the reactor and the flow rate through it. Frequently outgoing streams of real wastewaters do not have a definite and constant composition. Different operating conditions are analyzed, employing artificial and solar light with uniform and non-uniform illumination. Since model pollutants and artificial light are involved, very precise kinetic analysis and reactor design are complex and not exempt from difficulties, but possible [15, 30].

A common continuous flow reactor used for photocatalytic reactions is the Closed Loop Slurry Reactor (CLSR) [20]. This reactor recirculates a catalytic suspension through an illuminated column. A modification of the semi-batch reactor is used as reservoir where reagents can easily be added and samples taken from.

In a plug flow reactor (PFR), one or more fluid reagents are pumped through a pipe or tube. The chemical reaction proceeds as the reagents travel through the reactor. In this type of reactor, the reaction rate is a gradient; at the inlet (to the PFR) the rate is very high, but as the concentrations of the reagents decrease and the concentration of the product(s) increases, the reaction slows down.

Since it is futile to use highly sophisticated models for photocatalytic reactor performance, the photocatalytic plug flow reactor (PPFR) may seem to be an attractive alternative [29]. Starting from the general mass conservation equation, employing the following assumption of operating conditions:
(i) unsteady state;
(ii) isothermal performance;
(iii) unidirectional, incompressible, continuous and plug flow;
(iv) uniform concentrations in the reactor cross-sectional area;

(v) axial diffusion neglected in comparison to convective flow;
(vi) non-permeable reactor walls;
(vii) constant physical and transport properties.

Any differential volume of a photocatalytic plug flow reactor (PPFR) can be modelled as a small photocatalytic batch reactor because of the mixing assumptions in the cross-sectional area of the PPFR.

### 2.5.2 State of Photocatalyst

The majority of photocatalytic reactors used for water treatment is of the well mixed slurry type. Slurry reactors have larger photocatalytic activity compared to photocatalytic reactors with immobilized photocatalyst [12]. In the case of dispersed titanium dioxide an increase of photocatalytic efficiency, by at least a factor of 10, is reported compared to immobilized catalysts (fixed bed configuration) [32].

Slurry systems, on the other hand, requires separation of fine sub-micron particles $TiO_2$ (0.1 micron size) from the treated milk-like suspension. Separation steps complicate the treatment process and decrease the economical viability of the slurry reactor approach. Several techniques have been proposed including high-cost ultra-centrifugation and inexpensive, but time-consuming overnight settling.

Photocatalytic reactors with immobilized $TiO_2$ have suitable configurations for both air and water treatment. In typical fixed photocatalytic reactors, the photocatalyst can be coated or anchored (fixed) on the reactor walls around the light source casing or attached to a solid matrix. Typical $TiO_2$ supports are:

- Activated carbon
- Fiber optic cables
- Glass (beads or wool)
- Membranes
- Quartz sand
- Zeolites
- Silica gel
- Stainless steel

Since $TiO_2$ is not present in the water or air streams at any time, these reactors have the advantage of not requiring a catalyst recovery operation [35]. A comparison between the advantages and disadvantages of both suspended and immobilized catalyst reactors is given in Table 2 [29].

**Table 2** Comparison of slurry and immobilized reactors

| Slurry Reactors | Immobilized Reactors |
|---|---|
| *Advantages*<br>• Fairly uniform catalyst distribution<br>• High ratio of photocatalytic surface area to reactor volume<br>• Limited mass transfer<br>• Minimum catalyst fouling effects due to possible continuous removal and catalyst replacement<br>• Well-mixed particle suspension<br>• Low-pressure drop through reactor | *Advantages*<br>• Continuous operation<br>• Improved removal of organic material from water phase while using a support with adsorption properties<br>• No need for additional catalyst separation operation |
| *Disadvantages*<br>• Requires post-process filtration<br>• Important light-scattering and adsorption in particle suspended medium | *Disadvantages*<br>• Low light utilization efficiencies due to light scattering by immobilized photocatalyst<br>• Restricted processing capacities due to possible mass transfer limitations<br>• Possible catalyst deactivation and catalyst wash-out |

### 2.5.3 Irradiation Sources

Radiation absorption is the single, most distinct characteristic of photocatalytic reactors. Several questions remain to be answered regarding the economical competitiveness of large-scale applications. At the same time, research has yet to succeed in developing a comprehensive and sound understanding and description of all phenomena involved, with the challenge reaching its maximum when real wastewater and varying solar illumination become the implicated issues.

There are three central problems in designing a photocatalytic reactor:

(1) analysis of the reaction (paths, mechanisms, products, efficiencies, etc.) together with choice of the most efficient catalyst;

(2) analysis of the reaction kinetics and of methods for reactor design for different reactor geometries;

(3) provision of adequate irradiation for the entire reactor volume.

Since radiation absorption is the most distinct characteristic of photocatalytic reactors, it is possible to classify the most significant contributions to that form of quantitative work that can be useful for reactor design, according to the way in which this process is considered. Four processes may be present: emission, absorption, out-scattering and in-scattering (resulting from multiple scattering) [6].

Normally, with the exception of work performed at high temperatures, emission can be safely neglected, hence, it will not be considered for the case of photocatalytic reactions in water systems. When catalytic particles are present, the participating medium is macroscopically heterogeneous and scattering becomes important.

Two simplified models were presented in a two-part paper by Brucato and Rizzuti [36]: the first is a zero-reflectance model and the second a two-flux model. Both models are representative of two limiting conditions for the photon-particle interaction. The authors considered that when a photon impinges on the surface of a catalytic particle one can have: (i) total absorption (zero-reflectance model) and (ii) reflection in a purely back-scattering direction (two-flux model). The first model overestimates the photon absorption rate (all the impinging energy is absorbed) and the second underestimates the photon absorption rate because it computes reflection (a sort of macroscopic scattering) with its maximum influence. Since each of the models represents almost opposite situations, it is stated by the authors that the real performance of a heterogeneous system may lie somewhere between both predictions.

Photocatalytic reactors can be powered by solar light as 4-5% of the wavelengths of the solar spectrum are able to excite $TiO_2$. For low intensities, there is a first-order relation between rate of photoreaction and irradiation intensity. At higher levels of irradiation the relation becomes of fractional order. Increased inefficiencies with increasing irradiation is a significantly limiting factor in solar photoreactor applications.

One additional problem related to the use of non-concentrated solar illumination is combination of low irradiation rates with reactions that are usually slow in the liquid phase. In continuous systems this means that rather large average retention times will be needed. Under these circumstances the possibility of operating a reactor under unsteady state conditions during a significant part of day-light hours is always present. Knowledge of reactor performance during the first average retention time will thus be as important as knowing the same information under steady-state operations.

## 2.6 Kinetics

Chemical kinetics is a study of the rate and mechanism of a chemical reaction. A chemical reaction occurs when a chemical species' identity is lost via a change in the number or type of atoms present or when there is a change in its molecular structure [37]. The kinetics of photocatalytic reactions differs from conventional chemical reactions in the sense that the chemical substrate undergoing a change in photocatalytic oxidation or reduction can be treated empirically without consideration of the detailed mechanistic steps [3]. The photocatalytic reduction of $PtCl_6^{2-}$ in bulk-phase $TiO_2$, with ethanol as sacrificial reducing agent, occurs according to the following stoichiometry:

$$PtCl_6^{2-} + 2C_2H_5OH \xrightarrow{TiO_2, h\nu} Pt + 2H_3C_2OH + 4H^+ + 6Cl^- \quad (14)$$

The rate of platinum reduction, in a well-mixed slurry reactor, then conforms to the following standard kinetic relationship (Eq. 15) [38]:

$$-\frac{d[PtCl_6^{2-}]}{dt} = -\frac{d[C_2H_5OH]}{2dt} = \frac{d[Pt]}{dt} \quad (15)$$

Most often reaction rates are determined by measuring the concentration of the reacting species throughout the course of the reaction. A zero-order reaction is independent of the concentration (Eq. 16), and will result in a linear relationship between concentration and time [37]. Reactions of zero-order can occur when one

species is in such excess that its change in concentration is negligible. Equation 17 represents a first-order rate law for the disappearance of species A ($r$ = rate).

$$-r_A = k_A \quad (16)$$

$$-r_A = k_A C_A \quad (17)$$

The reaction rate constant for a first-order reaction can be determined from the slope of the plot of $\ln[A]/[A]_0$ versus time (Eq. 18).

$$\ln\frac{[A]}{[A_0]} = -kt \quad (18)$$

Benits et al. [39] investigated the photocatalytic oxidation of pentachlorophenol (PCP) and concluded that the reaction follows first-order kinetics. Accordingly, a plot of $\ln[PCP]_0/[PCP]$ versus time led to a straight line with slope $k$. A similar study was conducted by Ching et al. [40] for the degradation of gaseous formaldehyde. They found that the reaction was a pseudo first-order reaction and used Equation 18 as a simplified version of the Langmuir-Hinshelwood equation (see section 1.7.1) to calculate the rate constant, $k_r$.

The kinetics of catalytic reactions is an established field of research in heterogeneous catalysis [41]. Analysis of catalytic and photocatalytic kinetics in various reactions over solid catalysts is based essentially on the application of the Langmuir approach of ideal surfaces.

### 2.6.1 Langmuir – Hinshelwood Kinetics

In the Langmuir-Hinshelwood treatment of heterogeneous surface reactions, the rate of photocatalytic degradation [3] can be expressed in general terms for both the oxidant (e.g. $Pt^{2+}$) and the reductant (e.g. $C_2H_5OH$) as follows:

$$-\frac{d[Red]}{dt} = -\frac{d[Ox]}{dt} = k_d\theta_{Red}\theta_{Ox} \quad (19)$$

where $k_d$ is the photodegradation rate constant, $\theta_{Red}$ represents the fraction of the electron-donating reductant (e.g. ethanol) adsorbed to the surface, and $\theta_{Ox}$ represents the corresponding fraction of electron-accepting oxidant (e.g. platinum) adsorbed on to the surface. This treatment is subjected to assumptions that adsorption of both the oxidant and the reductant is a rapid equilibrium process in both the forward and reverse directions and that the rate-determining step of the reaction involves both species present in a monolayer at the solid-liquid interface.

An analogous expression (Eq. 20) can also be written for the oxidant [1]:

$$\theta_{ads} = \frac{K_e C_i}{1 + K_e C_i} \tag{20}$$

Langmuir-Hinshelwood kinetics utilizes both a reaction rate constant, $k_r$, and an adsorption equilibrium constant, $K_e$, to describe heterogeneous surface reactions. The Langmuir-Hinshelwood model assumes that the initial rate of a surface reaction ($R_i$) is proportional to the fractional coverage ($\theta_{ads}$) and that the adsorption equilibrium of the solute follows a Langmuir isotherm (Eq. 20 and 21)

$$R_i = \frac{dC_i}{dt} = \frac{k_r K_e C_i}{1 + K_e C_i} \tag{21}$$

where $C_i$ is the initial concentration of the solute. For dilute solutions ($C_i < 10^{-3}$M), $K_e C_i$ becomes << 1 and the reaction is of apparent first-order, whereas for concentrations > 5 x $10^{-3}$ M, ($K_e C_i >> 1$), the reaction rate is maximum and of zero-order [8]. Both $k_r$ and $K_e$ depend on the catalyst utilized and the disappearing species. Cassano et al [42] demonstrated that Langmuir-Hinshelwood kinetics is a simplified model since $k_r$ incorporates the local volumetric rate of radiation energy absorption and $K_e$ incorporates several kinetic rate constants.

Equation 21 stems from a mechanism allowing one relatively rapid (e.g. adsorption equilibrium) reaction followed by a single, slow surface reaction step [41]. It is important to note that equation (21) is used in enzyme catalysis and is known in somewhat modified form as the Michaelis-Menten equation [43]. Similar to photocatalytic data, linearization and application of double reciprocal plots (e.g. $1/R_i$ vs. $1/C_i$) is utilized in enzymatic catalysis as well. The values of both constants, $k_r$ and $K_e$, can be determined from a plot of $1/R_i$ vs. $1/C_i$ (Eq. 22).

$$\frac{1}{R_i} = \frac{1}{k_r K_e C_i} + \frac{1}{k_r} \quad (22)$$

It should be noted that the initial rate of the surface reactions must be determined experimentally at various levels of initial concentrations.

Kumar et al. [44] stated, using data from [45], that Langmuir kinetics cannot be approximated to zero-order reactions because of the significance of the $K_eC_i$ term. This conclusion was made when the entire data set for a certain range of conditions was used. At high substrate concentrations (zero-order reaction), the $K_eC_i$ term cannot be determined based on the limited data set from [45] as $K_eC_i >> 1$. Murzin found, contrary to Kumar, that Langmuir kinetics can be approximated to zero-order reactions for a certain range of experimental conditions and the rate is independent of the substrate concentration ($K_eC_i$ term). This is when only a subset of the data is used. If the entire data set is used for kinetic modelling, the $K_eC_i$ term becomes significant. The theoretical explanation for zero-order kinetics is complete coverage of active sites by the substrate, thus the presence of any additional substrate in the reaction milieu does not have any influence on the kinetics.

Schrank et al. [6] studied the photocatalytic reduction of Cr(IV) in order to determine the relationship between $K_e$ for both the reactional system (UV light and catalyst present) and the adsorption system (irradiation without a catalyst present). They found that, although there is no similarity between the two equilibrium constants, they are of the same magnitude, indicating that the reaction occurs mainly on the surface of the solid catalyst [2]. Various studies indicated that the reaction rate constant, $k_r$, is independent of the geometry of the reactor and the UV light source [3, 42].

An alternative method for calculating the reaction rate R and the reaction rate constant for photocatalytic reactions was proposed by Angelidis et al. [20] using mass balance equations over the inlet and outlet of a closed-loop flow reactor with a continuously stirred batch vessel as reservoir. This is represented in Section 2.6.2.

### 2.6.2 Mass Balance Equations

The kinetics was followed by the measurement of the platinum concentration at the inlet of the batch vessel at various times. In order to estimate the reaction rate at any time the value of the concentrations of platinum at the inlet and the outlet stream of the photoreactor is required. The mass balance equations of the two vessels (batch and photoreactor) were applied in order to calculate these concentrations as a function of the actually measured concentration at the inlet of the batch vessel. With the assumption that the batch vessel is a CSTR (continuous stirred tank reactor) (this assumption is a good approximation of the real conditions due to the vigorous mixing produced by the magnetic stirrer), the mass balance is

$$QC_{in} = QC_{out} + V\left(\frac{dC_{out}}{dt}\right) \tag{23}$$

where $Q$ is the volumetric flow in mL.min$^{-1}$, $C_{in}$ is the platinum concentration at the inlet stream in mg.L$^{-1}$ (measured concentration), $C_{out}$ is the platinum concentration at the outlet stream in mg.L$^{-1}$ (since the vessel is a CSTR, this concentration is equal to the platinum concentration in the batch vessel) and $V$ is the volume of the solution in the batch vessel, in mL, at any time $t$. The second mass balance for the photoreactor is given by

$$Q\mathrm{d}C_r = r_{Pt}\mathrm{d}V \tag{24}$$

where $C_r$ is the platinum concentration in the reactor in mg.L$^{-1}$, $r_{Pt}$ is the rate of platinum photodeposition in mg.L$^{-1}$.min$^{-1}$ and $V_r$ is the illuminated volume of the reactor in mL. With the assumption of a linear relationship between $C_r$ and $V_r$ (plug flow reactor) the reaction rate at any time $t$ is given by

$$r_{Pt} = Q\left(\frac{dC_r}{dV_r}\right) = \left(\frac{Q}{V_r}\right)(C_{in} - C_{out}) \tag{25}$$

Assuming plug flow in the piping connecting the two vessels, the following relationships exist between the inlet and outlet platinum concentrations:

$$C_{\text{in},t-t_a} = C_{r_{\text{out}}}$$
$$C_{\text{out},t-t_b} = C_{r_{\text{in}}}$$

where $t$ is the time elapsed from the beginning of the experiment when the lamps were turned on, $t_a$ is the time required for the plug front to travel from the outlet of the reactor to the inlet of the CSTR in min, $t_b$ is the time required for the plug front to travel from the outlet to the inlet of the CSTR in min. Thus Eq. (25) becomes

$$r_{\text{Pt}} = \left(\frac{Q}{V_r}\right)\left(C_{\text{out},t-t_b} - C_{\text{in},t-t_a}\right) \tag{26}$$

Since $t_b$ and $t_a$ are constant the establishment of relationships between $C_{\text{out},t}$ and $C_{\text{in},t}$ is required in order to calculate the reaction rate at any time $t$. The experimental data can be used to calculate the relationship between $C_{\text{in},t}$ and t. Two types of relationships connect these variables before the reaction reaches equilibrium: a single linear function for initial platinum concentrations between 25 and 75 mg.L$^{-1}$ ($C_{\text{in}} = \text{A} - \text{B}t$) and a double linear function for concentrations higher than 75 mg.L$^{-1}$ ($C_{\text{in}} = \text{A} - Bt$ for lower and $C_{\text{in}} = \text{A}' - \text{B}'t$ for higher $t$ values). Substitution of these linear relationships in Eq. (23) permits the solution of the differential equation and the calculation of $C_{\text{out}}$ as a function of $t$:

$$V\left(\frac{\text{d}C_{\text{out}}}{\text{d}t}\right) + \text{QC}_{\text{out}} = \text{A} - \text{B}t \tag{27}$$

and

$$\text{C}_{\text{out}} = \text{A} - \text{B}t + \left(\frac{V\text{B}}{Q}\right) + \text{C}\left(\text{EXP} - \left(\frac{Qt}{V}\right)\right), \tag{28}$$

where C is the integration constant for $t = 0$ and $C_{\text{out}} = C_{\text{out}_0}$ such that

$$\text{C} = C_{\text{out}_0} - \text{A} - \frac{V\text{B}}{Q}. \tag{29}$$

Eq. (28) becomes

$$C_{out} = A - Bt + \left(\frac{VB}{Q}\right) + \left(C_{out} - A - \left(\frac{VB}{Q}\right)\right)\left(EXP\left(-\left(\frac{Qt}{V}\right)\right)\right) \quad (30)$$

The value of V was not constant during each experimental run and was decreased by 10 $cm^3$ after each aliquot removal. In order to take into account this change, Eq. (30) was solved separately for each sampling interval.

$$C_{out} = A - B\Delta t + \left(\frac{VB}{Q}\right) + \left(C_{out\,i} - A - \left(\frac{VB}{Q}\right)\right)\left(EXP\left(-\left(\frac{Q\Delta t}{V}\right)\right)\right) \quad (31)$$

where $C_{out\,i}$ is the respective concentration at the end of the previous time period. For $t = 0$ it was assumed that $C_{out\,0} = A$. So

$$C_{in,t-t_a} = A - B(\Delta t - t_a) \quad (32)$$

and

$$C_{out,t-t_b} = A - B(\Delta t - t_b) \quad (33)$$

and the reaction rate can be calculated from Eq. (26).

### 2.6.3 Quantum Yield and Photonic Efficiencies

The quantum yield $\Phi$ is crucial in homogeneous photochemistry. However, in heterogeneous photocatalysis this term remains elusive since the number of absorbed photons remains experimentally difficult to assess. A comprehensive method to standardize and compare process efficiencies in heterogeneous photocatalysis has been proposed earlier by describing the relative photonic efficiency $\zeta_r$ [46]. The method of determining $\zeta_r$ was tested for the photocatalyzed degradation of phenol as the standard process and Degussa P25 $TiO_2$ as the standard photocatalyst. Photonic efficiencies ($\zeta_r$) are useful to assess process quantum yields once the actual quantum yield for a standard process ($\Phi_{stand}$, for a given photocatalyst and a standard organic substrate) has been rigorously determined. Thus

$$\Phi = \zeta_r \, \Phi_{stand} \tag{34}$$

Too often, heterogeneous photocatalysis literature uses the term quantum yield, which it has defined as the number of molecules converted relative to the total number of photons incident on the reactor walls, for a sometimes ill-defined reactor geometry and for a large spectral irradiation window (polychromatic radiation) rather than the number of absorbed quanta at a given wavelength to satisfy the photochemical definition of $\Phi$ in homogeneous phase. In the latter phase, the overall quantum yield $\Phi_{overall}$ expresses the number $N_{mol}$ of molecules undergoing an event (conversion of reactants or formation of products) relative to the number $N_{ph}$ of quanta absorbed by the reactant(s) or by the photocatalyst [47].

$$\phi_{overall} = \frac{N_{mol} / \mathrm{cm^{-3}s}}{N_{ph} / \mathrm{cm^{-3}s}} = \frac{\text{rate of reaction}}{\text{rate of absorption of radiation}} \tag{35}$$

Because the number $N_{ph}$ of absorbed photons is experimentally difficult to access owing to reflection, scattering, transmission (for transparent colloidal sols) and absorption by the suspended particulates, usage of the term quantum yield as defined in terms of incident photons in the literatrure on heterogeneous photochemistry has led to a high degree of confusion. The number of photons emitted by UV light absorbable by $TiO_2$ seems to be about 60-65%.

$\zeta_r$ from Eq. (34) can at a later stage be converted into the photochemically defined $\Phi$ once a protocol or method is found that gives the precise description of the number of absorbed quanta. A quantum yield $\Phi_{stand}$ is therefore specified for a given photocatalyst and a given substrate such that $\Phi = \zeta_r \, \Phi_{stand}$. Recent laser work from Serpone et al. [48], however, suggests that $\Phi$ cannot be larger than about 10% for $TiO_2$ photocatalyst.

# CHAPTER 3

# EXPERIMENTAL METHODS AND MATERIALS

## 3.1 Catalyst and Reagents

Commercially available $TiO_2$ P-25 from Degussa consisting of 70% anatase and 30% rutile, with a primary particle size of 30 nm, was employed throughout all experiments. Platinum solution ($H_2PtCl_6$) was obtained from Anglo Platinum in 20% HCl. Hydrochloric acid and ethanol (both from Saarchem) were of reagent grade and employed as received. Sodium hydroxide pellets (Saarchem) were employed to prepare a solution which was standardized by using borax. Deionised water produced by a Millipore Milli-Q Plus system was used for all experiments. Whatman no. 42 (Merck) ashless filter paper was used for the filtration of all sample solutions.

## 3.2 Photoreactors

### 3.2.1 Photocatalytic Batch Reactor

A 500 mL batch reactor was employed for the reduction of platinum(IV) chloride to platinum metal. A slurry type reactor was chosen with the catalyst particles suspended for its higher photocatalytic activity compared to that of immobilised photocatalyst reactors [12]. The reactor was vigorously stirred with a magnetic stirrer while water was recirculated through a water jacket on the outside of the reactor to achieve accurate temperature control. The water temperature was adjusted by a water-recirculating temperature control unit from Julabo. A 9 W germicidal UV lamp from Philips was employed as energy source. A schematic representation of the batch reactor can be seen in Figure 6 and a photograph is shown in Figure 7.

This reactor configuration was chosen in order to calculate the reaction rates and to investigate the influence of all parameters with the suspension exposed to the UV light for the entire duration of the experiment. In order to achieve this, the germicidal UV light had to be immersed in the slurry. A glass cover was chosen to protect the electrical components from the slurry. Initially perspex glass was used as a cover, but since perspex glass absorbs light within the visible and ultraviolet range, it was replaced with a quartz cover to successfully reduce platinum(IV) chloride. The reactor was covered with reflective foil and black tape in order to prevent loss of light from the UV light source as well as to eliminate reduction by sunlight.

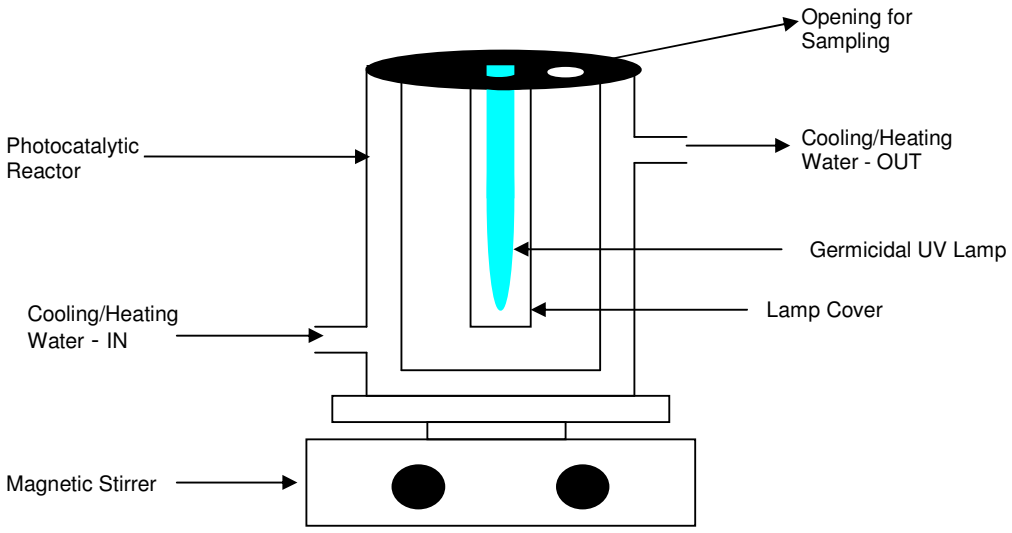


**Figure 6** Schematic representation of the photocatalytic batch reactor with immersed UV light and water jacket

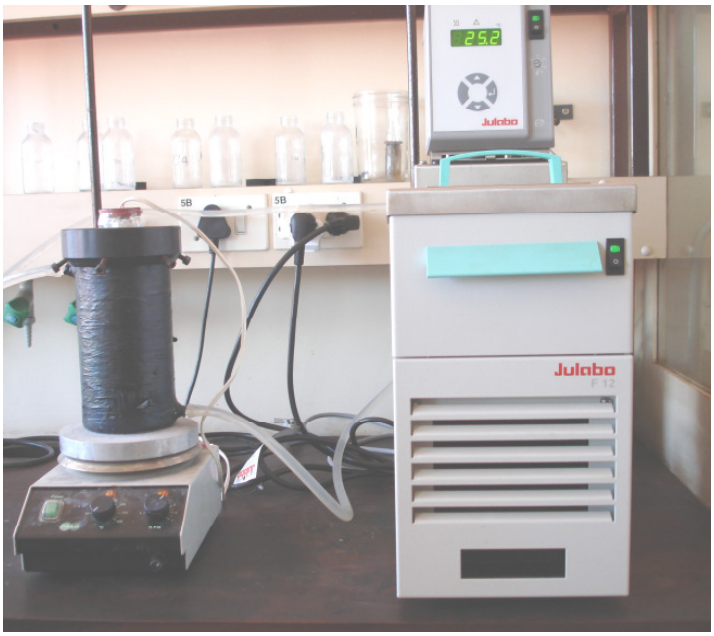


**Figure 7** Photograph of the photocatalytic batch reactor system with connected recirculating temperature control unit

### 3.2.2 Photocatalytic Flow Reactor

The flow reactor system used was similar to that used by Angelidis et al. and Kriek [16, 20, 27], except that a water jacket was added to the reservoir for accurate temperature control. The platinum(IV) chloride slurry was recirculated through the system at a rate of 500 mL/min using a peristaltic pump. The slurry was kept in suspension in the 500 mL reservoir by stirring vigorously with a magnetic stirrer. The 15 W (Philips) germicidal lamp was kept in place within a glass cylinder and sealed off at the ends by employing O-rings. The reactor had a volume of 91.6 mL and each differential volume of the slurry was exposed for approximately 9.5 seconds to the light source (assuming that perfectly mixed conditions were achieved in the reservoir). This reactor was also covered with foil and black tape to eliminate loss of light from the UV light source as well as to prevent reduction by sunlight. The schematic representation of the recirculating flow reactor setup is shown in Figure 8 and a photograph is given in Figure 9.

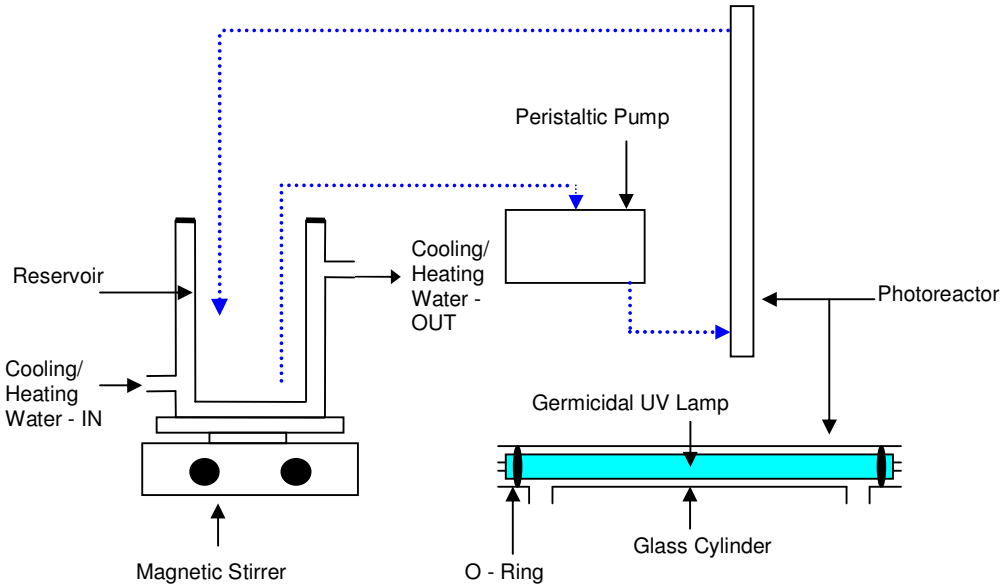


**Figure 8** Schematic representation of the photocatalytic flow reactor with the dotted line indicating the recirculating slurry


**Figure 9** Photograph of the photocatalytic flow reactor system with temperature control unit and peristaltic pump

## 3.3 Operating Conditions and Procedure

Numerous experiments were conducted for the kinetic investigation of initial reduction rates of platinum(IV) at various conditions. Three different sampling sequences were investigated. Sampling intervals were chosen as 0, 3, 5, 10, 20, 30, 40 and 60 minutes, respectively, where sampling was concentrated at the beginning of the 60 minute reaction time in order to determine initial reaction rates and calculate Langmuir-Hinshelwood constants at various experimental conditions. Sampling intervals were also chosen as 0, 20, 30, 33, 36, 39, 42, 45, 50 and 60 minutes respectively, with sampling concentrated in the middle of the 60 minute reaction time. Evenly distributed sampling was also investigated with sampling intervals of 0, 5, 10, 15, 20, 25, 30, 35, 40 and 50 minutes, respectively.

Since a number of parameters were investigated and both flow and batch reactor were employed, Langmuir-Hinshelwood constants were only determined when the influence of initial platinum(IV) concentration and initial ethanol concentration on $R_i$ were investigated. Langmuir-Hinshelwood kinetics was not applied to reactions where catalyst concentration, pH, temperature and light intensity were investigated..

During the study average reaction rates ($R_a$) were also determined and the influence each parameter had on $R_a$.

Reactions were carried out at various initial platinum(IV) concentrations. These concentrations were obtained by diluting the platinum solution received from Anglo Platinum. The dilution was done with HCl and deionised water such that a 1 M HCl concentration was maintained in 500 mL. The HCl was added first in order to prevent hydrolysis of the platinum. If the platinum (IV) solution were to be hydrolysed, the solution would turn from light yellow to brown and photocatalytic reduction would not be possible. The sacrificial reducing agent, ethanol, was then added. Sodium hydroxide was added to adjust the pH. The pH was measured with a Metrohm pH meter before the addition of the $TiO_2$ catalyst. After the desired pH was obtained, the catalyst was added. The slurry was stirred for two to five minutes to ensure complete mixing and a homogeneous suspension, before turning on the 9 watt germicidal UV lamp (batch reactor). For the recirculating flow reactor, the slurry was recirculated at a rate of 500 mL/min using a peristaltic pump from YASKAWA for 2 minutes before turning on the 15 watt germicidal UV lamp. The total reaction time

was 60 minutes, during which 10 mL samples were taken at specified time intervals. Each 10 mL sample taken was filtered twice to ensure that all the fine catalyst particles were removed.

Three baseline experiments were run with no $TiO_2$, no UV light and no ethanol. The effect light intensity has on the reduction of the platinum(IV) chloride solution was investigated in the recirculating flow reactor. The UV light source was covered by black film and taped with black tape to absorb the UV light. The 15 W lamp was used either uncovered or with 25%, 50% or 75% of its surface area covered.

Experimental conditions investigated can be seen in Table 3 – 5.

**Table 3** Experimental matrix with sampling at 0, 3, 5, 10, 20, 30, 40 and 60 minutes, employing the photocatalytic flow reactor

| **$[PtCl_6^{2-}]$ (ppm)** | **$[C_2H_5OH]$ ($g.L^{-1}$)** | **$[TiO_2]$ ($g.L^{-1}$)** | **Light intensity (W)** |
|---|---|---|---|
| 20;40;60;80 | 6 | 2 | 15 |
| 20;40;60;80 | 3 | 2 | 15 |
| 20;40;60;80 | 12 | 2 | 15 |
| 20;40;60;80 | 6 | 1 | 15 |
| 20;40;60;80 | 6 | 4 | 15 |
| 20;40;60;80 | 3 | 1 | 15 |
| 20;40;60;80 | 3 | 4 | 15 |
| 20;40;60;80 | 12 | 1 | 15 |
| 20;40;60;80 | 12 | 4 | 15 |
| 20;40;60;80 | 6 | 2 | 3.75 |
| 20;40;60;80 | 6 | 2 | 7.5 |
| 20;40;60;80 | 6 | 2 | 11.25 |

***All reactions were carried out at a constant pH of 3.0 and temperature of 25 ˚C**

**Table 4** Experimental conditions with sampling at 0, 20, 30, 33, 36, 39, 42, 45, 50 and 60 minutes for flow and batch reactor

| **$[PtCl_6^{2-}]$ (ppm)** | **$[C_2H_5OH]$ ($g.L^{-1}$)** | **$[TiO_2]$ ($g.L^{-1}$)** | **Light intensity (W)** |
|---|---|---|---|
| 15, 25, 50, 75, 100, 120 | 6 | 2 | 15 (Flow)<br>9 (Batch) |
| 25, 50, 75, 100 | 0, 3, 6, 8, 11 | 2 | 15 (Flow)<br>9 (Batch) |
| 50 | 6 | 0, 2, 3, 4 | 15 (Flow)<br>9 (Batch) |
| 50 | 6 | 2 | 0, 3.75, 7.5, 11.25 & 15 (Only Flow) |

***All reactions were carried out at a constant pH of 3.0 and temperature of 25 ˚C**

**Table 5** Experimental conditions with sampling at 0, 5, 10, 15, 20, 25, 30, 35, 40 and 50 minutes for batch and flow reactor

| **$[PtCl_6^{2-}]$ (ppm)** | **$[C_2H_5OH]$ ($g.L^{-1}$)** | **$[TiO_2]$ ($g.L^{-1}$)** | **pH** | **Temperature (˚C)** | **Light intensity (W)** |
|---|---|---|---|---|---|
| 50 | 6 | 2 | 1.5, 3.0, 4.5, 6.0 | 25 | 15 (Flow)<br>9 (Batch) |
| 100 | 12 | 2 | 3 | 12.5, 25, 50, 75 | 15 (Flow)<br>9 (Batch) |

## 3.4 Analysis

### 3.4.1 Inductively Coupled Plasma Analysis

An Inductively Coupled Plasma (ICP) spectrometer was used to follow the reduction of platinum in solution. For sampling interval 0, 3, 5, 10, 20, 30, 40 and 60 minutes, ICP analysis was conducted at the university. The ICP instrument was calibrated using prepared standards, having concentrations of 0, 5, 15, 25, 50, 75, 100 ppm

platinum(II) chloride. The standards matrix was similar to that of the actual samples with regard to the platinum, ethanol and hydrochloric acid concentrations as to ensure accurate results.

Due to some technical difficulties with experimental runs for sampling intervals 0, 20, 30, 33, 36, 39, 42, 45, 50 and 60 minutes as well as 15, 20, 25, 30, 35, 40 and 50 minutes, ICP analysis was conducted by an independent company employing an Inductively Coupled Plasma – Mass Spectrometer (ICP-MS). The main practical difference between the ICP and the ICP-MS is that for the ICP-MS the samples had to be diluted prior to being analysed. The prepared samples were sent within the same week as being collected and the results were received three to four weeks later.

### 3.4.2 Nuclear Magnetic Resonance Spectrometry

Nuclear Magnetic Resonance (NMR) was utilised to determine whether any ethanol was left at the end of the 50 and 60 minute experiments. This was investigated to determine whether or not any reaction would take place after this time period or whether the reaction time should be increased, especially for experiments conducted at high initial platinum(IV) concentrations.

A reference sample was prepared with 12 g/L ethanol. Phenol of equivalent molar concentration was added to the ethanol. The conditions of the reference sample was similar to that of an actual sample exposed to photocatalytic reduction, with 1 M HCl, 100 ppm platinum(IV) chloride and a pH of 3. Two platinum(IV) sample solutions (of high initial platinum(IV) concentrations) obtained at 50 min and 60 min, respectively, were analysed. The same amount of phenol was added to the actual samples as to the reference sample. Both the reference and two samples were diluted 1:10 with $D_2O$ prior to analysis.

The two samples were analysed to determine the actual concentration of the ethanol present with respect to the reference sample. From the NMR graphs, peaks were obtained for phenol, ethanol and water. Since the phenol was constant in both the reference and actual samples a relationship could be obtained from the integral calculated over the phenol peak as well as the integral formed over the ethanol peak.

With the ethanol concentration known in the reference sample, the remaining ethanol could be calculated in the actual samples.

# CHAPTER 4

# RESULTS AND DISCUSSION

The reduction of platinum(IV) solution could be visually observed over time as the slurry turned from pure white to various shades of grey depending on the extent of reduction. Figure 10a indicates the colour of the pure $TiO_2$ powder and Figure 10b shows the catalyst after complete reduction of platinum(IV) was achieved.

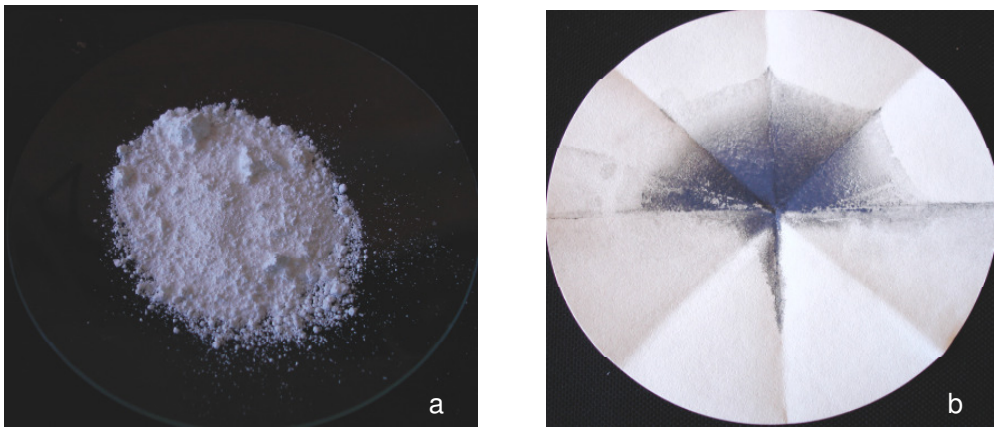


**Figure 10 a)** Pure white $TiO_2$ powder and **b)** $TiO_2$ powder containing reduced Pt metal

The reduction in platinum(IV) was followed by ICP-MS. Initial concentrations were calculated, but the actual concentrations read by ICP-MS indicated some severe discrepancies from intended initial concentrations. The inconsistency can be due to various experimental errors in the dilution process required for the ICP-MS, since both the provided standards as well as the samples had to be diluted prior to analysis. This inconsistency made it (visually) difficult to compare results. For this reason some concentration data were plotted as normalised concentrations ($C/C_i$). However, for calculation of all reaction rates, rate constants and adsorption equilibrium constants, actual concentrations (as read by the ICP-MS) were used.

## 4.1 Induction Period

Experiments for the photocatalytic reduction of Pt(IV) were conducted and Langmuir-Hinshelwood kinetics was employed for the determination of the reduction rate. The Langmuir-Hinshelwood kinetics yields both the reaction rate constant $k_r$ as well as the adsorption equilibrium constant $K_e$. To determine these constants the initial reduction rate had to be plotted against the initial platinum(IV) concentration (see Equation 22). The initial reduction rate can be obtained from the first couple of data points showing the change in platinum(IV) concentration over time. This should be calculated by fitting a straight line through the first 20 min of each experimental run. The change in platinum(IV) concentration in solution was determined by ICP-MS analysis.

Experiments were conducted with sampling intervals of 0, 3, 5, 10, 20, 30, 40 and 60 minutes, respectively. Langmuir-Hinshelwood kinetics is only useful when a series of experimental runs are carried out at various initial platinum(IV) concentrations during which all other parameters are kept constant. Experiments were conducted with the recirculating flow reactor. The proposed experimental matrix is indicated in Table 3.

A first set of experiments was conducted. Initial platinum(IV) concentrations of 15 ppm, 20 ppm, 40 ppm, 60 ppm, 80 ppm and 100 ppm were evaluated. Figure 11 indicates the results obtained for the following conditions:

$[TiO_2]$ = 2 g/L;
ethanol = 6 g/L;
pH = 3;
temperature = 25˚C;
light intensity = 15 W.

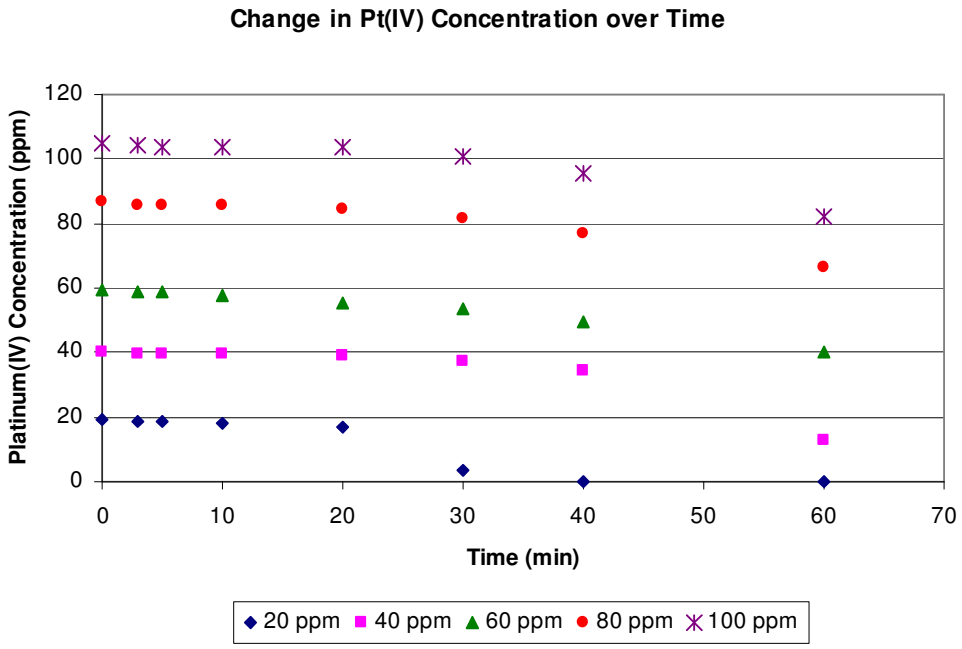


**Figure 11** Reduction of various Pt(IV) concentrations over time

Normalised Pt(IV) concentrations ($C/C_i$) were plotted in Figure 12 to aid in the visual interpretation of the results obtained.

The results show a distinct induction period exist during which very little Pt(IV) is reduced, and that the initial reaction rate should be determined over the initial data points following the induction period as shown by the solid lines in Figure 13. More normalised graphs indicating the induction period over various operating conditions can be seen in Appendix A.

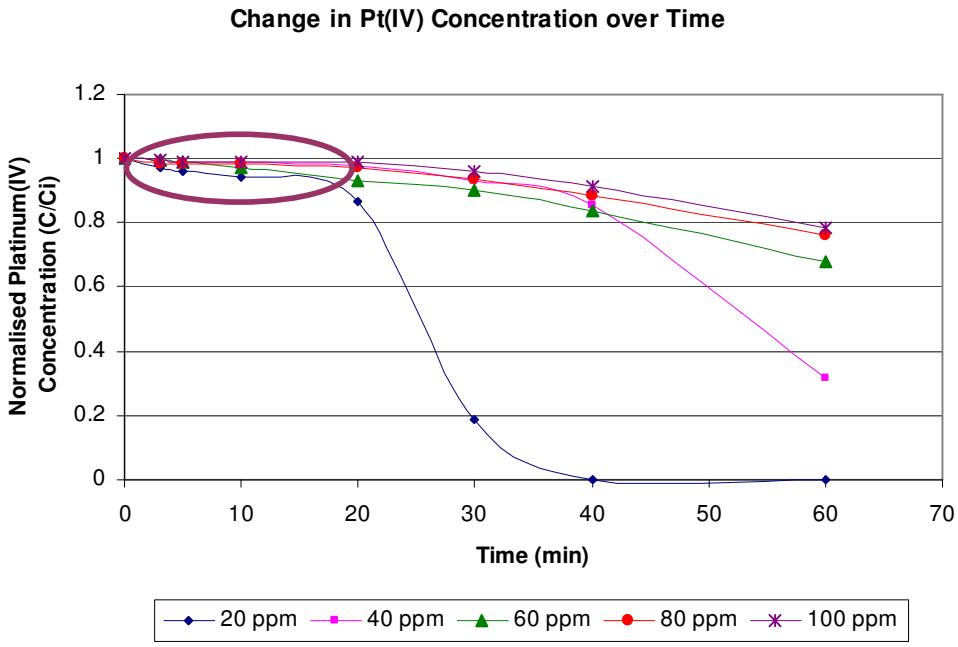


**Figure 12** Reduction of Pt(IV) indicating an induction period for the first 20 minutes

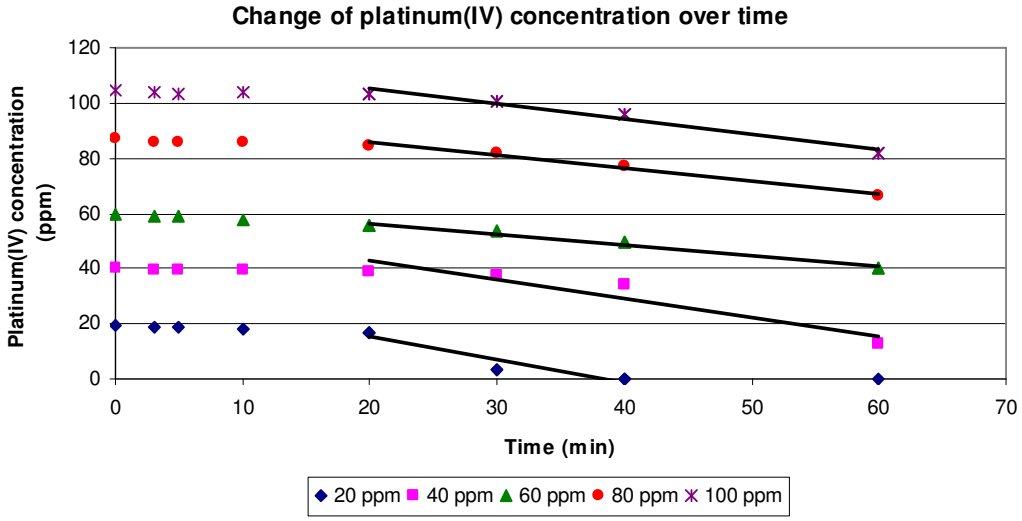


**Figure 13** Indication of the initial reduction of Pt(IV) after the induction period

An important question is what the reason for the induction period is. In the following paragraph a plausible explanation is given.

Initially reduction is slow, because an initial percentage of Pt metal should be present on the catalyst surface. Platinum metal stabilises the excited electron, generated when the photocatalyst is activated, by trapping the electron in the conduction band (cb) and moving it to the surface of the adsorbed platinum (Figure 14). When platinum islands are deposited on the surface of the $TiO_2$ particle, a Schottky barrier ($\Phi_b$) is formed between the $TiO_2$ and metal particles that acts as sufficient electron traps which decreases the $e^-/h^+$ recombination rate. This explanation is supported by work done by Siemon *et al*. [51], who compared the photocatalytic activity of $TiO_2$ and $Pt/TiO_2$ for the oxidation of EDTA and the reduction of Cr(VI) to investigate the essential presence of platinum metal on the surface. Both the EDTA oxidation rate and the Cr(VI) reduction rate is increased in the case of platinised $TiO_2$. Stabilisation of the electron not only limits the recombination of the electron/hole pair, but also makes the electron on the surface more readily available for reduction [10, 52]. This improves the photocatalytic activity of the catalyst, and increased reduction rates are observed until one of the other critical parameters is exhausted.

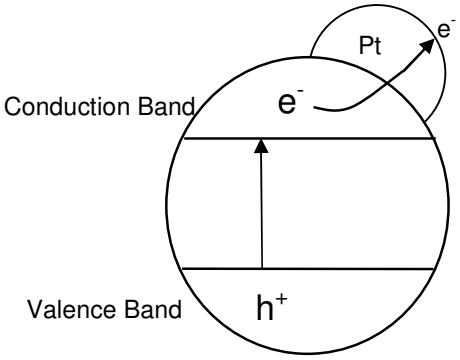


**Figure 14** Schematic representation of stabilisation of generated electrons through metal deposition on $TiO_2$

Due to the existence of an induction period the sampling intervals were adapted for all experiments. In addition to the initial sample at 0 minutes, samples were only taken after 20 minutes (average duration of induction period). All parameters were to

be evaluated with data taken at 0, 20, 30, 33, 36, 39, 42, 45, 50 and 60 minutes respectively, unless otherwise specified.

According to Langmuir-Hinshelwood kinetics, the initial reaction rate has to be determined over those data points where initial reduction takes place. The initial reaction rate was therefore calculated after the induction period to determine the Langmuir-Hinshelwood constants as well as to determine the influence each of the parameters investigated had on the initial reaction rate.

## 4.2 Influence of Initial Platinum(IV) Concentration

Experiments were conducted on both the recirculating flow reactor and the photocatalytic batch reactor. In order to determine the effect that the initial platinum(IV) chloride concentration has on the overall reduction rate, six experimental runs were carried out at initial concentrations of 15, 25, 50, 75, 100 and 120 ppm, respectively. For all of these reactions the other parameters were kept constant at:

Ethanol = 6 g/L;
$TiO_2$ = 2 g/L;
pH = 3;
temperature = 25 ˚C;
light Intensity = 15 W (flow reactor) and 9 W (batch reactor).

The reduction profile of platinum(IV) can be seen in Figure 15 for the recirculating flow reactor and in Figure 16 for the batch reactor. The lines on the graphs indicate the time interval over which initial reaction rates were calculated, using Equation 36.

$$R_i = -\frac{C_2 - C_1}{t_2 - t_1} \tag{36}$$

For both reactors reduction can be clearly seen for all initial values of platinum(IV) chloride concentrations. It should be noted that for the high initial concentrations not all the platinum(IV) was fully reduced within the 60 minute interval of irradiation.

Even running experiments for additional time did not fully reduce the high initial platinum(IV) concentrations. The explanation for this is given in Section 4.3.

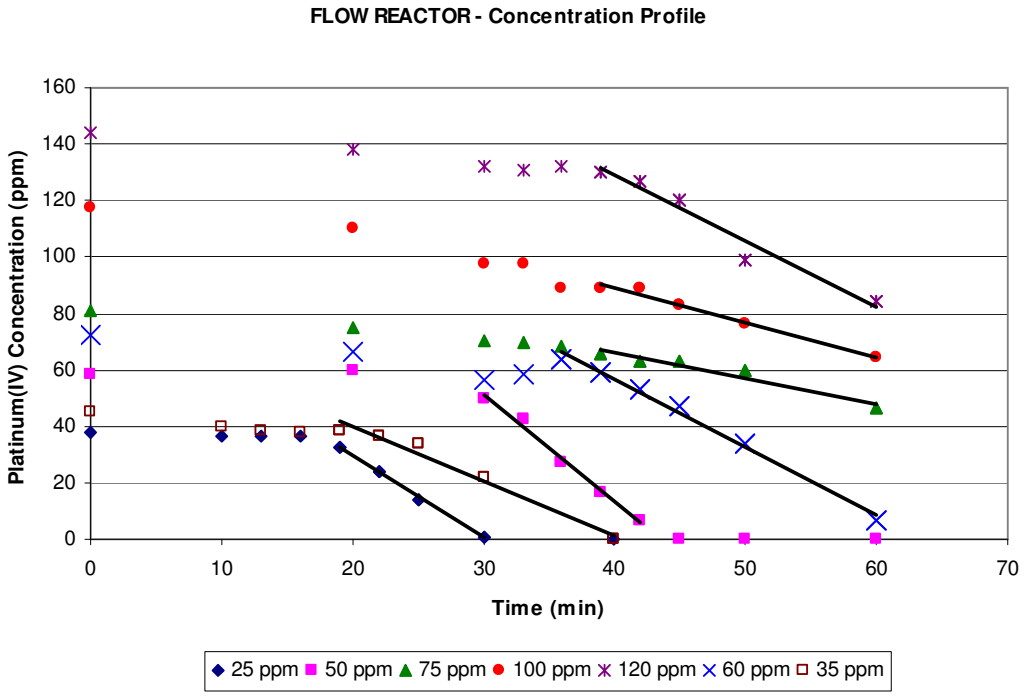


**Figure 15** Photocatalytic reduction of Pt(IV) in the re-circulating flow reactor

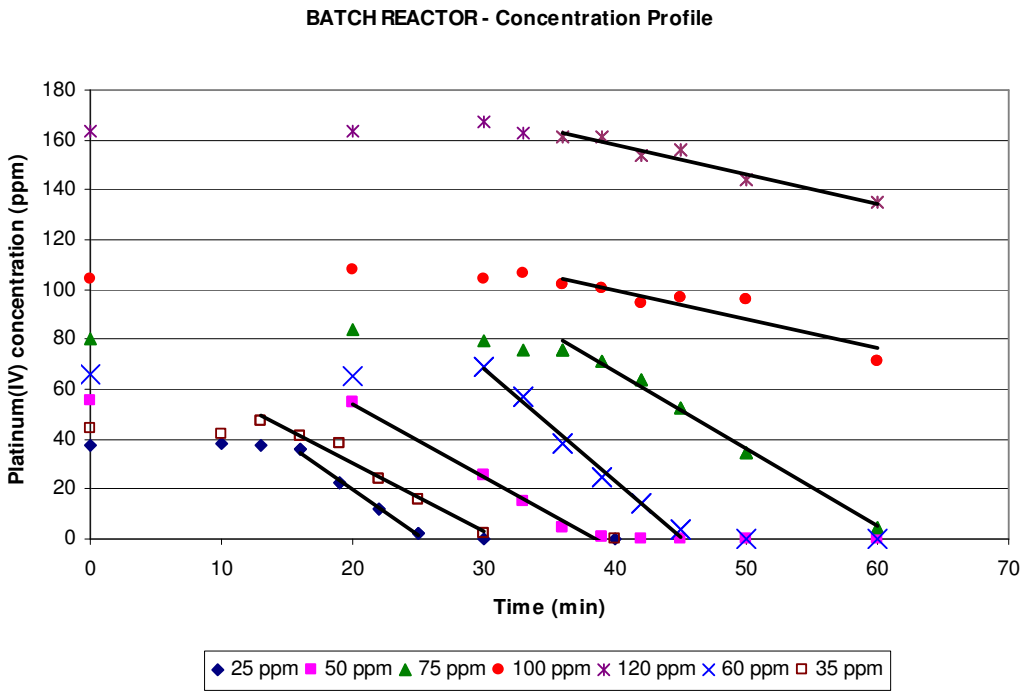


**Figure 16** Photocatalytic reduction of Pt(IV) in a batch reactor

The initial reaction rate for each of the individual platinum(IV) concentrations was determined and the inverse plotted against the inverse of the initial concentrations.

It can be seen from Figure 17 that the reaction rate is independent of the initial platinum(IV) concentration even though not all concentrations were fully reduced as mentioned previously. The reaction is zero-order with regard to the initial platinum(IV) concentration.

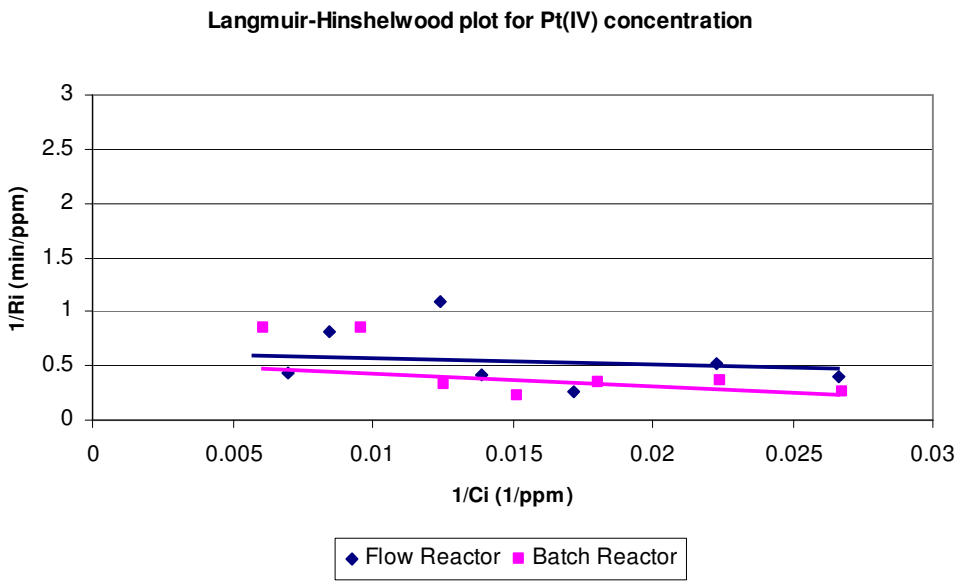


**Figure 17** Relationship between $R_i$ and initial platinum(IV) concentration

## 4.3 Influence of Sacrificial Reducing Agent Concentration

Without the presence of a SRA the recombination of the electron-hole pair would occur within nanoseconds and minimal photocatalytic activity would be possible. In this study ethanol was used as SRA. A baseline experiment was conducted with no ethanol in which it was observed that no reduction of the platinum(IV) took place.

To study the effect of the initial SRA concentration on the reaction rate as well as its effect on the Langmuir-Hinshelwood constants, experiments were conducted with 3, 6, 8 and 11 g/L of ethanol for each of four platinum(IV) chloride concentrations (25, 50, 75, and 100 ppm). For these reactions all other parameters were kept constant at:

$[TiO_2]$ = 2 g/L;
pH = 3;
temperature = 25 ˚C;
light intensity = 15 W (flow) and 9 W (batch).

The reduction of platinum(IV) was plotted against time using normalised Pt(IV) concentrations ($C/C_i$) to aid in the visual interpretation of the reduction trends. Figure 18 (flow reactor) and Figure 19 (batch reactor) clearly indicate that for high ethanol concentrations all platinum(IV) was reduced even at very high initial platinum(IV) concentrations. Reduction graphs for 3, 6 and 8 g/L ethanol can be found in Appendix B.

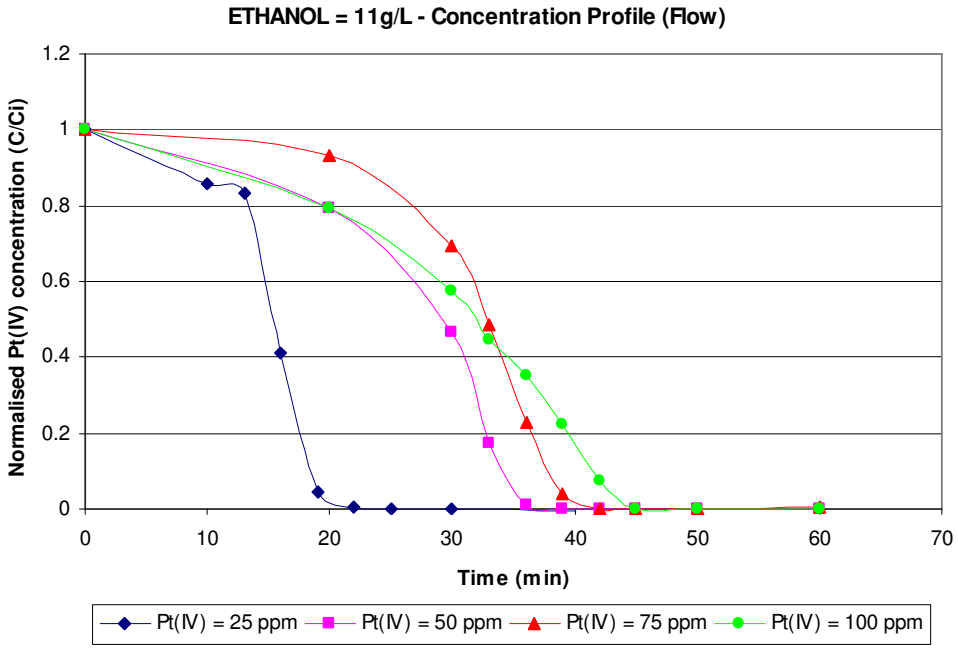


**Figure 18** Reduction profile for the recirculating flow reactor at 11 g/L ethanol

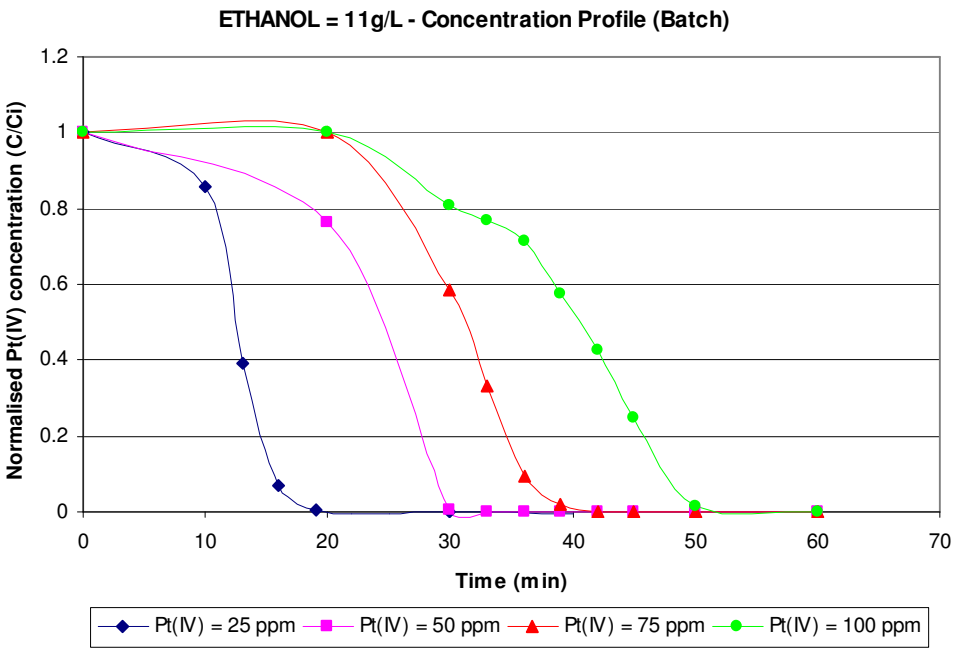


**Figure 19** Reduction profile for the batch reactor at 11 g/L ethanol

The initial reduction rate was determined, as before, by calculating the change in platinum(IV) concentration over time at the end of the induction period for each of the ethanol concentrations. The Langmuir-Hinshelwood graph was plotted for each ethanol concentration. Figure 20 indicates the Langmuir-Hinshelwood graph for 11 g/L ethanol as a representative example. Again the graphs for 3, 6 and 8 g/L ethanol can be seen in Appendix B. Figure 20 confirms that the data fit the Langmuir-Hinshelwood theory fairly well, and the values of the different constants of this theory are presented in Table 6.

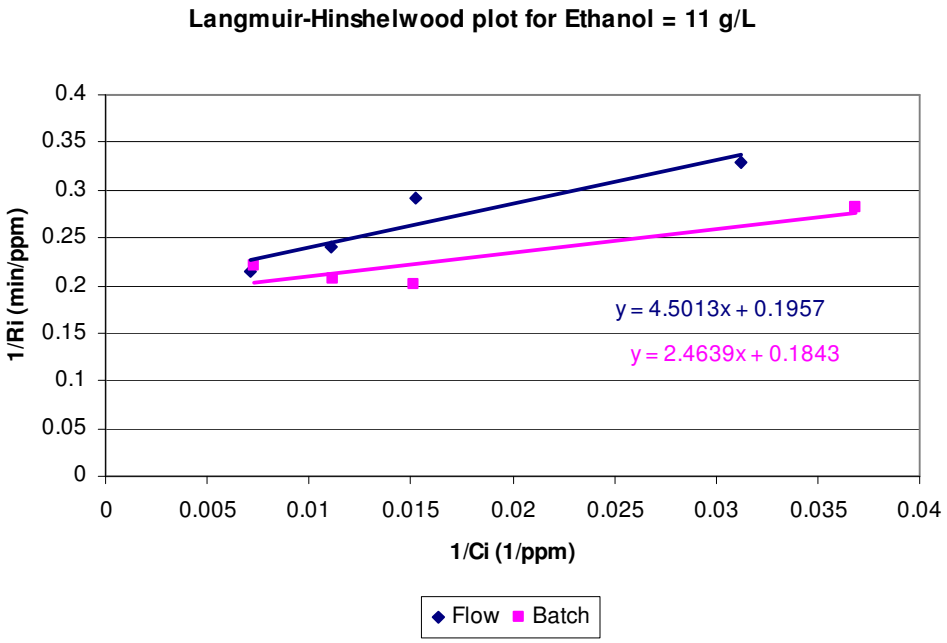


**Figure 20** Relationship between the reaction rate and initial Pt(IV) concentration

**Table 6** Determined Langmuir-Hinshelwood rate and equilibrium constants

| **Initial Ethanol Concentration (g/L)** | **$k_r$ (ppm/min)** | | **$K_e$ (1/ppm)** | |
|---|---|---|---|---|
| | **Batch** | **Flow** | **Batch** | **Flow** |
| 3 | 0.300 | 0.304 | -0.029 | -0.044 |
| 6 | 1.20 | 0.756 | -0.035 | -0.032 |
| 8 | 2.47 | 2.27 | -0.050 | -0.053 |
| 11 | 5.43 | 5.11 | 0.075 | 0.039 |

For all reactions at different ethanol concentrations it was observed (similar to Section 4.2) that the reduction process is independent of the platinum(IV) concentration, provided that there was sufficient (excess) ethanol present.

As noted before in Section 2.6.1, Murzin [41] stated that the $K_eC_i$ term becomes insignificant if a subset of data, under certain experimental conditions, is used. In this Section various ethanol concentrations were evaluated for four different platinum(IV) concentrations. It was found that the $K_e$ term is approximately zero

(either small positive of small negative), with regard to each set of ethanol concentrations investigated. In the event where there was sufficient ethanol present > 8 g/L all the platinum was reduced for all four initial platinum(IV) concentrations, but when there was insufficient ethanol present the reaction rate decreased for high platinum(IV) concentrations and therefore a negative $K_e$ term was observed.

Table 7 indicates the initial reaction rate for 50 ppm Pt(IV) as obtained from the reduction graphs as well as the calculated reaction rate using the Langmuir-Hinshelwood rate constants determined in Table 6. The results in Figure 21 (calculated) and Figure 22 (actual) clearly shows that a very strong linear dependency was obtained with regard to the initial ethanol concentration. It is clear that the reduction rate is directly dependent on the ethanol concentration and that the reaction is therefore first-order with regard to SRA concentration.

**Table 7** Actual initial reaction rate and calculated reaction rate for Pt(IV) = 50 ppm

| **Initial Ethanol Concentration (g/L)** | **$R_i$ (ppm/min) Actual at [Pt(IV)] ≈ 50 ppm** | | **$R$ (ppm/min) Calculated for [Pt(IV)] = 50 ppm** | |
|---|---|---|---|---|
| | **Batch** | **Flow** | **Batch** | **Flow** |
| 3 | 1.83 | 0.434 | 0.685 | 0.557 |
| 6 | 2.94 | 3.49 | 2.80 | 2.02 |
| 8 | 4.26 | 4.93 | 4.12 | 3.65 |
| 11 | 4.98 | 3.428 | 4.29 | 3.38 |

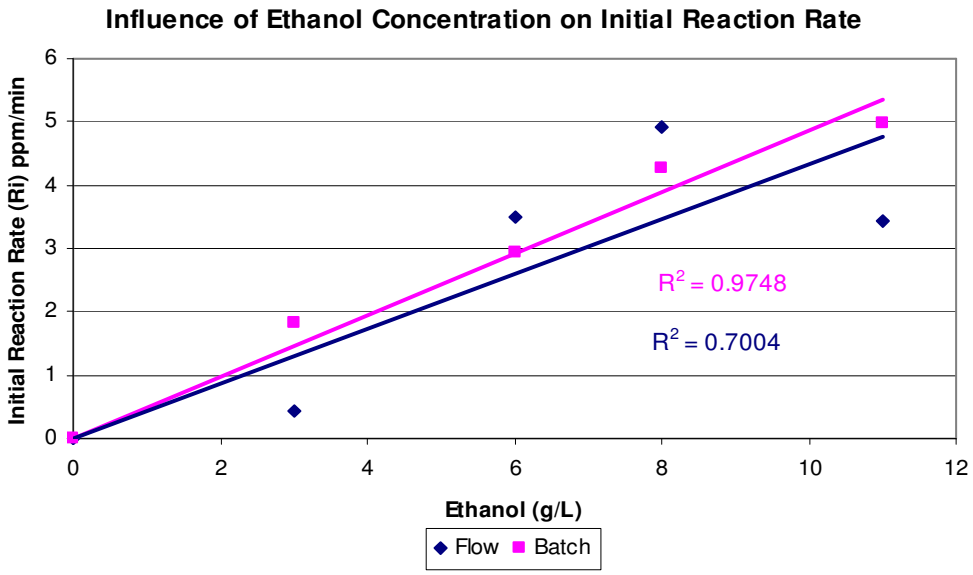


**Figure 21** Dependency of calculated reaction rates on initial ethanol concentration

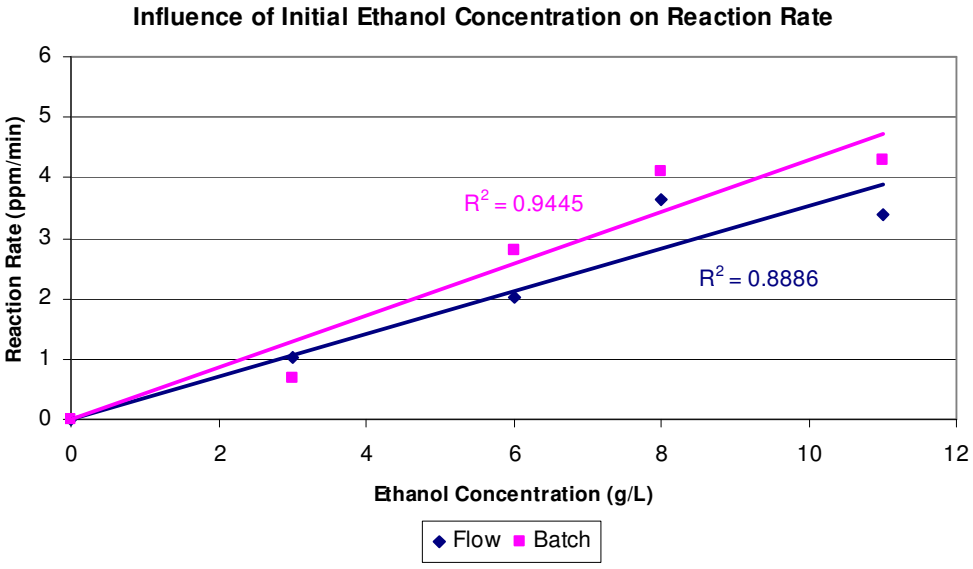


**Figure 22** Dependency of actual reaction rates on initial ethanol concentration

Similar to reaction rate, $R_i$, the strong linear dependence on initial ethanol concentration can also be demonstrated by utilising the Langmuir-Hinshelwood reduction rate constant $k_r$ as can be seen in Figure 23.

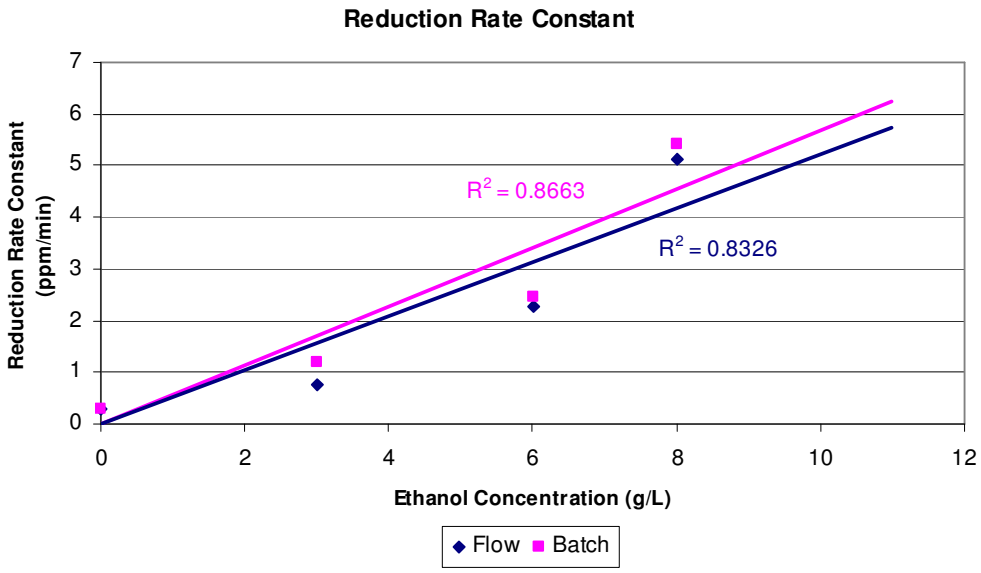


**Figure 23** Linear dependence of initial ethanol concentration on reduction rate constant

The fact that the rate is directly dependent on the ethanol concentration and that very little reduction is observed at low ethanol concentrations and high platinum concentrations, may explain what was observed in Section 4.2. When the influence of platinum(IV) concentration was tested, it was found that at even sufficient ethanol concentrations (6 g/L), the reduction rate slowed down after some time for high platinum concentrations as was seen in Figure 15 and 16. Very little or no reduction took place after 60 minutes for concentrations higher than 100 ppm.

In order to explain this phenomenon, nuclear magnetic resonance (NMR) spectra were taken of samples at time t = 50 minutes for the reactions with 6 g/L ethanol in order to determine the amount of ethanol still present at that time. It was clear from the results that at this point only 3 g/L of ethanol remained present in solution. This is similar to the amount of ethanol present for which little or no reduction took place

for high initial platinum(IV) concentrations, as can be seen in the reduction graphs for 3 g/L ethanol in Appendix B.

## 4.4 Effect of Catalyst concentration

In order to determine the influence the initial catalyst concentration has on the initial reaction rate, experiments were conducted with 0, 2, 3 and 4 g/L $TiO_2$, respectively. The other parameters were kept constant at:

$[PtCl_6^{2-}]$ = 50 ppm;
ethanol = 6 g/L;
temperature = 25˚C;
pH = 3;
light intensity = 15 W (flow) and 9 W (batch).

As previously mentioned, Langmuir-Hinshelwood kinetics was not used to evaluate the rate constant and equilibrium constant since this would require all experiments to be conducted at various platinum(IV) concentrations. This would have amounted to a vast number of experiments and therefore only the influence that the $TiO_2$ concentration had on the reaction rate was determined.

The reduction graphs (Appendix C) was used to determine the initial reduction rate as before. The initial reduction rate was then plotted against the respective $TiO_2$ concentrations. Figure 24 shows that there was a strong increase in the reduction rate with an increase in the catalyst concentration until it reached a concentration of 3 g/L, after which a steady decline in the reduction rate was observed. A very good correlation was observed between the batch and the re-circulating flow reactor, which confirmed the results obtained.

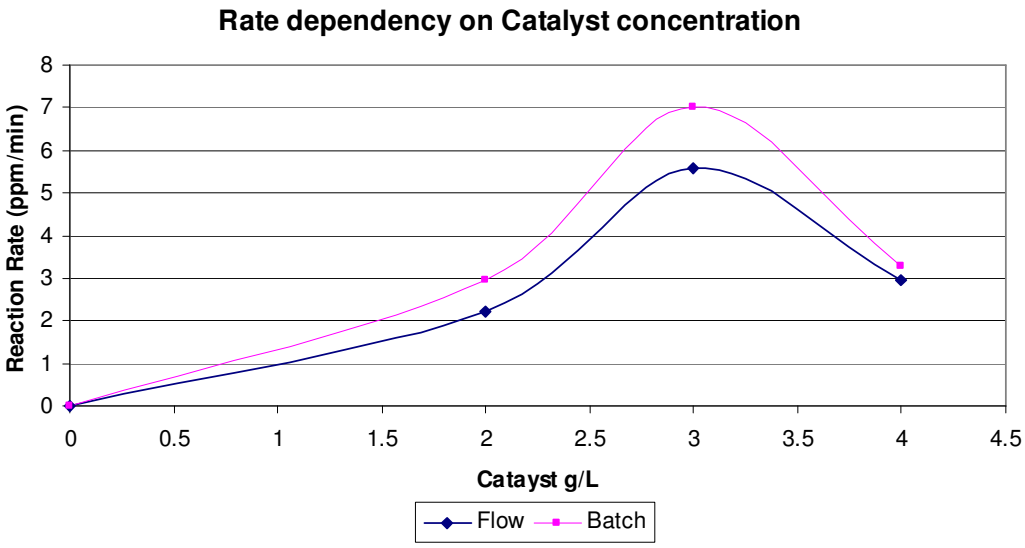


**Figure 24** Influence of the $TiO_2$ concentration on the initial reaction rate for the flow and batch reactor

Without any catalyst present no reduction occurred, since the activation of a catalyst by UV light is vital for photocatalytic processes as mentioned in Section 2.1. With the addition of $TiO_2$ reduction took place, and the more $TiO_2$ added the more particles were available for activation, and the reduction rate increased until a maximum was reached (3 g/L). After more than 3 g/L of $TiO_2$ was added, the reduction rate decreased. This observation was due to the fact that the $TiO_2$ slurry became very dense and the radius that the UV light could travel was limited (Figure 25). This meant that less light reached the catalyst particles and could be activated for reduction. Herrmann [8] stated that the critical limit of the catalyst depends on the reactor geometry and the working conditions of the photoreactor, in this study the critical value of 3 g/L was obtained for both the batch and flow reactor.

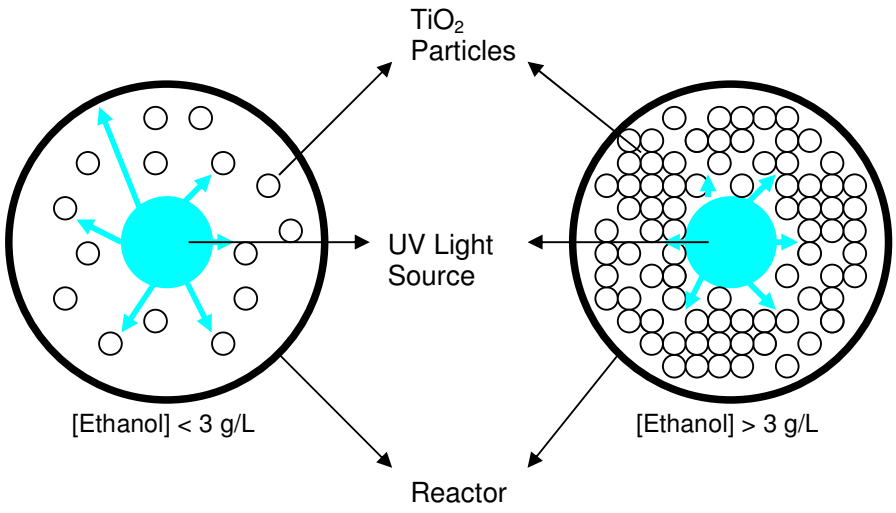


**Figure 25** Schematic representation of the path the UV light travels within a reactor at low and high catalyst concentrations

## 4.5 Effect of pH

In order to photoreduce a chemical species, the potential (V) of the conduction band for the semiconductor photocatalyst must be more negative than the reduction potential of the chemical species [6]. The energy level of the bottom of the conduction band is a measure of the reduction strength of the photogenerated electrons. The positions of both the conduction and valence bands are pH dependent. The increase of the pH in solution makes the positions of the valence band and conduction bands to shift to more cathodic potentials, at 25˚C, as per Equation 36 and 37.

$$E_{CB}(V) = -0.05 - 0.059\ \text{pH} \quad (36)$$

$$E_{VB}(V) = 3.15 - 0.059\ \text{pH} \quad (37)$$

The influence of pH on the initial reduction rate was determined for pH values of 1.5, 3.0, 4.0, and 5.5, respectively. The reduction of Pt(IV) concentration was plotted against time and the initial reaction rates determined. The reduction graphs can be

seen in Appendix D. These reduction graphs were then used to determine the initial reaction rate and were plotted against the corresponding pH value. The results can be seen in Figure 26.

The graph shows a type of S-curve, with minimal difference between the reaction rate and pH of 1.5 and 3.0 as well as 4.0 and 5.5, but a very strong increase in reaction rate between pH 3.0 and 4.0. These results are in accordance to what was observed by Kriek [16] when he studied the influence of pH as a means of selectively reducing Pt(IV), Rh(III) and Pd(II) species.

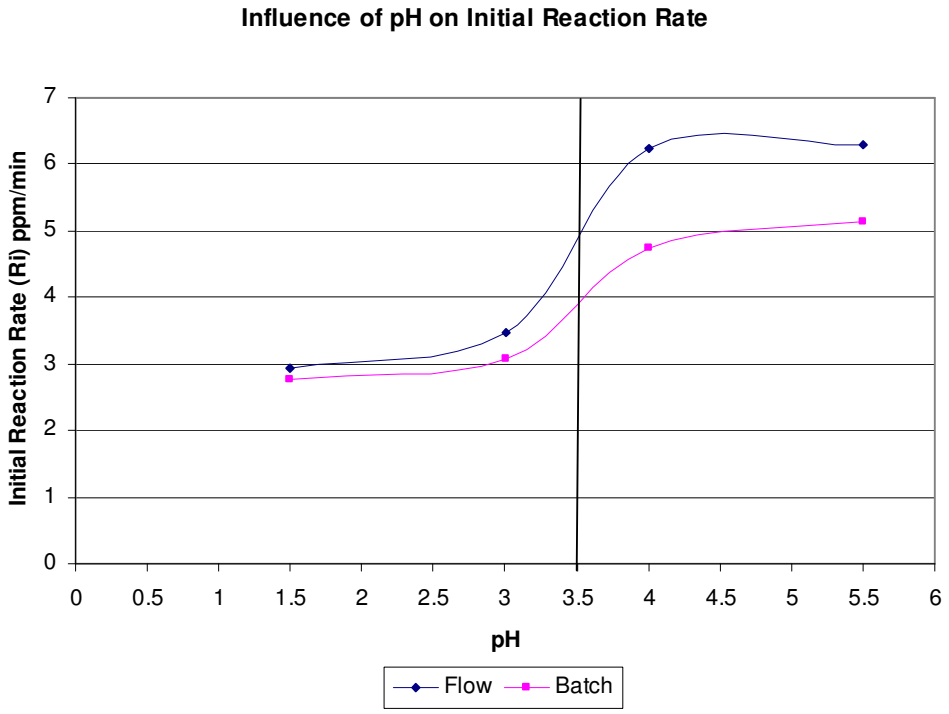


**Figure 26** Influence of the pH on the initial reaction rate in a flow and batch reactor

The dependence of the reduction rate on pH can be attributed to the modification of $TiO_2$ charge. The iso-electric point for $TiO_2$ Degussa P-25 is reported in literature to be between a pH of 6 and 7 [9, 53, 54]. The surface of $TiO_2$ will therefore be positively charged at pH lower than 6 and negatively charged at pH higher than 7 (Figure 29). Since the surface at pH 4 is more negatively charged than at pH 1.5 and the chloride ions are absorbed less on the catalyst surface (ethanol-chloride

adsorption competition) an increase in reduction rate was observed with an increase in pH.

From the graph the $pK_a$ value can be obtained, which is 3.5 for both the recirculating flow and the batch reactor. The larger the $pK_a$ value the smaller the extent of dissociation.

$$pK_a = - \log K_a \quad (35)$$

The $K_a$ value for the photocatalytic reduction of platinum(IV) is therefore $3.162 \times 10^{-4}$.

The $pK_a$ value of 3.5 obtained in Figure 26 also closely correlates to the pH value in Figure 27 where almost equal amounts of TiOH and $TiOH_2^+$ are present. This is the critical pH value for which lower pH values result in reduced reduction rates (more $TiOH_2^+$ present) and higher pH values result in improved reduction rates. When the pH value was studied over a wider range, as was done by Kriek [16], it was found that the reduction rate decreases again from pH values 7 to 12 and a $pK_b$ value of approximately 9.7 was obtained. The $pK_b$ value again closely relates to the critical pH value in Figure 27 where equal amounts of TiOH and $TiO^-$ are present. This led to the conclusion that the best photocatalytic reduction rate for platinum(IV) can be obtained at pH values for which the catalyst particles are neutral.

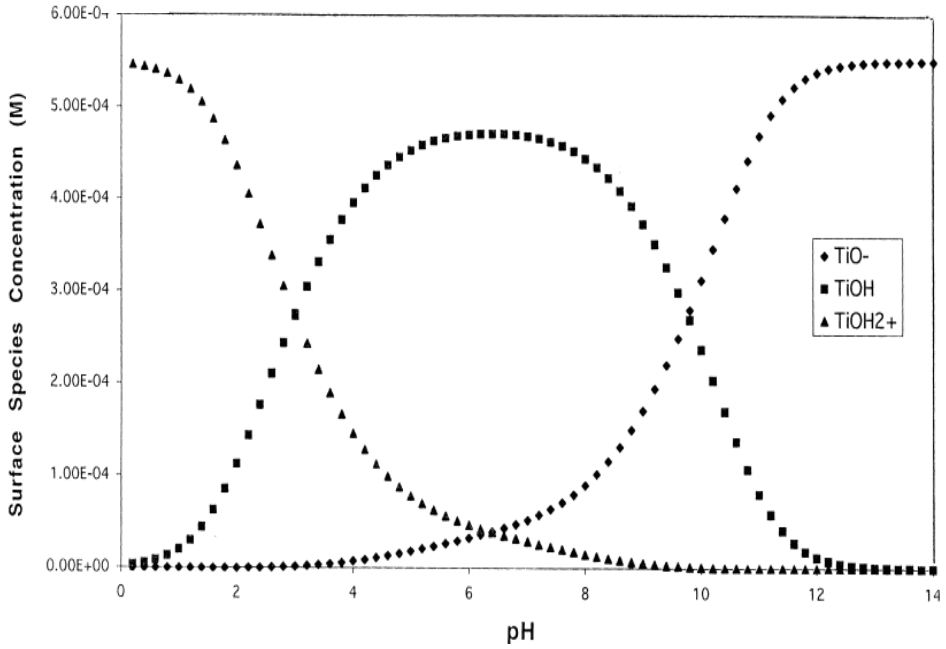


**Figure 27** $TiO_2$ Degussa P-25 speciation as a function of pH [54]

## 4.6 Effect of Temperature

The influence of temperature on the initial reaction rate was determined for temperatures 12.5, 25, 50 and 75˚C. Temperatures higher than 75˚C where not investigated as the boiling point of ethanol is at around 79˚C. As before, the Pt(IV) concentration graphs (Appendix D) was used to determine the initial reaction rates. The temperatures, in kelvin, were plotted against the obtained initial reaction rates in Figure 28. From the graph a linear dependency on the temperature was obtained with a slight tendency to stabilise or reduce at 75 ˚C. This observation might be due to the heating of the ethanol, where the ethanol (Section 4.2.2) was determined to be a critical rate controling parameter.

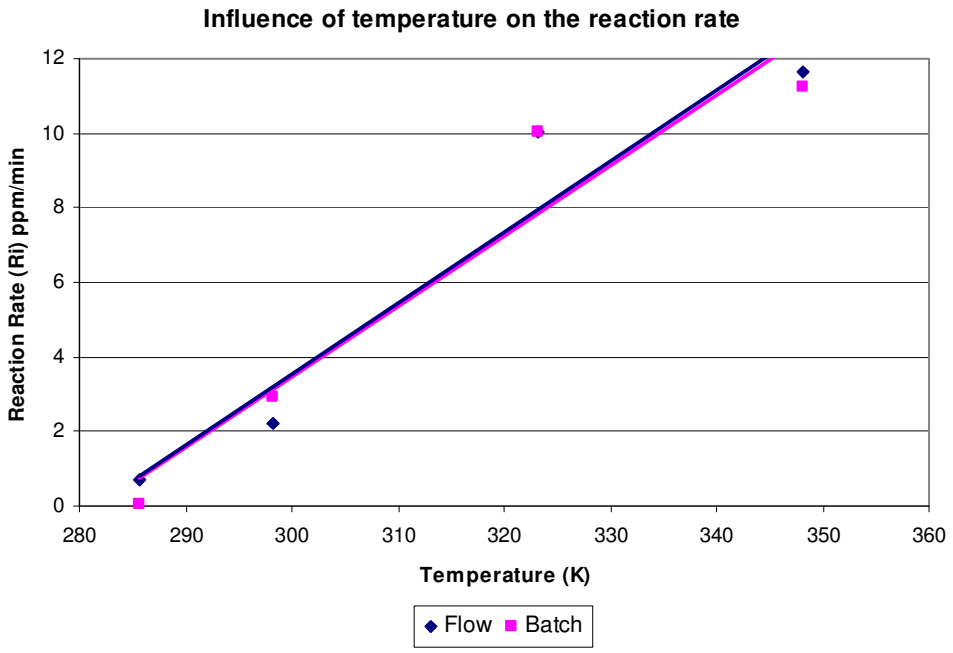


**Figure 28** Influence of the temperature on the initial reaction rate for the flow and batch reactor

Literature states that, because of photonic activation, the photocatalytic system does not require heating and operates at room temperature in most cases. The true activation energy, $E_t$, is nil, whereas the apparent activation energy $E_a$ is often very small (a few kJ/mol) in the medium temperature range (20˚C ≤ θ ≤ 80˚C). However, at very low temperatures (-40˚C ≤ θ ≤ 0˚C), the activity decreases and the apparent activation energy $E_a$ increases [8].

The Arrhenius equation for the determination of the activation energy is:

$$k(\mathrm{T}) = Ae^{\frac{-E_a}{RT}} \tag{38}$$

and

$$\ln k = \ln A - \frac{E_a}{R\mathrm{T}} \tag{39}$$

In Figure 29 ln $k$ is plotted against 1/T (K). From the graph it appeared that two regions existed for both the flow or batch reactor. The activation energy, $E_a$, was calculated for both regions and can be seen in Table 9. In both regions the activation

energy is low, especially in the lower temperature range. This supports the fact that very low activation energies are required for photocatalytic processes since the photocatalyst is generally light activated.

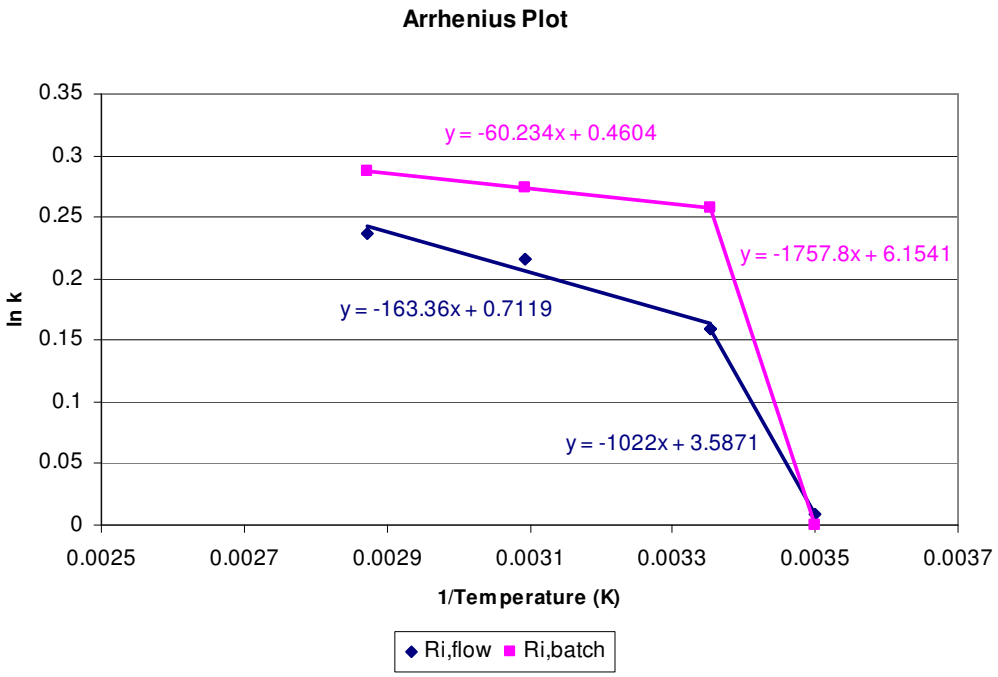


**Figure 29** Arrhenius plot for determining the activation energy

**Table 8** Activation energy for the photocatalytic reduction of platinum(IV)

| | **12.5 ˚C to 25 ˚C** | **25 ˚C to 75 ˚C** |
|---|---|---|
| Flow Reactor | 0.50 kJ/mol | 14.6 kJ/mol |
| Batch Reactor | 1.36 kJ/mol | 8.5 kJ/mol |

## 4.7 Effect of Light intensity

The influence of light intensity was determined for the photocatalytic recirculating flow reactor. This was achieved by covering parts of the reactor with black film and taping it with black tape to prevent percentages of UV light to be available for photo reduction. 0, 25, 50 and 75 % of the lamp surface was covered, respectively. An experiment was also conducted with no UV light present. Two sets of experiments were conducted at conditions indicated in Table 9.

**Table 9** Experimental conditions for determining the of influence light intensity on reaction rates

| **Experiment Set** | **Sampling Times (min)** | **Light Intensity (Watt)** | **Reaction Rate (ppm/min)** | **Constant Parameters** |
|---|---|---|---|---|
| **(1)** | 0, 3, 5, 10, 20, 30, 40, 60 | 0; 3.75; 7.5; 11.25; 15 | *$R_{a,1}$ | $[PtCl_6^{2-}]$ = 50 ppm; ethanol = 6 g/L; $[TiO_2]$ = 2 g/L; temperature = 25 ˚C; pH = 3. |
| **(2)** | 0, 20, 30, 33, 36, 39, 42, 45, 50, 60 | 0; 3.75; 7.5; 11.25; 15 | *$R_{a,2}$ $R_i$ | $[PtCl_6^{2-}]$ = 50 ppm; ethanol = 6 g/L; $[TiO_2]$ = 2 g/L; temperature = 25 ˚C; pH = 3. |

* Where $R_{a,1}$ is the average reduction rate for the first set of experiments and $R_{a,2}$ is the average reduction rate for the second set of experiments.

When no UV light was present, no reduction of the Pt(IV) took place and the $TiO_2$ remained pure white. At 100% of light (15 watt), complete reduction was achieved within 45 minutes. The reduction in Pt(IV) concentration, for both experimental sets, were plotted against time and can be seen in Appendix D. From the reduction graphs, reaction rate was determined and plotted against the light intensity calculated in W (e.g. 25% x 15 W = 3.75 W).

As seen in Figure 30 similar trends were observed with regard to all three reaction rates investigated ($R_i$, $R_{a,1}$ and $R_{a,2}$). Reaction rates increased very slowly initially (up to 7.5 watt) followed by rapid increases. It can also be seen from Figure 30 that initial reaction rates, $R_i$, are very similar to those for up to 75% UV light intensity, thereafter a more rapid increase was observed for initial reaction rates. This confirms that reduction over the first 20 minutes is very slow (induction period) and results in lower averages. After the induction period the reaction increases rapidly. With less light present to activate $TiO_2$ catalyst, the reduction rate seems to experience an extended induction period with very little reduction taking place.

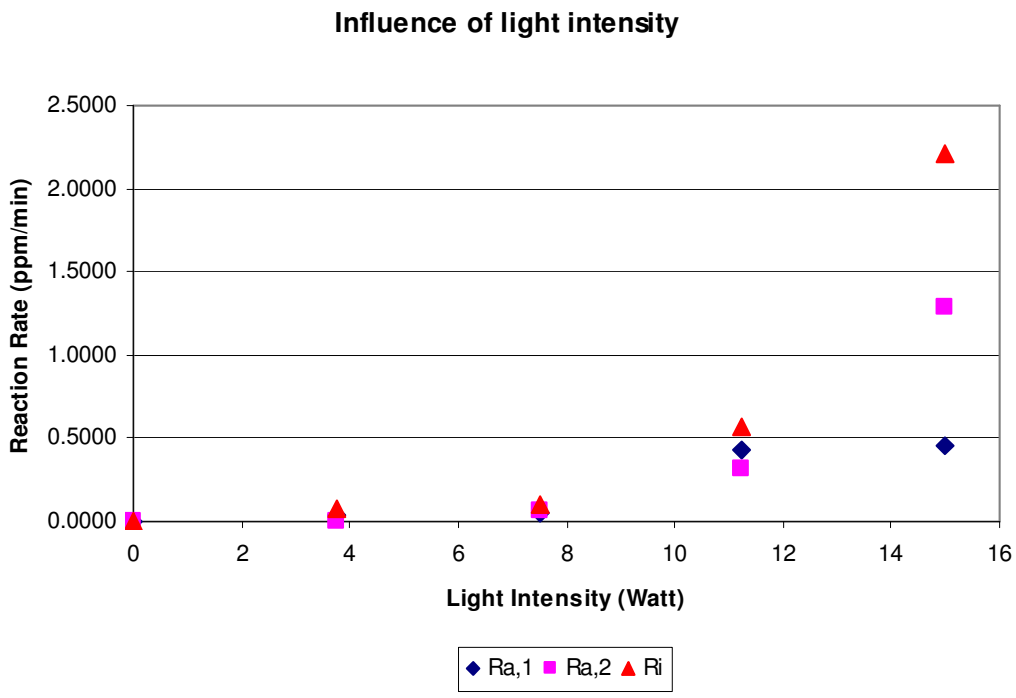


**Figure 30** Influence of light intensity on reaction rates for the photocatalytic flow reactor

These results are not completely in line with the expectation that there would be a linear increase in reduction with increase in intensity. When each of the reaction rates ($R_{a,1}$, $R_{a,2}$, $R_i$) were individually plotted against the light intensity, Figure 31 - 33, it could be seen that average reaction rates best fitted a linear profile.

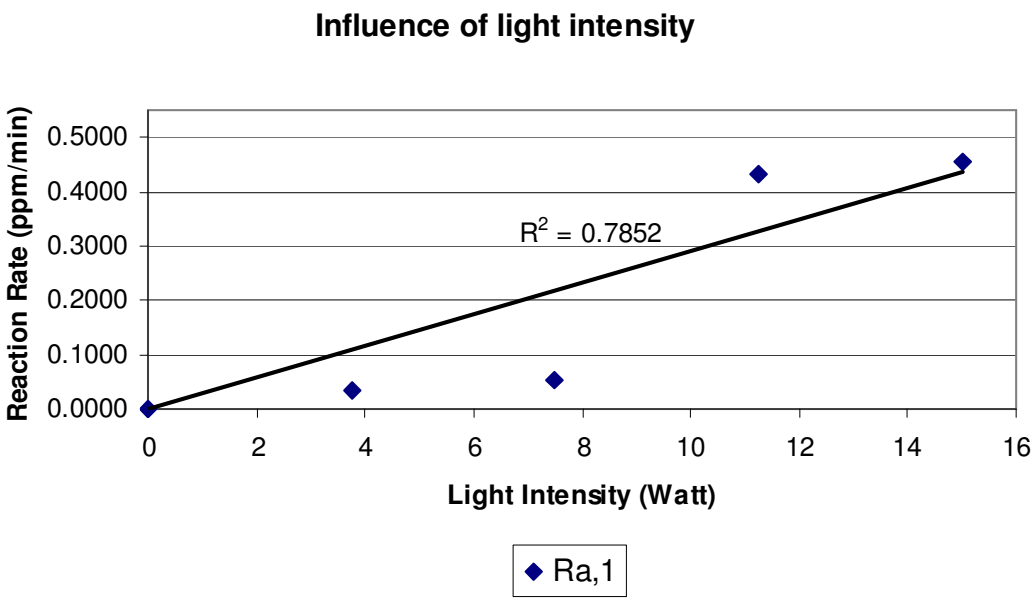


**Figure 31** Influence of light intensity on average reaction rates for the first set of experiments

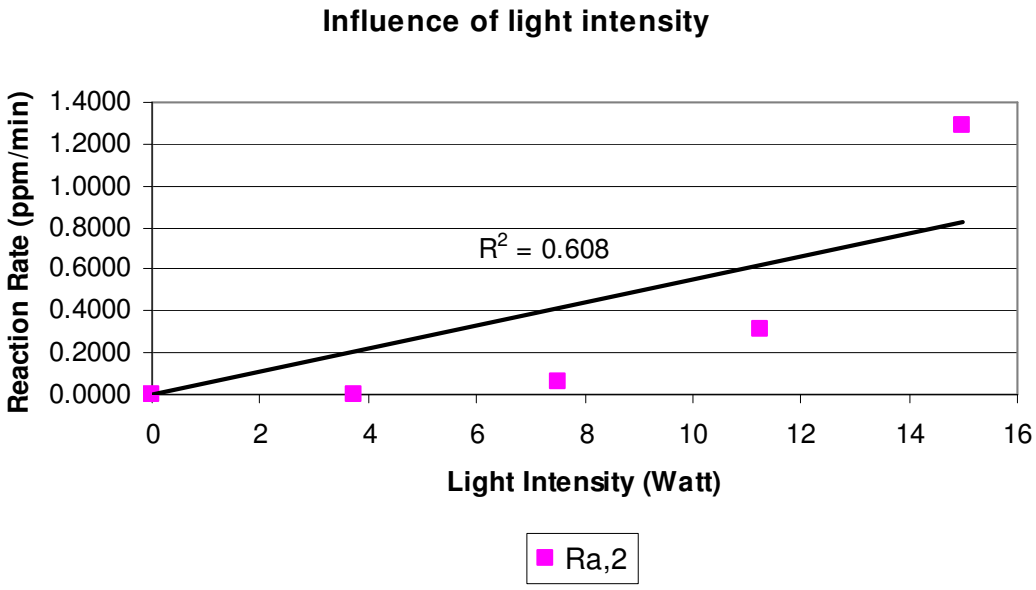


**Figure 32** Influence of light intensity on average reaction rates for the second set of experiments

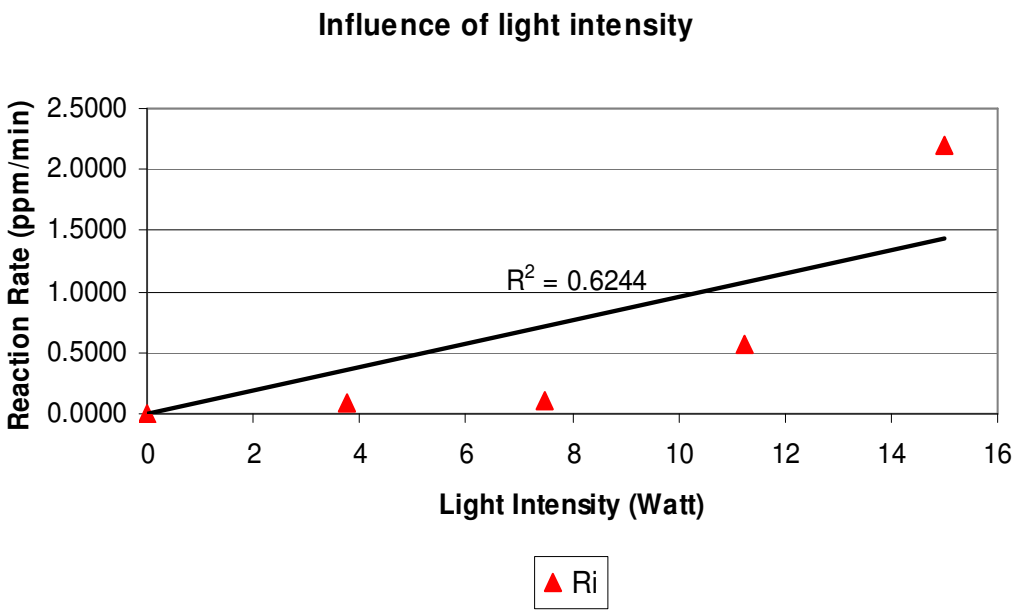


**Figure 33** Influence of light intensity on initial reaction rates in the photocatalytic flow reactor

The fact that the results do not fit a perfect straight line might be due to the method utilised for covering the lamp. Two possible explanations can be given for the results obtained.

Firstly, with no black tape covering the lamp, light (within the lamp) can either be absorbed by catalyst particles or be reflected back (scattered) within the reactor, until eventually absorbed by catalyst particles [6]. When part of the lamp is covered, reflected light could have been absorbed by the black film and tape, resulting in less light available for catalyst activation than the anticipated 25, 50 or 75 % stated.

Secondly, with the lamp uncovered it was determined that each particle spent approximately 9.5 seconds exposed to the UV light source (assuming perfectly mixed conditions in the reservoir). With parts of the lamp covered, each particle will spend only 2.4 seconds exposed to light for lamp coverage of 75% (again assuming perfectly mixed conditions). This method of covering the lamp therefore has rather reduced the time catalyst particles were exposed to UV light as opposed to reducing the light intensity.

These results call for more investigation in future studies, with better methods for determining the influence of light intensity on the initial reduction rate.

# CHAPTER 5

# CONCLUSION

As a first step towards the optimisation of a photocatalytic batch and recirculating flow reactor various parameters such as initial platinum(IV) concentration, initial ethanol concentration, catalyst concentration, pH, temperature and light intensity were investigated on initial and average reduction rates of platinum(IV). Langmuir-Hinshelwood kinetics was applied to some of the parameters (initial platinum(IV) concentration and initial ethanol concentration) in order to determine and compare the reduction rate constant $k_r$ and the adsorption equilibrium constant $K_e$.

The experiments were carried out for various sampling intervals. With sampling concentrated at the beginning of the experimental run, very low initial reduction rates were observed and in some instances negative reduction rate constants, $k_{r,}$ and adsorption equilibrium constants, $K_e$ were obtained. This led to the identification of an induction (generation) period at the beginning of the reduction process. During the induction period only a small percentage of platinum is deposited on the catalyst surface. These platinum pockets then acts as traps for the generated electrons, and reduces the recombination rate between the electron/hole pairs that are formed. Increased reduction rates were only observed after the induction period.

The discovery of the induction period led to experiments to beconducted with sampling concentrated in the middle of each experimental run, generally after the 20 minute induction period. Experiments were carried out for both the batch and recirculating flow reactor. Results indicated that both initial and average reduction rate are independent of the initial platinum(IV) concentration and first-order with regard to the initial ethanol concentration. At high initial ethanol concentrations all platinum(IV) reduced regardless of the initial platinum(IV) concentration. For low initial ethanol concentrations little or no reduction took place for high initial platinum(IV) concentrations. In experimental runs where the ethanol concentration

was in access of 12 g/L the induction period was virtually eliminated and maximum reduction in short periods of time was observed.

The influence of catalyst concentration showed an increase in reduction rate with an increase in $TiO_2$ up to an optimum concentration of 3 g/L, after which a decrease in reduction rate was observed. This is due to the increased density of the suspension.

Determination of the influence of pH on the reduction rate proved to be a complex parameter as both the catalyst surface charge as well as positions of the conduction and valance band is pH dependent. Results indicated a strong increase in reduction rate from pH 3 to pH 4. The $pK_a = 3.5$ corresponds to the pH value at which equal amounts of TiOH and $TiOH_2^+$ species are present in the system.

The influence that temperature has on the reduction rate was investigated for 12.5 ˚C to 75 ˚C. Temperatures higher that 75 ˚C were not investigated as ethanol starts to evaporate at higher temperatures. A linear relationship was obtained with greater reduction rates at higher temperatures. The Arrhenius plot indicated two regions for both reactors with low activation energies in all cases.

Determination of the influence of light intensity suffered some difficulties. This parameter was only investigated for the recirculating flow reactor as the UV light source had to be covered by black tape. Very low reduction rates were obtained for all intensities except when 100% of the UV light was utilised. This indicated that the method for testing light intensity was not adequate.

It was generally observed that average reduction rates were lower than that of initial reduction rates, due to the incorporation of the induction period in the average rates. All trends remained similar to that of initial reaction rates, except in the case of light intensity where a better linear fit was observed for average reaction rates. Experiments conducted under exactly the same conditions with sampling intervals either concentrated at the beginning or in the middle of the experimental run, generally showed little difference in the average reaction rates. The slight differences observed, were due to the different analytical methods used, ICP vs. ICP-MS.

During all experiments very good correlations were obtained between the batch and flow reactor, with all parameters indicating similar trends. There was no significant

difference between the two reactors even though the batch reactor had a UV light source at 9 W and the flow reactor at 15 W. This may be a good starting point for future studies as to correlate the reactor configuration and the light intensity. Future studies can also investigate better ways of varying the light intensity. This will allow to test both the effect that the reactor type as well as the light intensity has on the photocatalytic reduction of platinum(IV).

# REFERENCES


1. Litter, M.I., Applied Catalysis B: Environmental, 1999. **23**: p. 89-114.
2. Schrank, S.G., Jose, H.J., and Moreira, R.F.P.M., Journal of Photochemistry and Photobiology A: Chemistry, 2002. **147**: p. 71-76.
3. Hoffmann, M.R., Martin, S.T., Choi, W., and Bahnemann, D.W., Chemical Review, 1995. **95**: p. 69-96.
4. Prairie, M.R., Evans, L.R., Stange, B.M., and Martinez, S.L., Environmental Science Technology, 1993. **27**: p. 1776-1782.
5. Devipriya, S., and Yesodharan, S., Solar Energy Materials and Solar Cells, 2005. **86**: p. 309-348.
6. Chen, D., and Ray, A.K., Chemical Engineering Science, 2001. **56**: p. 1561-1570.
7. Kish, H., *What is Photocatalysis*, in *Photocatalysis: Fundamentals and Applications*, N. Serpone, Editor. 1989, Wiley-Interscience. p. 650.
8. Herrmann, H., Catalysis Today, 1999. **53**: p. 115-129.
9. Carrier, M., Perol, N., Herrmann, J., Bordes, C., Horikoshi, S., Paisse, J.O., Baudot, R., and Guillard, C. , Applied Catalysis B: Environmental, 2006. **65**: p. 11-20.
10. Hufschmidt, D., Bahnemann, D., Testa, J.J., Emilio, C.A., and Litter, M.I., Journal of Photochemistry and Photobiology A: Chemistry, 2002. **148**: p. 223-231.
11. Rajeshwar, K., Journal of Applied Electrochemistry, 1995. **25**: p. 1067-1071.
12. Macias, T.L., *The Design and Evaluation of a Continuous Photocatalytic Reactor Utilizing Titanium Dioxide in Thin Films of Mesoporous Silica* in *Chemical Engineering*. 2003, Mississippi State University. p. 125.
13. Greenwood, N.N., and Earnshaw, A., *Chemistry of the Elements*. 1997, Oxford: Butterworth-Heinemann.
14. Ollis, D.F., and Turchi, C.S., Journal of Catalysis, 1990. **122**: p. 179-192.
15. Alfano, O.M., Bahnemann, D., Cassano, A.E., Dillert, R., and Gosllich, R., Catalysis Today, 2000(58): p. 199-230.
16. Kriek, R.J., *Separation of Pt(IV), Pd(II) and Rh(III) through Differential Photocatalytic Reduction*, in *Chemistry*. 1994, University of Stellenbosch: Stellenbosch. p. 142.
17. Ollis, D.F., Pelizzetti, E., and Serpone, N., Environmental Science Technology, 1991. **25**(9): p. 1523.
18. Wang, C.M., Heller, A., and Greischer, H., Journal of the Americal Chemical Society, 1992. **114**: p. 5230.
19. Kanki, T., Yoneda, H., Sano, N., Toyoda, A., and Nagai, C., Chemical Engineering Journal, 2004. **97**: p. 77-81.

20. Angelidis, T.N., Koutlemani, M., and Poulios, I., Applied Catalysis B: Environmental, 1998. **16**: p. 347-357.
21. Rajeshwar, K., Chenthamarakshan, C.R., Ming, Y., and Sun, W. , Journal of Electoanalytical Chemistry, 2002. **538-539**: p. 173-182.
22. Prairie, M.R., Evans, L.R., and Martinez, S.L., Chemical Oxidation, 1992. **2**: p. 428.
23. Prairie, M.R., Strange, B.M., Evans, L.R., and Martinez, S.L., in: Ollis, D.F., Al-Ekabi, H., ed. *Photocatalytic Purification and Treatment of Water and Air*. 1994, Elsevier: Amsterdam. 353.
24. Liangbo, F., Hanqing, W., Zhensheng, J., Qinglin, L., and Mengyang, S., Journal of Photochemistry and Photobiology A: Chemistry, 1991. **56**: p. 89.
25. Serpone, N., Borgarello, E., and Pelizzetti, E., in: Schiavello, M., ed. *Photocatalysis and Environment*. 1988, Kluwer Academic Publishers: Dordrecht. 527.
26. Ward, M.D., and Bard, A.J., Journal of Physical Chemistry, 1982. **86**: p. 3599-3602.
27. Kriek, R.J., Engelbrecht, W.J., and Cruywagen, J.J., Journal of South African Institute of Minerals and Metallurgy 1995. **9**: p. 73-76.
28. Borgarello, E., Serpone, N. Pelizetti, E., and Barbeni, M., Journal of Photochemistry 1986. **33**: p. 34-37.
29. De Lasa, H., Serrano, B., and Salaices, M., *Photocatalytic Reaction Engineering*. 2004, London: Springer.
30. Bahnemann, D., Dockelman, D., Goslich, R., and Weichgrebe, M., Solar Energy Mater 1991. **24**: p. 564-583.
31. Cassano, A., Martin, C., Brandi, R., and Alfano, O., Industrial and Engineering Chemistry Research, 1995. **34**: p. 2155-2201.
32. Mukherjee, P.S., and Ray, A.K., Chemical Engineering Technology, 1999. **22**(3): p. 253-260.
33. Segawe, G., Brandi, R.J., Bahnemann, D., and Cassano, A.E. , Chemical Engineering Science, 2003. **58**: p. 2587-2599.
34. Segawe, G., Brandi, R.J., Bahnemann, D., and Cassano, A.E., Chemical Engineering Science, 2003. **58**: p. 2601-2615.
35. Ray, A.K., and Beenackers, A., Catalysis Today, 1998. **40**(1): p. 73-83.
36. Brucato, A., and Rizzuti, L., Industrial and Engineering Chemistry Research, 1997. **36**(11): p. 4748-4755.
37. Fogler, H.S., *Elements of Chemical Reaction Engineering*. 1999: Prentice: Upper Saddle River.
38. Kormann, C., Bahnemann, D.W., and Hoffmann, M.R., Environmental Science Technology, 1991. **25**: p. 494-500.
39. Benitez, F.J., Acero, J.L., Real, F.J., and Garcia, J., Chemosphere, 2003. **51**(8): p. 651-662.
40. Ching, W.H., Leung, M., and Leung, D.Y.C., Solar Energy, 2004. **77**: p. 129-135.
41. Murzin, D.Y., Catalysis Communications, 2008. **9**: p. 1815-1816.

42. Cassano, A.E., Alfano, O.M., and Cabrera, m.I. , Journal of Catalysis, 1997. **172**: p. 370.
43. Cornish-Bowden, A., *Fundamentals of Enzyme Kinetics*. third ed. 2004, London: Portland Press.
44. Kumar, K.V., Prokodi, K., and Rocha, F. , Catalysis Communications, 2008. **9**: p. 82.
45. Poulios, I., Micropoulou, E., Panou, R., and Kostopoulou, E., Applied Catalysis B: Environmental, 2003. **41**: p. 345.
46. Serpone, N., Sauve, G., Koch, R., Tahiri, H., Picat, P., Piccinini, P., Pelizetti, E., and Hidaka, H., Journal of Photochemistry and Photobiology A: Chemistry, 1993. **73**: p. 11.
47. Serpone, N., Sauve, G., Koch, R., Tahiri, H., Picat, P., Piccinini, P., Pelizetti, E., and Hidaka, H., Journal of Photochemistry and Photobiology A: Chemistry, 1996. **94**: p. 191-203.
48. Serpone, N., Lawless, D., Khairutdinov, R., and Pelizzetti, E., Journal of Physical Chemistry, 1995. **99**: p. 16655.
49. Ku, Y., Jung, I.-J., , Water Research, 2001. **35**: p. 132-136.
50. Lin, W.-Y., Wei, C., Rajeshwar, K.,, Journal of Electochemical Society, 1993. **140**: p. 2475-2482.
51. Siemon, U., Bahnemann, D., Testa, J.J., Rodriquez, D., Litter, M.I., Bruno, N., Journal of Photochemistry and Photobiology A: Chemistry, 2002. **148**: p. 247-255.
52. Li, F.B., Li, X.Z., Chemosphere, 2002. **48**: p. 1103-1111.
53. Sauer, T., Cesconeto Neto, G., Jose, H.J., Moreira, R.F.P.M., Journal of Photochemistry and Photobiology A: Chemistry, 2002. **149**: p. 147-154.
54. Nedoloujko, A., Kiwi, J., Water Research, 2000. **34**(14): p. 3277-3285.

# APPENDIX A

# REDUCTON GRAPHS: THE INDUCTION PERIOD

All concentrations is normalised ($C/C_i$) for better visual representation of data.

## The reduction of platinum(IV) with 3 g/L ethanol

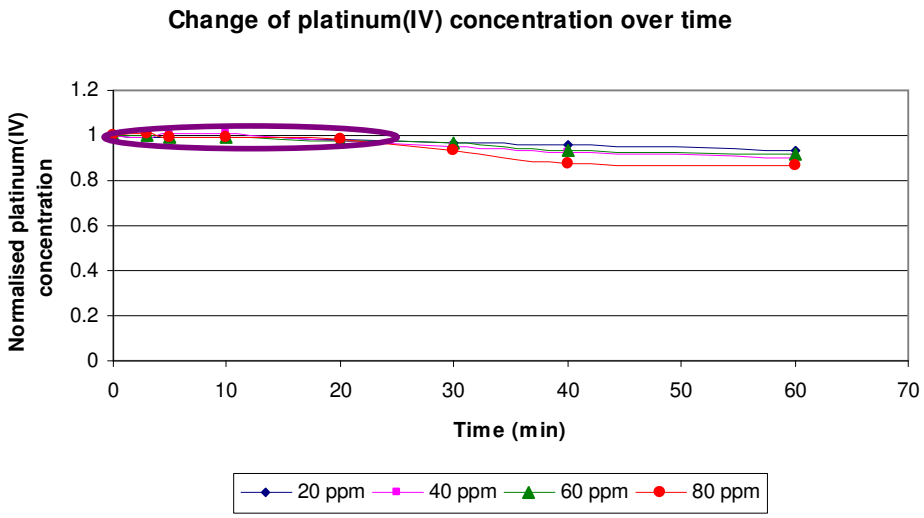


## The reduction of platinum(IV) with 6 g/L ethanol

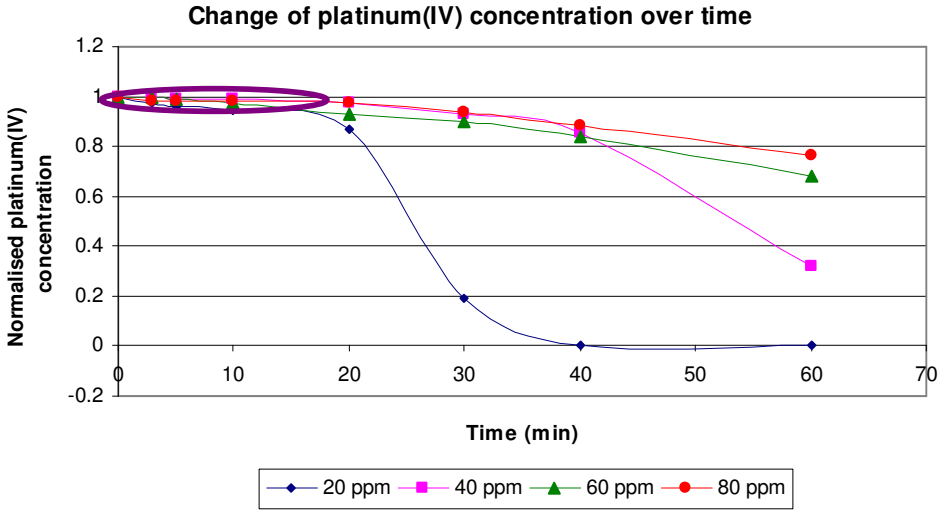

## The reduction of platinum(IV) with 12 g/L ethanol

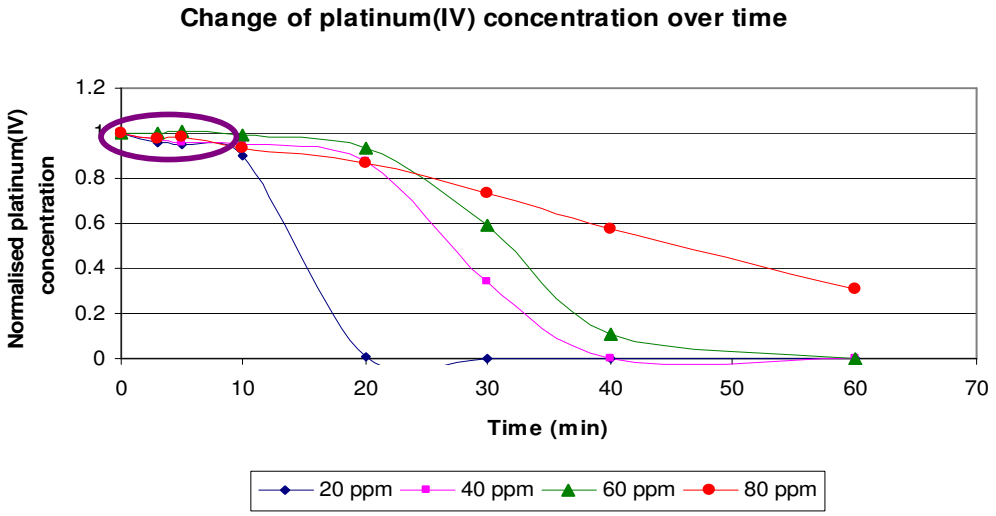


## Reduction dependency of 20 ppm platinum(IV) at various initial ethanol concentrations.

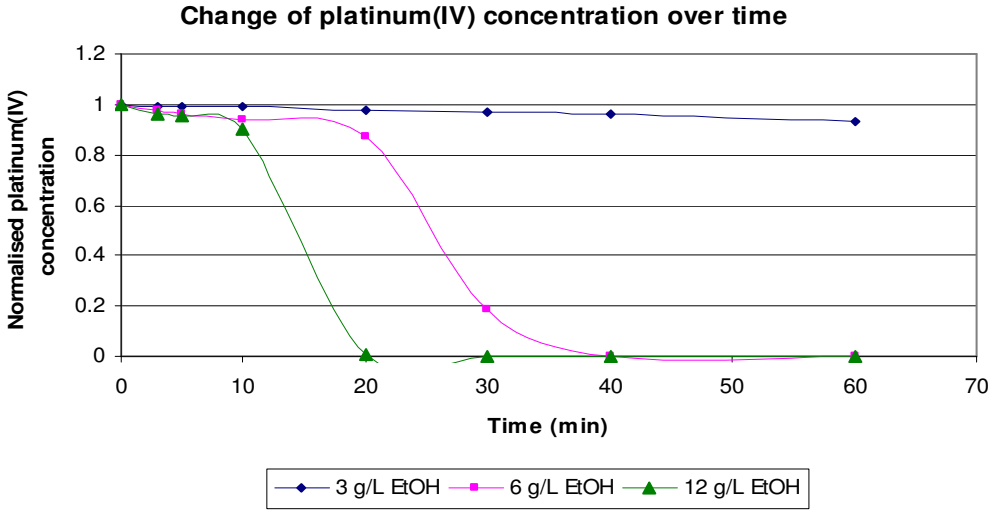

**Reduction dependency of 40 ppm platinum(IV) at various initial ethanol concentrations.**

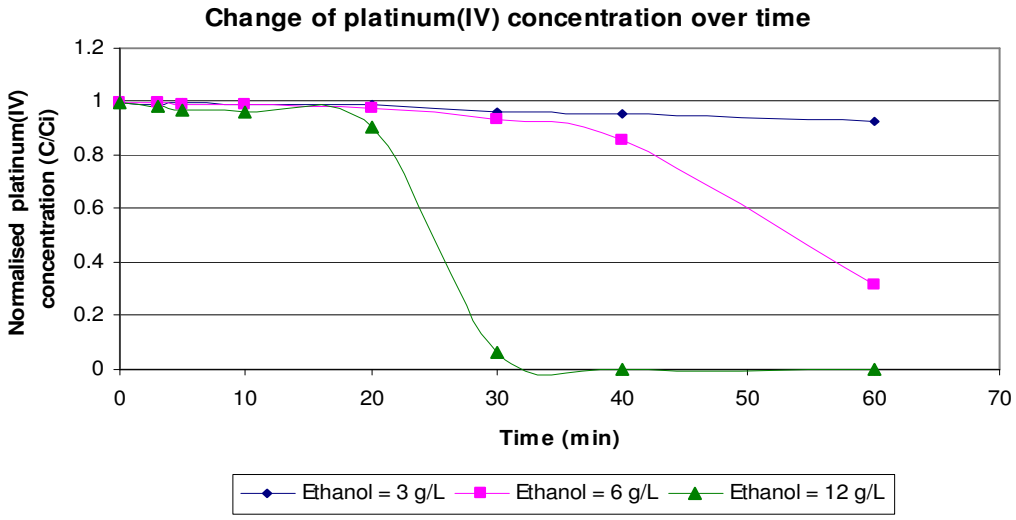


**Reduction dependency of 60 ppm platinum(IV) at various initial ethanol concentrations.**

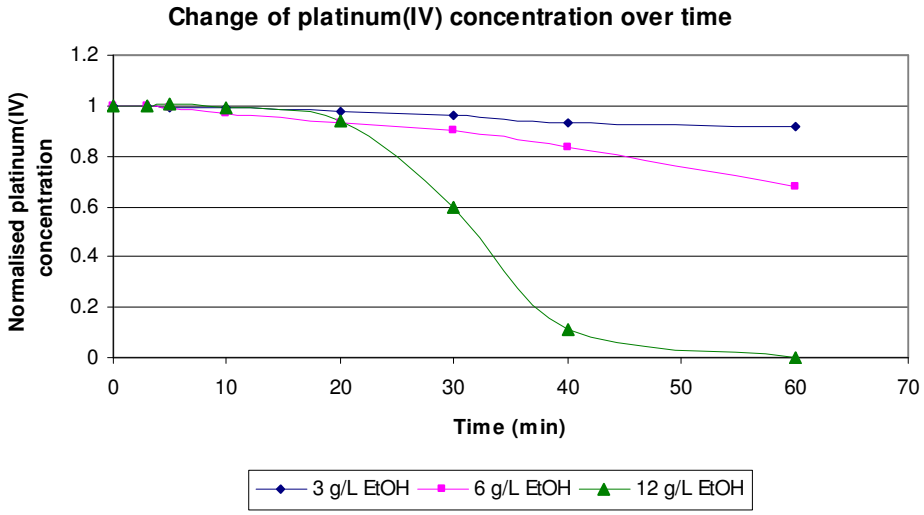

**Reduction dependency of 80 ppm platinum(IV) at various initial ethanol concentrations.**

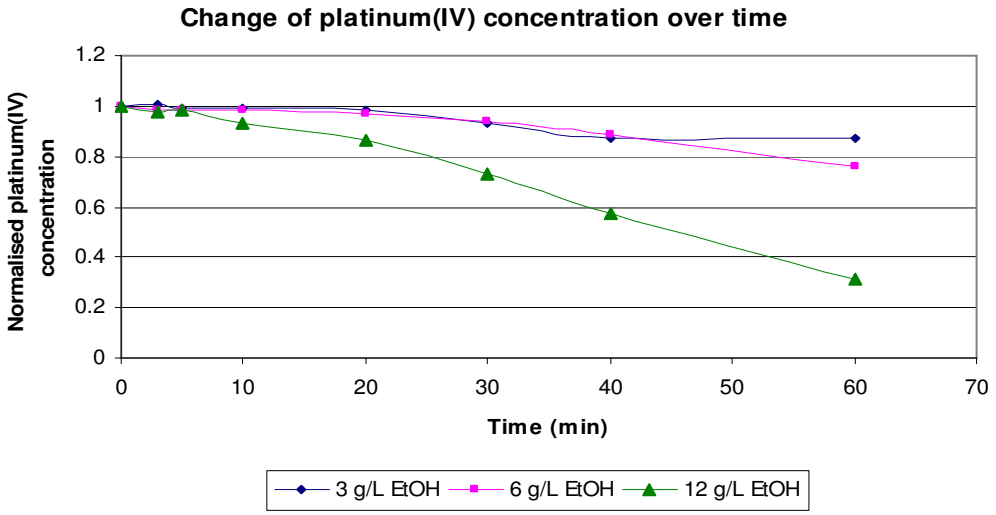


**The reduction of platinum(IV) with 1 g/L $TiO_2$.**

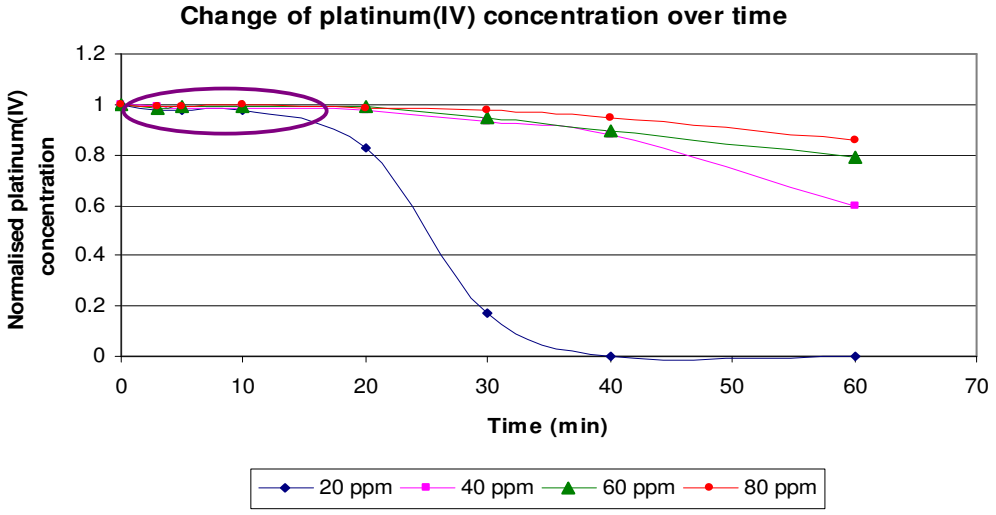

## The reduction of platinum(IV) with 2 g/L $TiO_2$.

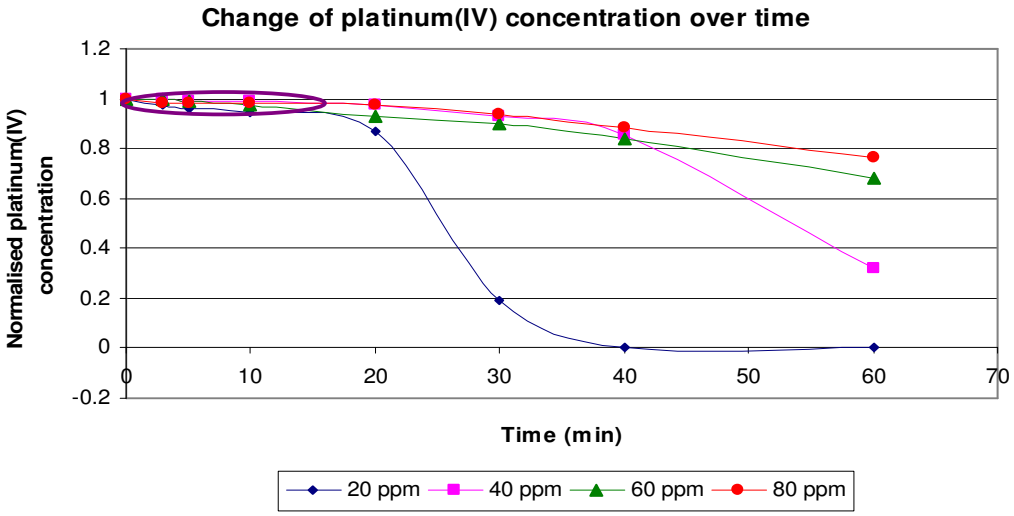


## The reduction of platinum(IV) with 4 g/L $TiO_2$.

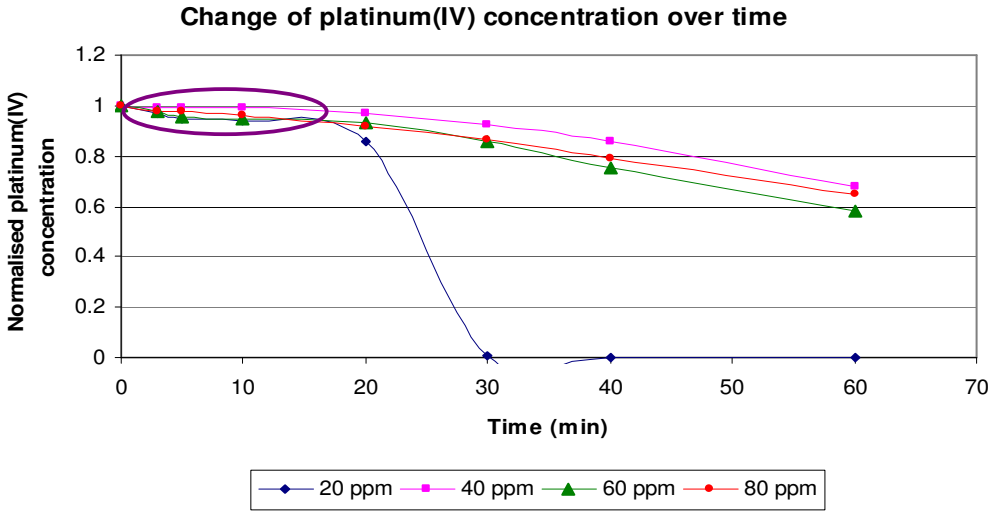

**Table below indicated low reduction rate constants and calculated reduction rates when Langmuir-Hinshelwood constants were calculated over the induction period.**

| **Reaction Conditions** (pH = 3, Temp = 25˚C, Light = 100%) | $k_r$ **ppm/min** | $K_e$ **1/ppm** | **R (50ppm) ppm/min** |
|---|---|---|---|
| EtOH = 6 ; $TiO_2$ = 2 | 0.0813 | -0.665 | 0.084 |
| EtOH = 3 ; $TiO_2$ = 1 | 0.0203 | -0.066 | 0.029 |
| EtOH = 6 ; $TiO_2$ = 1 | 0.0411 | 0.175 | 0.037 |
| EtOH = 12 ; $TiO_2$ = 1 | 0.3489 | 0.023 | 0.188 |
| EtOH = 3 ; $TiO_2$ = 2 | -0.1684 | -0.005 | 0.052 |
| EtOH = 12 ; $TiO_2$ = 2 | 0.1634 | -0.097 | 0.206 |
| EtOH = 3 ; $TiO_2$ = 4 | -0.1857 | -0.006 | 0.075 |
| EtOH = 6; $TiO_2$ = 4 | 0.1486 | 0.088 | 0.121 |
| EtOH = 12 ; $TiO_2$ = 4 | 0.5606 | -0.157 | 0.642 |

# APPENDIX B

# REDUCTON AND LANGMUIR-HINSHELWOOD GRAPHS: INITIAL ETHANOL CONCENTRATION

**Reduction of platinum(IV) over time for ethanol concentrations of 11, 8, 6 and 3 g/L, respectively.**

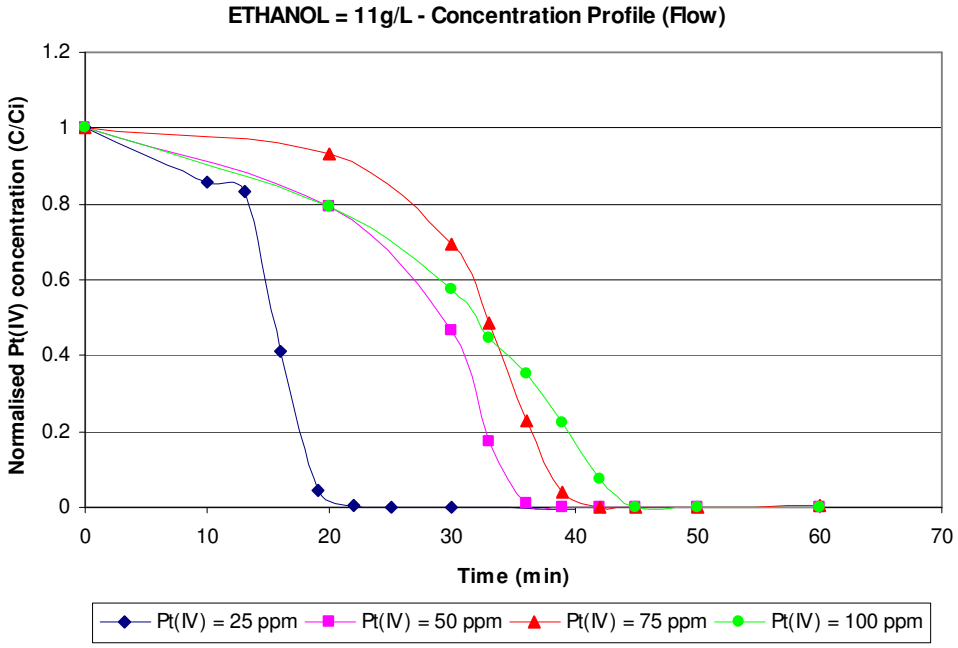


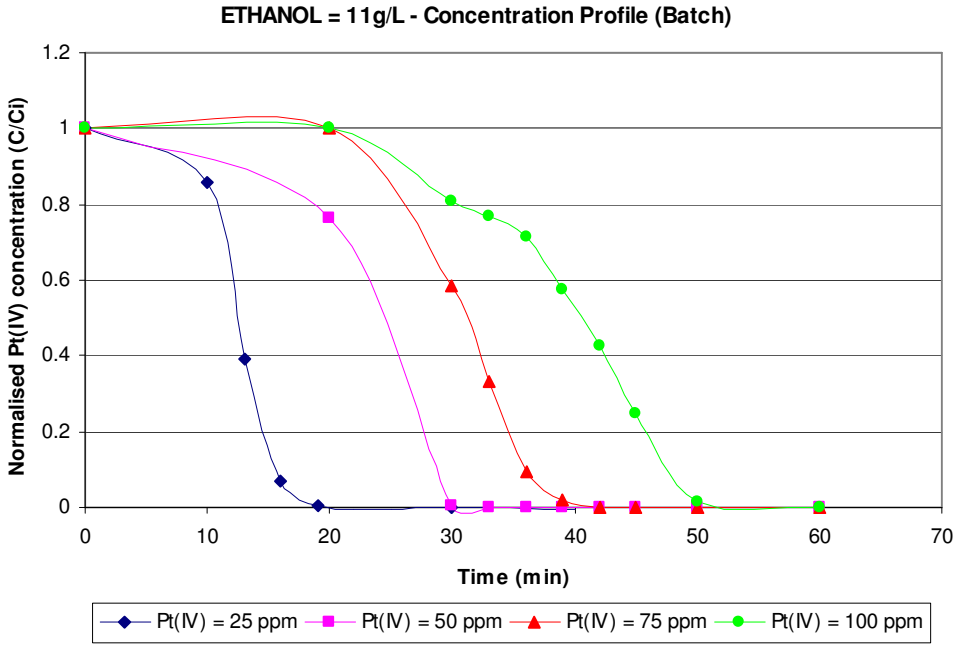

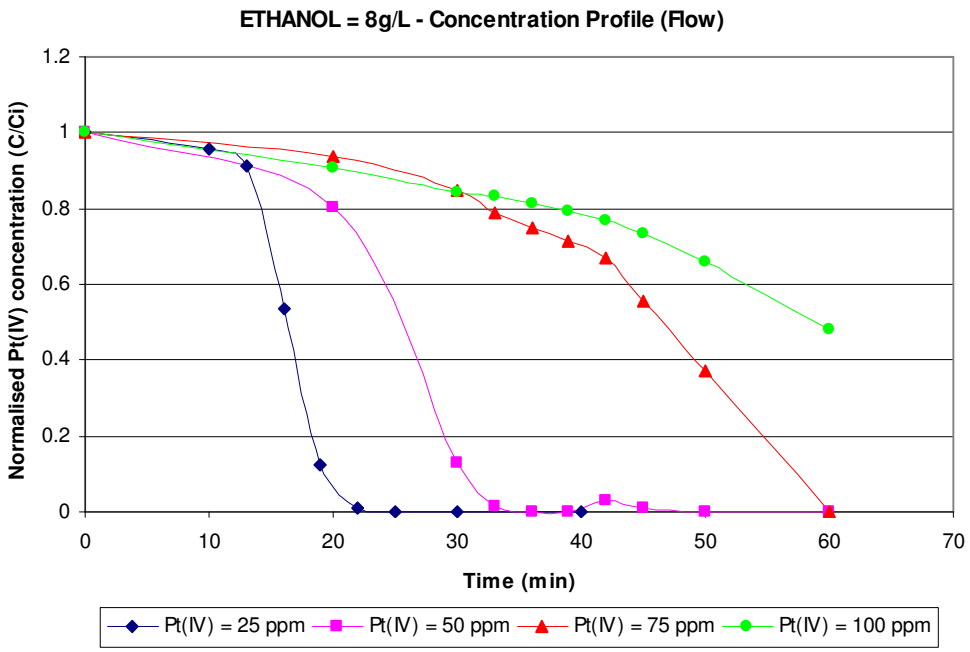
ETHANOL = 8g/L - Concentration Profile (Flow)
Normalised Pt(IV) concentration (C/Ci)
1.2
1
0.8
0.6
0.4
0.2
0
0
10
20
30
40
50
60
70
Time (min)
Pt(IV) = 25 ppm
Pt(IV) = 50 ppm
Pt(IV) = 75 ppm
Pt(IV) = 100 ppm

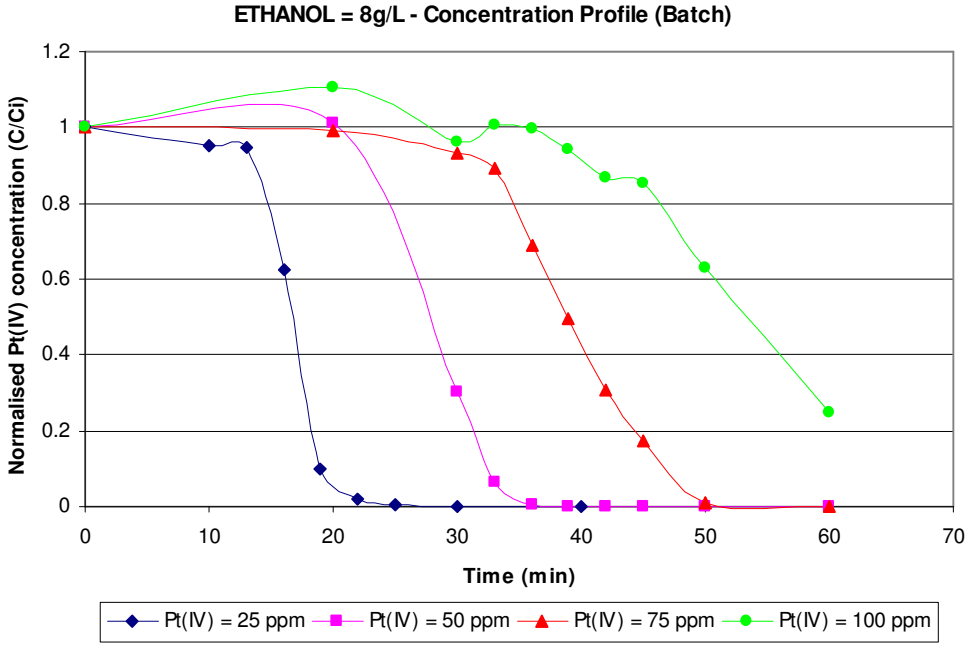
ETHANOL = 8g/L - Concentration Profile (Batch)
Normalised Pt(IV) concentration (C/Ci)
1.2
1
0.8
0.6
0.4
0.2
0
0
10
20
30
40
50
60
70
Time (min)
Pt(IV) = 25 ppm
Pt(IV) = 50 ppm
Pt(IV) = 75 ppm
Pt(IV) = 100 ppm

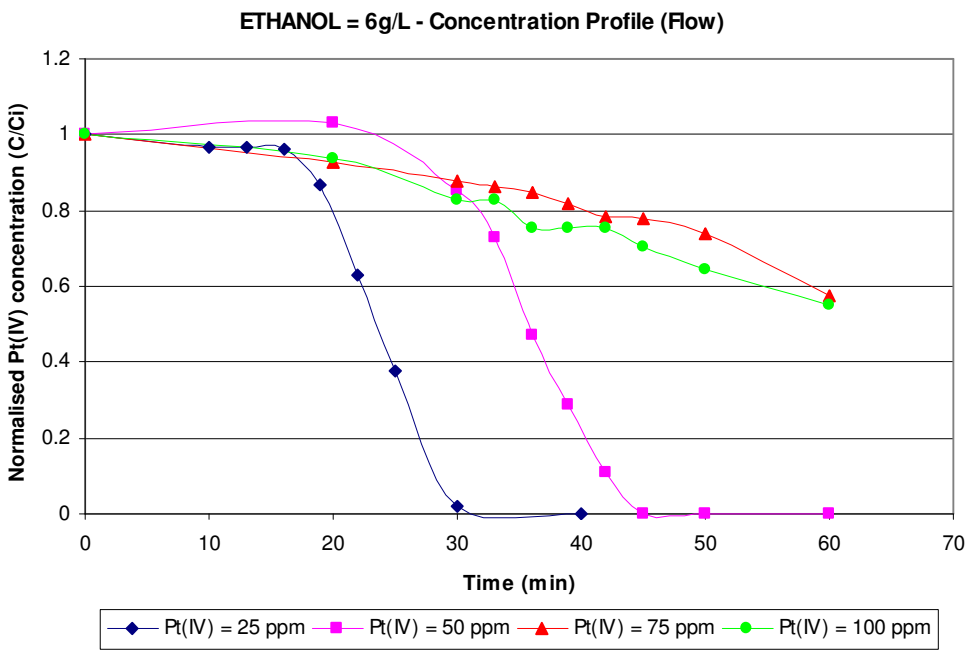
ETHANOL = 6g/L - Concentration Profile (Flow)
Normalised Pt(IV) concentration (C/Ci)
1.2
1
0.8
0.6
0.4
0.2
0
0
10
20
30
40
50
60
70
Time (min)
Pt(IV) = 25 ppm
Pt(IV) = 50 ppm
Pt(IV) = 75 ppm
Pt(IV) = 100 ppm

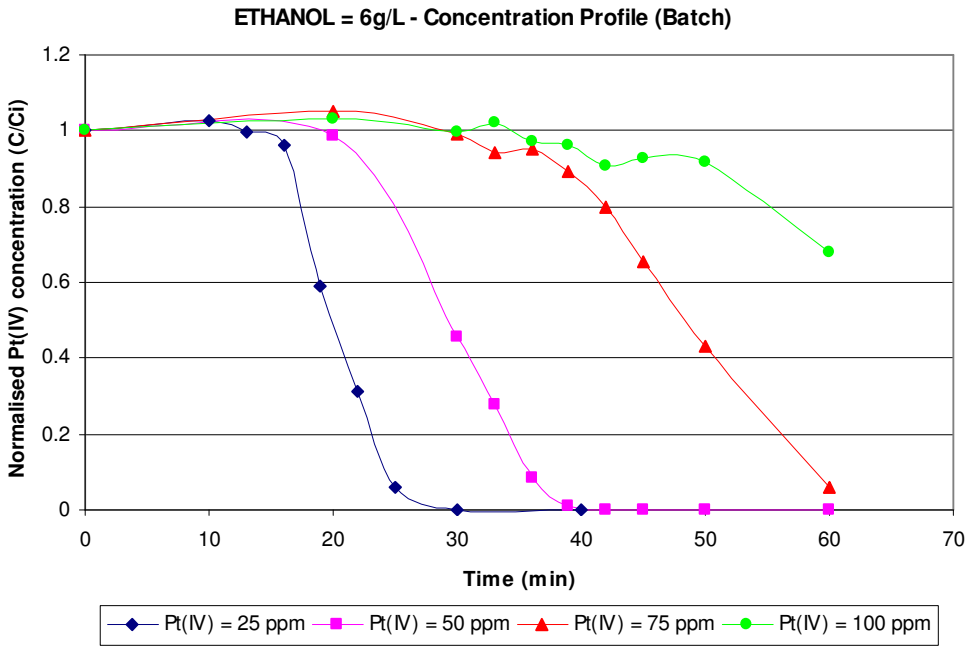
ETHANOL = 6g/L - Concentration Profile (Batch)
Normalised Pt(IV) concentration (C/Ci)
1.2
1
0.8
0.6
0.4
0.2
0
0
10
20
30
40
50
60
70
Time (min)
Pt(IV) = 25 ppm
Pt(IV) = 50 ppm
Pt(IV) = 75 ppm
Pt(IV) = 100 ppm

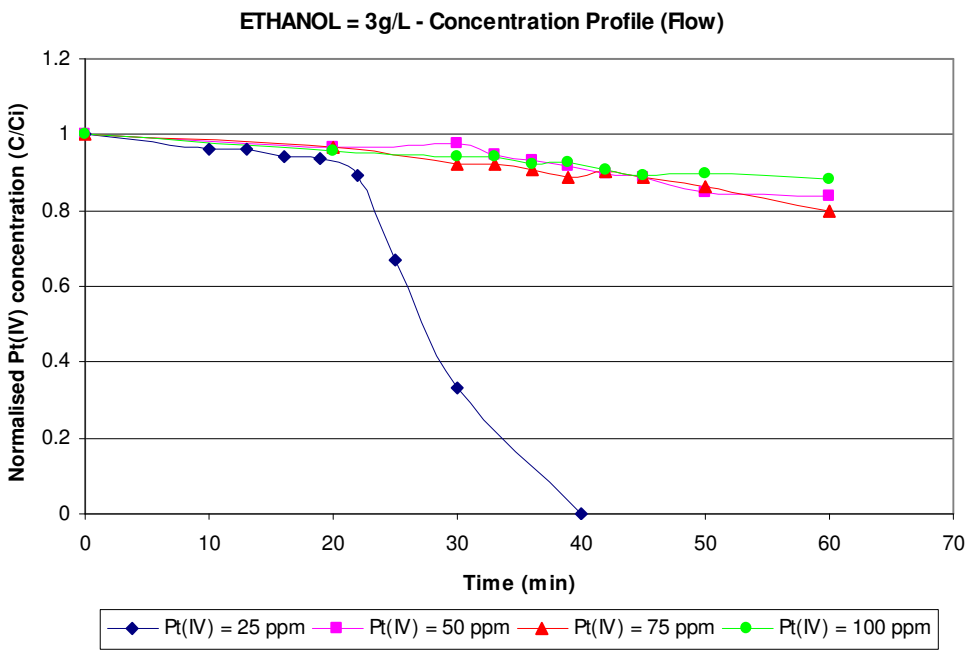
ETHANOL = 3g/L - Concentration Profile (Flow)
Normalised Pt(IV) concentration (C/Ci)
1.2
1
0.8
0.6
0.4
0.2
0
0
10
20
30
40
50
60
70
Time (min)
Pt(IV) = 25 ppm
Pt(IV) = 50 ppm
Pt(IV) = 75 ppm
Pt(IV) = 100 ppm

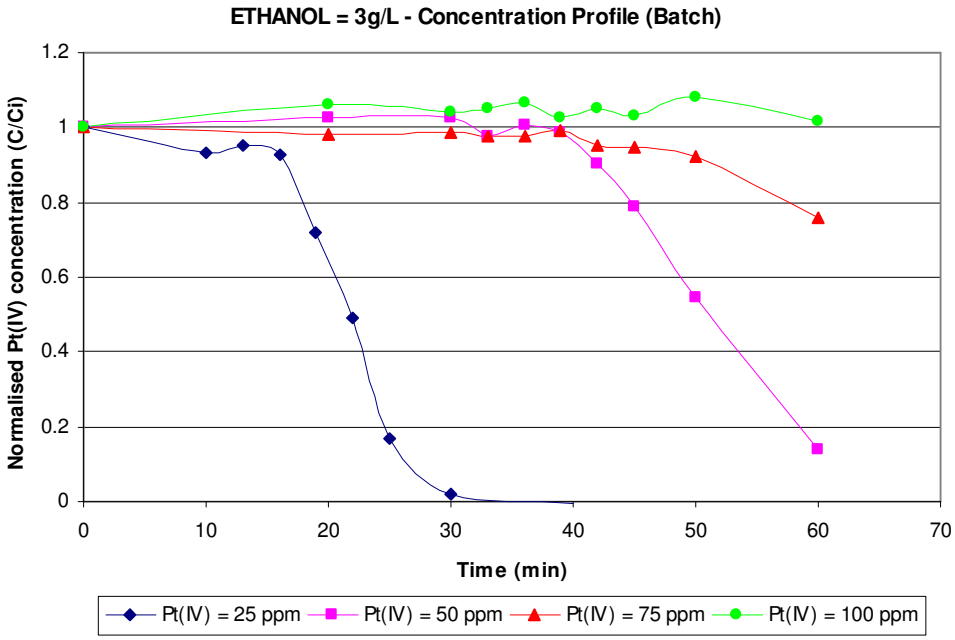
ETHANOL = 3g/L - Concentration Profile (Batch)
Normalised Pt(IV) concentration (C/Ci)
1.2
1
0.8
0.6
0.4
0.2
0
0
10
20
30
40
50
60
70
Time (min)
Pt(IV) = 25 ppm
Pt(IV) = 50 ppm
Pt(IV) = 75 ppm
Pt(IV) = 100 ppm

Langmuir-Hinshelwood plot for Ethanol = 8g/L

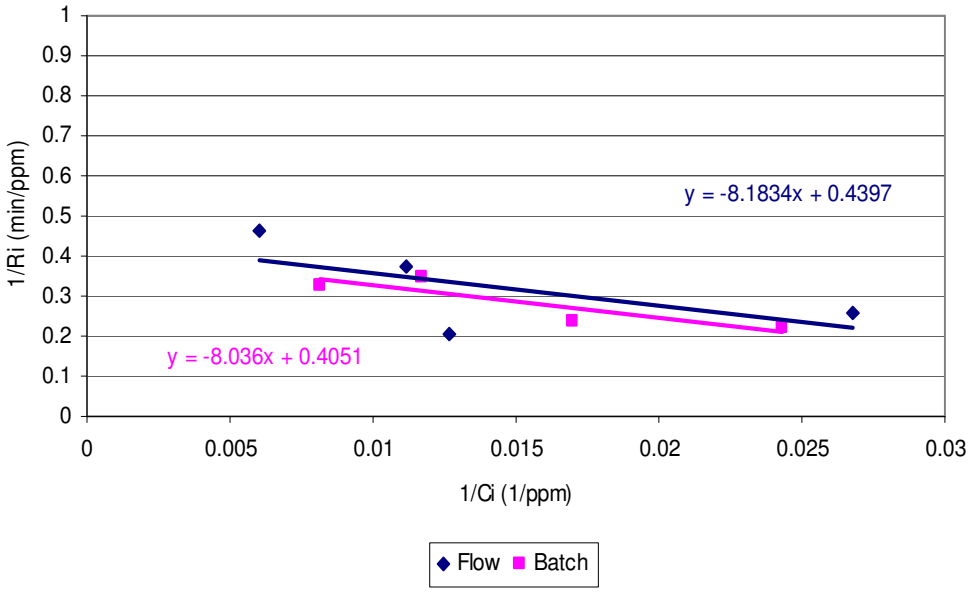


Langmuir-Hinshelwood plot for Ethanol = 6g/L

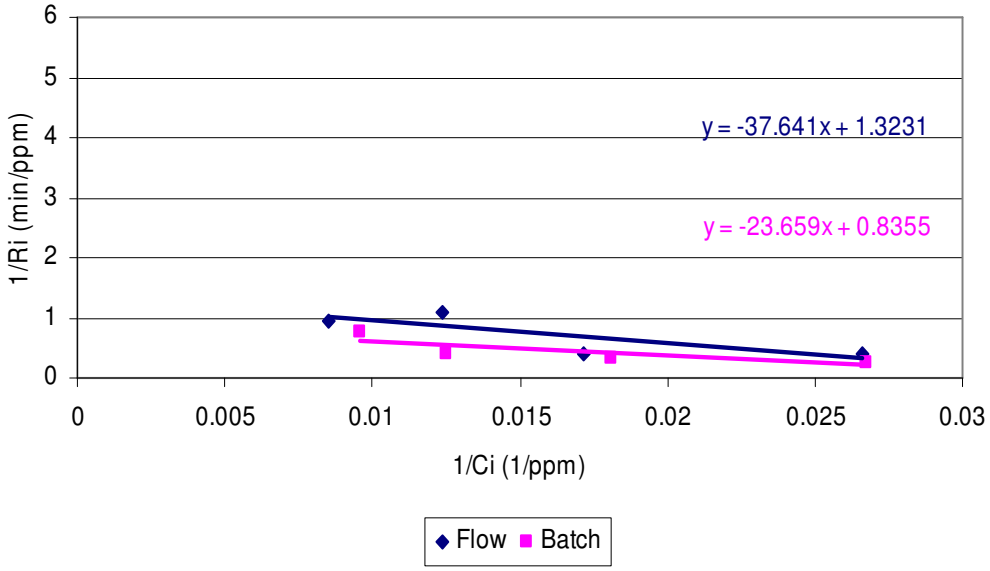

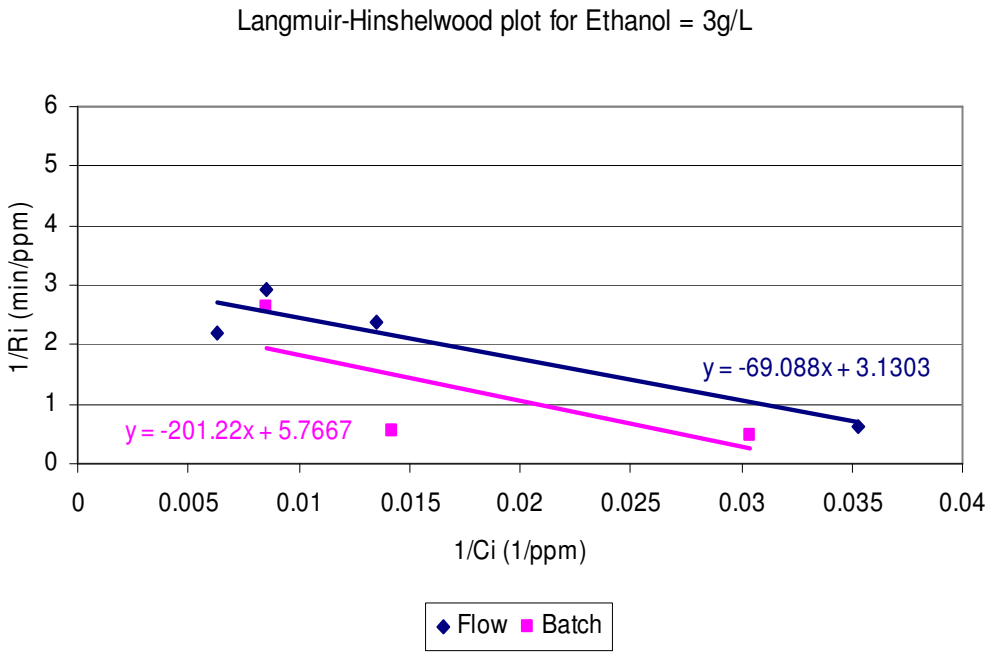
Langmuir-Hinshelwood plot for Ethanol = 3g/L
1/Ri (min/ppm)
6
5
4
3
2
1
0
0
0.005
0.01
0.015
0.02
0.025
0.03
0.035
0.04
1/Ci (1/ppm)
y = -69.088x + 3.1303
y = -201.22x + 5.7667
Flow
Batch

# APPENDIX C

# REDUCTION GRAPHS: CATALYST CONCENTRATION

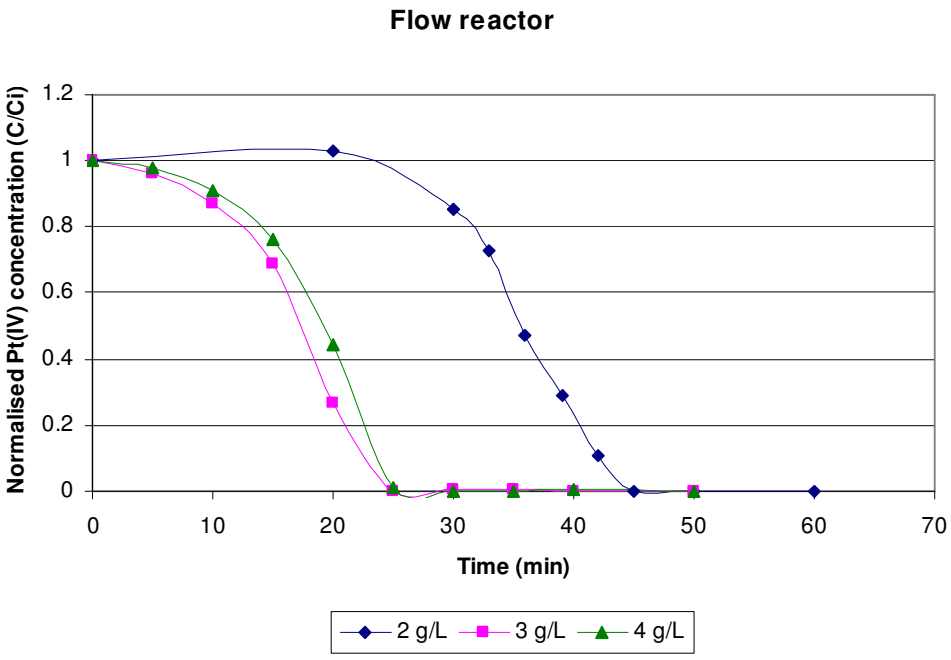
Flow reactor
Normalised Pt(IV) concentration (C/Ci)
1.2
1
0.8
0.6
0.4
0.2
0
0
10
20
30
40
50
60
70
Time (min)
2 g/L
3 g/L
4 g/L

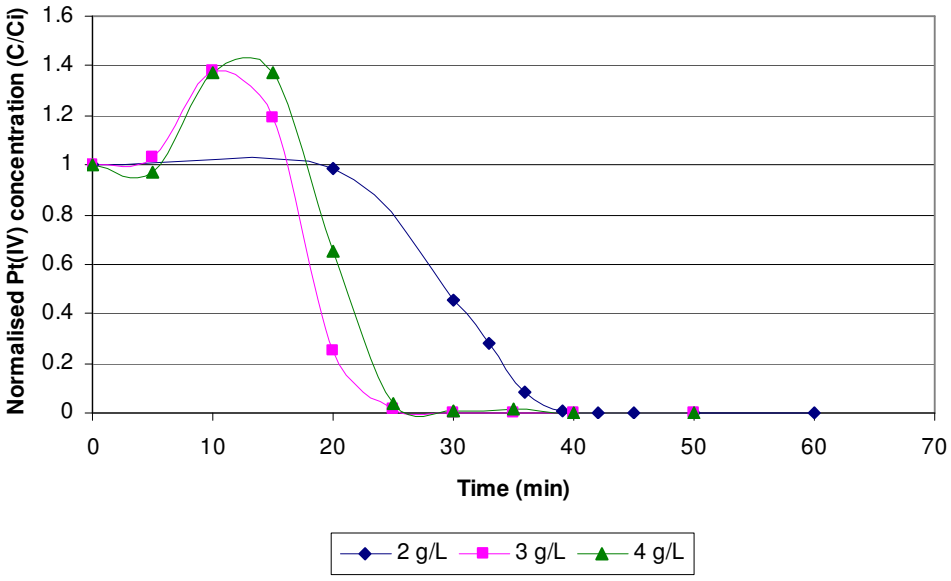
Batch Reactor
Normalised Pt(IV) concentration (C/Ci)
1.6
1.4
1.2
1
0.8
0.6
0.4
0.2
0
0
10
20
30
40
50
60
70
Time (min)
2 g/L
3 g/L
4 g/L

# APPENDIX D

# REDUCTION GRAPHS: pH, TEMPERATURE AND LIGHT INTENSITY

**Reduction in Platinum(IV) with pH 1.5, 3. 4.5 and 5.5 respectively.**

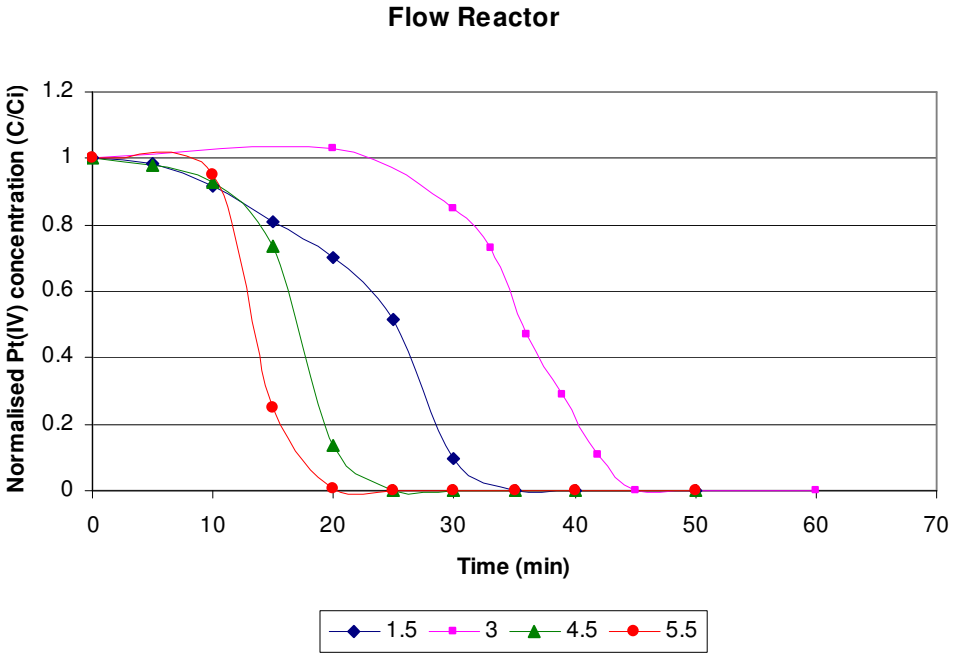


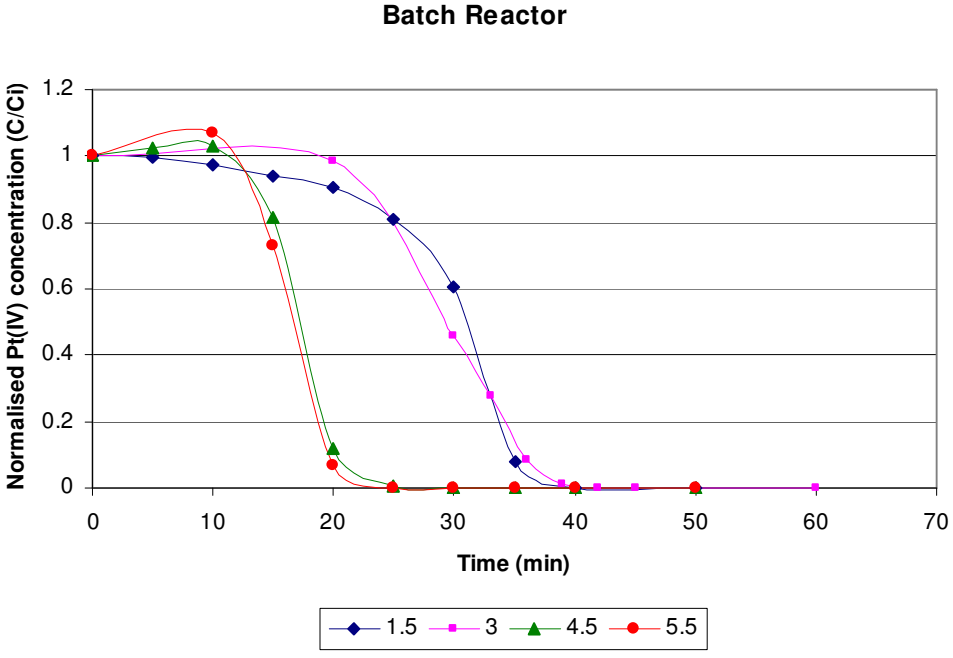

**Reduction of Platinum(IV) at temperatures 12.5 ˚C, 25 ˚C, 50 ˚C and 75 ˚C, respectively.**

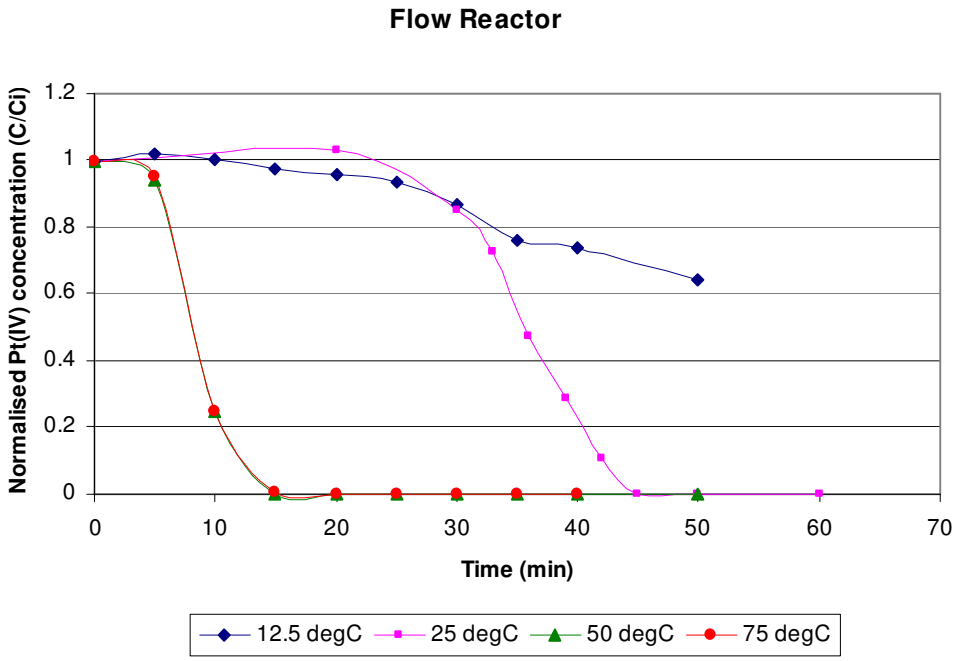


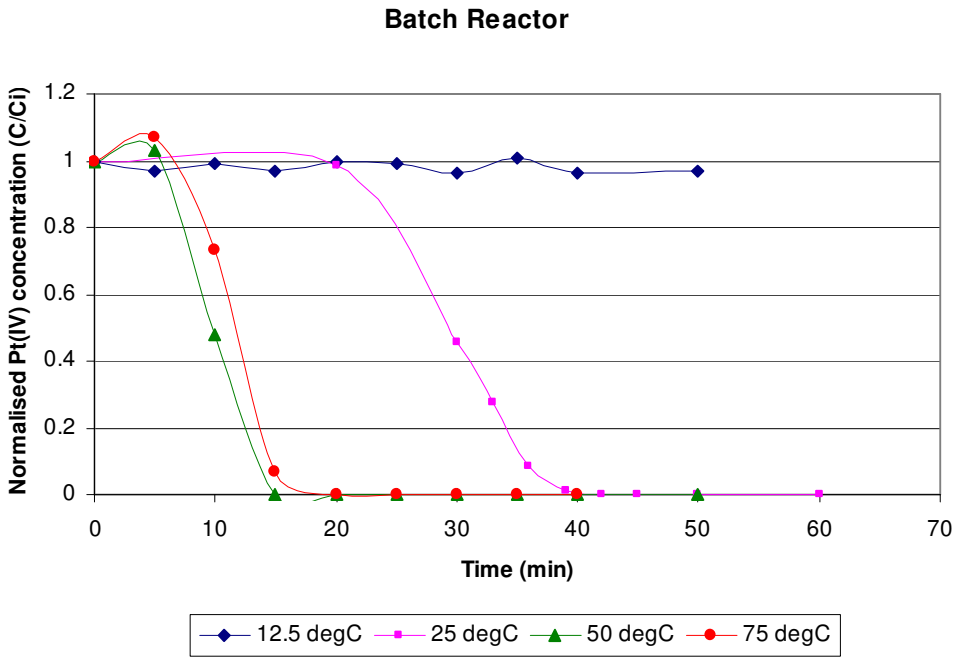

## Reduction of Platinum(IV) with 25%, 50%, 75% and 100% UV light present.

Below graph was used to determine Ra,1 as per Table 9 and Figure 32.

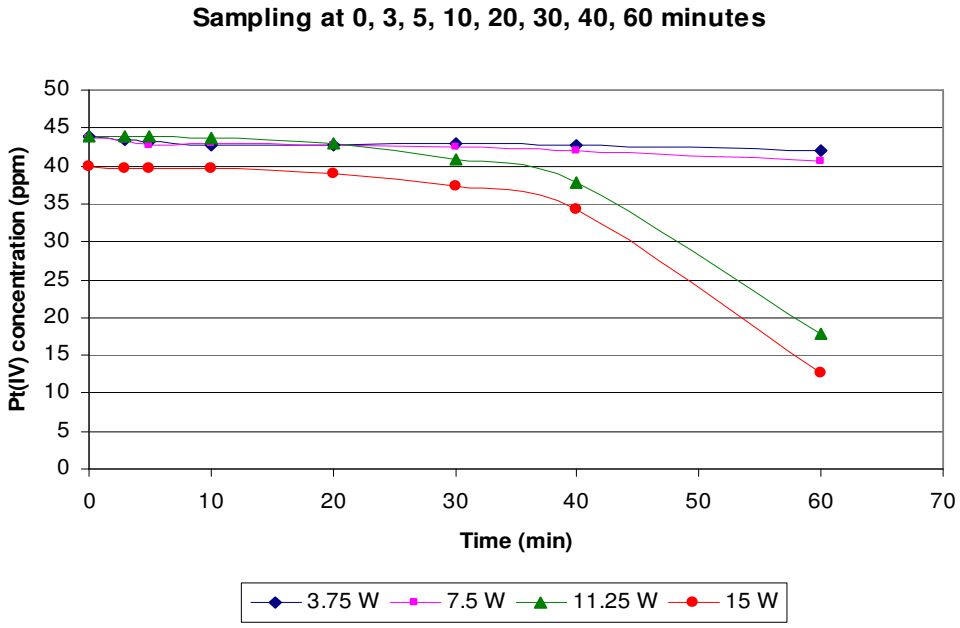


Below graph was used to determing Ra,2 and Ri as per Table 9 and Figure 33 and 34.